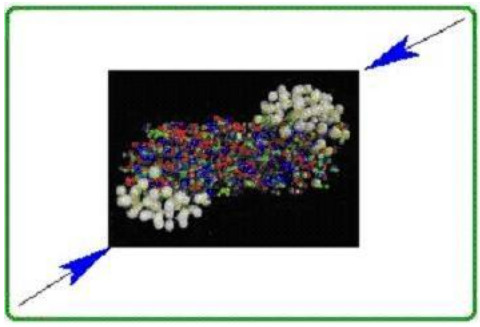

High Energy

High Intensity

Hadron Beams

Proceedings of the 4th CARE-HHH-ABI Workshop on
"Simulation of BPM Front-End Electronics and Special Mechanical Designs"
Lüneburg (Germany); 30th of November and 1st of December 2006

Edited by K. Wittenburg[1]

1) DESY, Hamburg, Germany

Abstract

This report contains the final proceedings of the 4th meeting in the framework of the CARE-HHH-ABI networking, held 30th of November and 1st of December 2006, in Lüneburg (Germany), with the subject: " Simulation of BPM Front-End Electronics and Special Mechanical Designs ".

The purpose of the event is:

- To discuss in detail technology issues related to the subjects.
- To understand the specifications for upcoming new hadron facilities
- To propose concrete work packages for the coming years in order to meet the specified objectives.

Proceedings of the 4th CARE-HHH-ABI Workshop
"Simulation of BPM Front-End Electronics and Special Mechanical Designs"
Lüneburg (Germany); 30th of November and 1st of December 2006

The European Community wants to reinforce the communication between scientific laboratories of similar nature in the field of high energy high intensity hadron beams. For this reason a so called "networking" program has been defined, which over the next five years will join experts in the field of beam instrumentation and related controls activities. The principle purpose of these meetings is to exchange knowledge on well defined subjects. (CARE-N3 networking for HHH, i.e. for high energy, high intensity hadron beams). These events are not in concurrence with more general instrumentation workshops like DIPAC or BIW.

The fourth event of this nature is proposed by Kay Wittenburg (DESY), Andreas Peters (GSI) and H. Schmickler (CERN) with the following topic:
" Simulation of BPM Front-End Electronics and Special Mechanical Designs"
The purpose of the event will be:
- To discuss in detail technology issues related to the subjects.
- To understand the specifications for upcoming new hadron facilities
- To propose concrete work packages for the coming years in order to meet the specified objectives.

For these objectives we consider important the experience from the major three European laboratories working with hadron beams (DESY; GSI; CERN) and experience from other institutes.

Participants:

CERN	Jose Gonzalez	jose.luis.gonzalez@cern.ch
	Lars Soeby	lars.soby@cern.ch
	Christian Boccard	christian.boccard@cern.ch
	Jocelyn Tan	jocelyn.tan@cern.ch
	Clara Palau	clara.palau.montava@cern.ch
	Hermann Schmickler	hermann.schmickler@cern.ch
DESY	Silke Vilcins	Silke.Vilcins@desy.de
	Nicoleta Baboi	nicoleta.baboi@desy.de
	Kay Wittenburg	Kay.Wittenburg@desy.de
	Dirk Noelle	Dirk.Noelle@desy.de
	Thomas Traber	traber@win.desy.de
	Matthias Werner	Matthias.Werner@desy.de
	Jorgen Lund-Nielsen	jorgen.Lund-Nielsen@desy.de
GSI	Andreas Peters	A.Peters@gsi.de
	Peter Forck	P.Forck@gsi.de
	Wolfgang Kaufmann	w.kaufmann@gsi.de
	Marcus Schwickert	m.schwickert@gsi.de
	Piotr Kowina	p.kowina@gsi.de
CEA	Claire Simon	claire.simon@cea.fr
RAL	P.G.Pine	B.G.Pine@rl.ac.uk

	Alex Pertica	A.Pertica@rl.ac.uk
Globes	Mr. Gothmann	juergen.gothmann@globes.de
electronics	Farzard Kialashaki	fkialashaki@safetysystem.com
Kyocera	Florian Wurster	Florian.Wurster@Kyocera.de
	Michikazu Nagata	Michikazu.Nagata@Kyocera.de
	Koichi Iwamoto	kouichi.iwamoto.xm@kyocera.jp
FNAL	Manfred Wendt	manfred@fnal.gov

Agenda:

1st half day: BPM sensor technology – simulation tools and results

Chair: A.Peters (GSI)

2nd half day: BPM technology – simulation of electronics, measurements

Chair: H.Schmickler (CERN)

3rd half day: Cold BPM technology

Chair: K.Wittenburg (DESY)

BPM simulations for the FAIR SIS100 synchrotron using Microwave Studio

P. Kowina for the GSI Beam Diagnostic Group,
Gesellschaft für Schwerionenforschung GSI, Darmstadt, Germany

Abstract

In the present contribution results of a simulation of linear-cut Beam Position Monitors (BPMs) based on a design using metal coated ceramics are compared for two different geometries. The investigated BPMs will be used in the SIS100 synchrotron at the FAIR facility. The simulations were performed using CST Suite 2006. The main goals of the design optimisation were pick-up sensitivity and linearity of the position determination. The effects often observed in BPMs, like resonances or cross–talks, are discussed together with methods of their reduction. In the last part the questions concerning mechanical challenges in the BPM design are addressed and partially answered.

Contents

1 Introduction to the Fair Facility

The **F**acility for **A**ntiproton and **I**on **R**esearch (**FAIR**), presently under design at GSI, will enable production of intense beams for the full spectrum of ion — starting from antiprotons up to the radioactive beams of uranium ions. The ions will be accelerated up to the maximal energies of 35 GeV or 45 GeV per nucleon depending on the ion type and charge state. The variety of different injectors, synchrotrons and storage rings, see Fig. 1, allows to cover almost all operational modes like slow extraction of the high charge state ions, pulse extraction of the beams with extremely high intensities or storing of the antiprotons (or ions) e.g. for on–beam experiments, see Ref. [1]. The Beam Position Monitors (BPMs) presented in this contribution will be a part of the beam instrumentation of the superconducting heavy ion synchrotron SIS100. The SIS100 has circumference of 1084 m and is one of the two main synchrotrons in the FAIR accelerator complex. It consists superconducting, fast ramped (4 T/s) magnets with a maximal magnetic flux of 2.1 T. The SIS100 parameters are calculated for two design beams: 4×10^{13} protons at energy of 29 GeV and 5×10^{11} U^{+28} ions with an energy of 1.5 GeV/u. The features of SIS100 require a special design of BPMs that considers, for instance, operation of the device at liquid helium temperature.

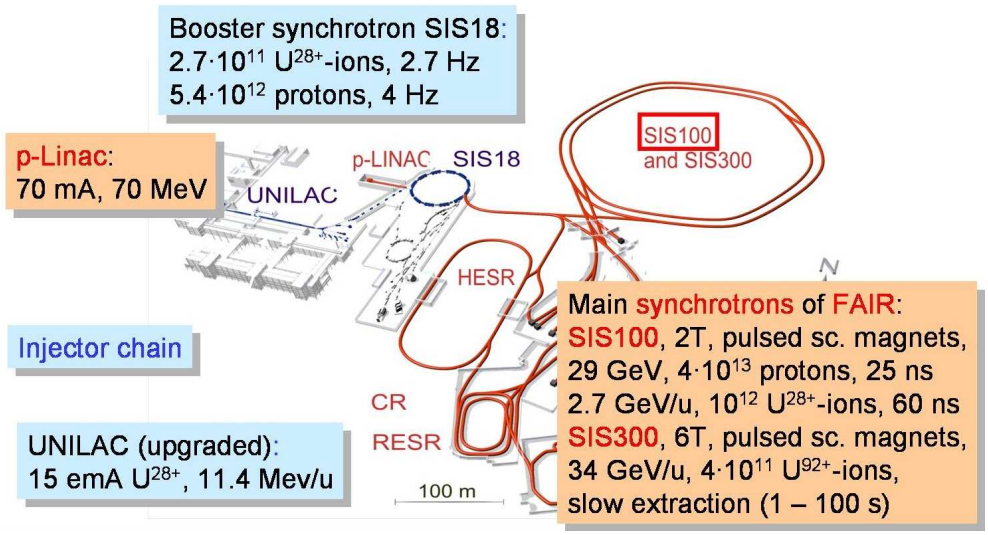

Figure 1: FAIR facility. The present GSI facility, depicted with blue colour, will be used as an injector for the future accelerators and beam lines marked with red colour and being presently under design.

1.1 Positioning of BPMs in the SIS100 lattice

All 84 BPMs will be installed in the cryostats of the quadrupole doublets [1, 2]. In the arcs the BPMs will be located directly behind the horizontally focusing (second in doublet) quadrupole, see Fig. 2 (top). In this position the horizontal β-function reaches its maximum. On the contrary, in the straight sections the

BPMs will be installed in the middle of the quadrupole doublet at the maximum of the vertical β-function, Fig. 2 (bottom). For almost all operation modes the average phase advance of the betatron oscillations between subsequent BPMs will be smaller than 90^{o}. As it is stated in Ref. [3], this is sufficient for the unambiguous closed orbit correction feedback system.

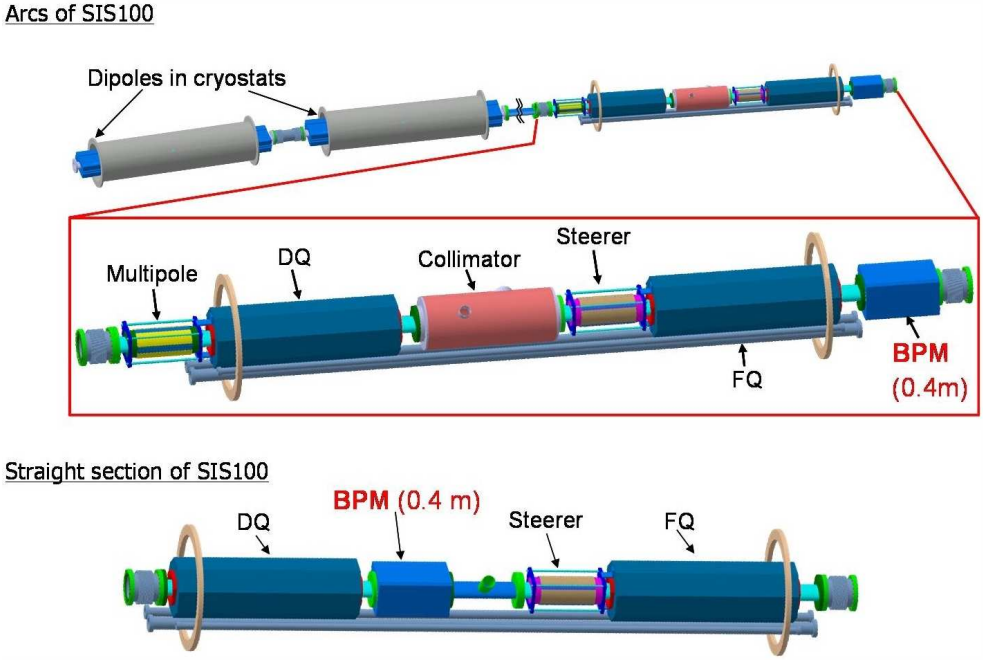

Figure 2: Positioning of the BPMs in the SIS100 lattice.

2 Parameters of SIS100 BPMs

For the foreseen bunch frequencies of 0.5 MHz $< f_b <$ 2.7 MHz and aspired bunch lengths the designed BPM should show a good response in the frequency range from $\sim$ 0.1 MHz to 100 MHz. Due to the relatively large bunch length (in comparison to the length of the BPM) and the bunch frequency in the order of a few MHz, the linear cut type BPMs are preferred. The high linearity of the position determination, typical for this BPM style, is advantageous for beams that are transversally large and have a complex charge distribution.

All BPM components have to be suitable for vacuum pressure better than 10^{-11} mbar. Two design types ware taken into account: i) design based on metal electrodes and ii) design based on metal coated Al_2O_3 ceramics. A construction with metal electrodes benefits from its simplicity. In contrast, the advantage of a ceramic solution is a compact construction allowing easy positioning and good mechanical stability in the cryogenic environment. In order to reach the desired position accuracy of 100 μm [4], the mechanical stability has to be about 50 μm. It seems that this can be achieved only with a BPM design based on a metal coated Al_2O_3 ceramics (type ii)).

A smooth passage of the beam pipe aperture between subsequent elements in the lattice prevents a beam–to–ground impedance jump, which is crucial for beam stability. Therefore, the aperture of the BPM is identical to the aperture of the proceeding quadrupole chamber.

The preliminary design of the SIS100 BPM is shown in Fig. 3. The elliptic ceramic pipe is coated on the inner side with 30 μm of PtAg metal layer. In this

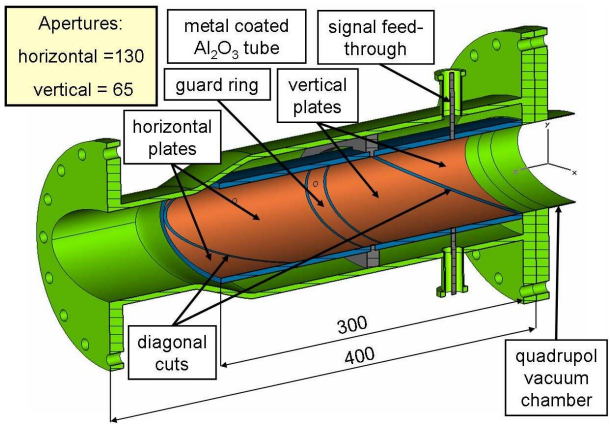

Figure 3: Preliminary design of the SIS100 BPM.

metal coating the electrode shapes are formed by cutting out grooves. Available total detector length of 400 mm (flange–to–flange) allows to equip of all BPMs with electrodes for both, horizontal and vertical beam position measurement.

2.1 Dynamic of the signal amplitude

For the minimal current of the beam that is expected in the SIS100 in low intensity operation mode 10^8 charges per cycle will be spread over 100 ns long bunches. Assuming a beam of bunches with parabolic density distribution circulating in the synchrotron ring with the velocity of light and investigated BPM geometry with 125 mm long signal plates with plate–to–ground capacity of 45 pF, the expected peak voltage will be as low as 1.1 mV [5]. This is barely sufficient to obtain a detectable difference signal, even with high impedance preamplifiers directly mounted on the signal feed-through. At the other extremum (i.e. for the intense proton beam) 4×10^{13} charges will be compressed into a single 25 ns long bunch [1]. For such beams, the maximal expected amplitude reaches 1.8 kV. In this case the preamplifier protection becomes necessery. The huge dynamic range of over 120 dB requires not only a special electronics [6], but also a very careful BPM design. In particular the relative distances between electrodes, guard rings and chamber elements have to be large enough to prevent discharges.

3 FEM simulations

As a tool for simulations CST Suite 2006 was used [7]. This software uses the Finite Element Method (FEM). All BPM components, i.e. caramic tube, chassis, feed–throughs etc. were defined using materials with realistic permitivity and

conductance. All simulation were performed using the Time Domain Solver in the bandwidth of 200 MHz. The usage of the Time Domain Solver was predicted by:

- the simulation duration which — in the contrast to the Frequency Domain Solver — does not depend on number of frequency steps [7].
- the discrete S-parameter port can be defined for the Time Domain Solver only. This is necessery when BPM outputs are defined with an impedance of 1MΩ.

The hexahedral mesh grid was used being the only possibility when using the Time Domain Solver. For the simulated BPM models the number of single mesh cells ranges from 1×10^6 to 3×10^6, depending strongly on the model complexity. The number of mesh cells is blowed up mainly by components that are oriented diagonaly in respect to the main axis, (like e.g. the separating ring in the diagonal cut). A broad band Gauss shaped signal was used as the excitation signal with the rms width of 5 ns, which covers the frequency band from 0–200 MHz. The electrode outputs were defined as diescrete S–parameter ports with characteristic impedance of 50 Ω for the resonance and cross–talk investigation, and 1 MΩ for the senvitity determination, respectively.

3.1 Investigation of "low frequency" resonances and reduction of the plate–to–plate cross talk

Elliptic BPM geometry is already too complicated for the clear three dimentional representation of the electric fiels. Therefore, the next two topics will be discused basing on the investigations of the SIS18 BPMs (see Fig. 4 left) and BPMs build for the HIT facility discussed more precisely in Ref. [8].

In the simulations the electrode outputs were defined as discrete S–parameter ports with the characteristic port impedances of 50 Ω. This is equivalent to measurements using two–port Network Analyser. For the capacitive BPM the S11-parameter (reflection) should be consistent with 0 dB over the whole interesting frequency range. Any sharp minium in S11 spectrum indicates resonant behavior of the BPM for this given frequency. This resonance makes the BPM insensitive for this given frequency. The frequency spectrum of S21–parameter (transmision) is a matter of coupling (plate–to–plate cross–talk) between the electrodes in the tested pair.

3.1.1 "Low frequency" resonances

All structures have characteristic eigen–resonances with the base frequency mainly given by longest geometrical size of the structure. The *low frequency* resonances are those resonances that apear in the interesting bandwidth — in this case — up to 200MHz. In the BPM shown in Fig. 4 (left) the RF signal is connected with the one of the horizontal plates. As it can be seen on the three dimensional plot of the electric fields in Fig. 4 (right), the signal amplitude on this plate, is one order of magnitude smaller than the amplitude of the resonance wich is excited on the opposite BPM side – on the vertical plates. This poor separation between the vertical and horizontal part of BPM is caused by insufficient connection of the middle guard ring with the BPM chassis. It is

made out of 1 mm thick cupper wire. Such type of connection does not provide a good ground definition for the higher frequency components of the signal.

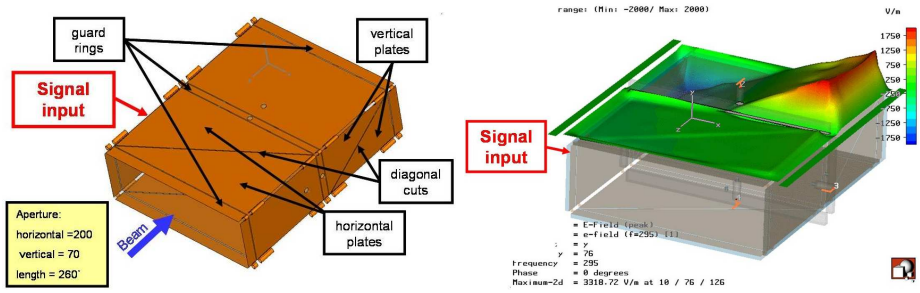

Figure 4: SIS18 BPM (1989) (left) and resonant behaviour observed at 295 MHz (right).

The massive middle guard ring connected directly to the BPM chassis, used in the advanced BPM design for the HIT facility (shown in Fig. 5), allows for separation between orthogonal BPM electrodes better than -40 dB [8]. This divides the BPM into two separate pieces and in consequence shift the first possible resonance far beyond 400 MHz.

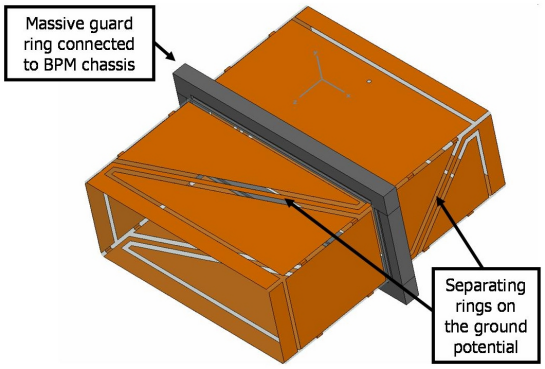

Figure 5: Advanced BPM design for the HIT facility.

3.1.2 Reduction of the plate–to–plate cross–talk

The next problem in the BPMs based on the ceramics is the poor electrical separation between the adjacent signal plates, see Fig.6 (left). This strong plate–to–plate cross–talk is caused by the large ceramic permittivity ϵ_r=9.6 which induces a big coupling capacitance. The larger the coupling the smaller is the difference of the output signals for a given beam displacement. This deteriorates the BPM position sensitivity. In the simulations the cross–talk has been investigated for i) horizontal plates (left-right), ii) vertical plates (top–bottom) and mixed combinations like top–left etc. The separation between the two adjacent horizontal plates for the BPM shown in Fig. 4 (left) is -8 dB at the maximum (i.e. at $\sim$ 20 MHz), and is depicted in Fig. 6 (right) with a dashed line. An insertion of the separating ring in the diagonal cut between the adjacent plates (Fig. 5) increases the plates separation to -21 dB indicated by the solid line in Fig. 6 (right).

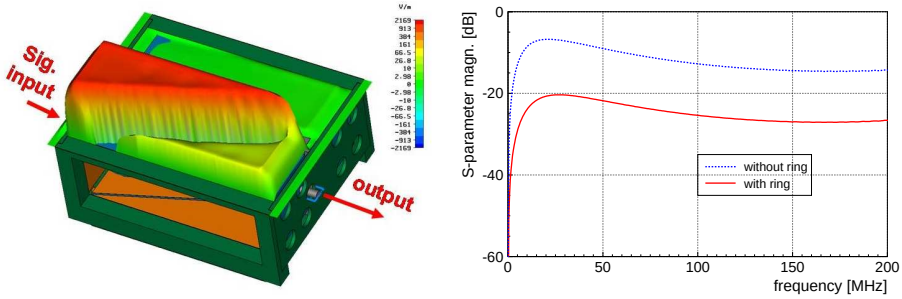

Figure 6: Left: cross–talk between the adjancent horizontal plates for the SIS18 like BPM. Right: corss–talk frequency spectrum of [S21]-parameter (transition) obtained in the simulations for the BPMs with and without separating ring.

The results of the simulations are verified by the measurements of the HIT BPMs that were performed using a network analyser, see Fig. 7.

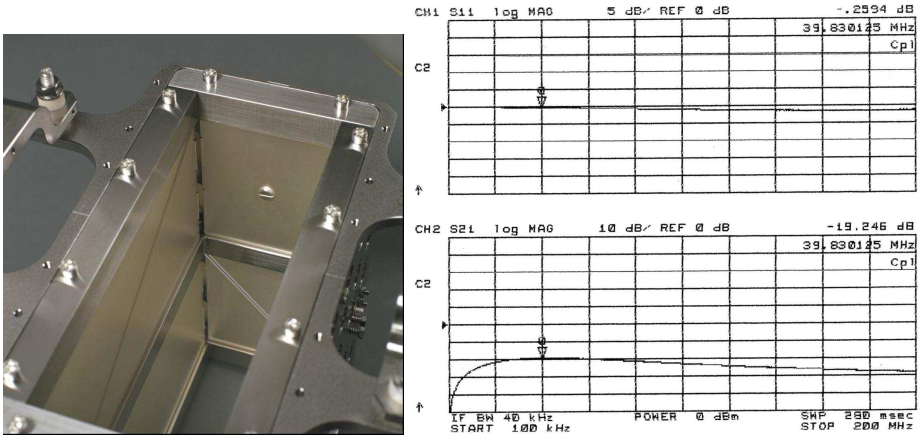

Figure 7: BPM for the HIT facility (left), and measurements performed using a Network Analyser: reflection [S11] (right top) and transition [S21] (right bottom).

3.2 Optimization of the position sensitivity

The *position sensitivity* is the response of the BPM (expressed as the difference of the electrode signals ΔU normalized to their sum ΣU) to changes in the beam position and is given by:

$$\Delta x = K\frac{\Delta U}{\Sigma U} + \delta x \tag{1}$$

The parameter K is usually called *pick-up constant*. The *pick-up offset* δx represents a misalignment of the electrical center with respect to the geometrical center of the BPM.

In the simulations the BPM with beam inside was treated as a semi–coaxial TEM wave guide. The ion beam was approximated by a cylinder of a Perfect Electric Conductor (PEC) with a diameter of 1.5 mm and a length corresponding to the length of the vacuum chamber. The beam was spanned between two wave

guide ports defined on both ends. All four electrode outputs were defined as S-parameter ports with a characteristic impedance of 1 MΩ. All simulations were performed using the time domain solver in the bandwidth of 200 MHz. The simulated beam position was swept in the horizontal plane in the range ±50 mm in 10 mm steps.

The position sensitivity of the BPMs was calculated from the S-parameters expressed in the frequency domain:

$$\frac{S_{right\leftarrow in} - S_{left\leftarrow in}}{S_{right\leftarrow in} + S_{left\leftarrow in}} = \frac{\frac{U_{right}}{U_{in}} - \frac{U_{left}}{U_{in}}}{\frac{U_{right}}{U_{in}} + \frac{U_{left}}{U_{in}}} = \frac{\Delta U_{hor}}{\Sigma U_{hor}}\,, \tag{2}$$

where the S-parameters are given by the output/input voltage ratio [9]. For each beam position the full set of the S-parameters was analyzed for both horizontal and vertical planes.

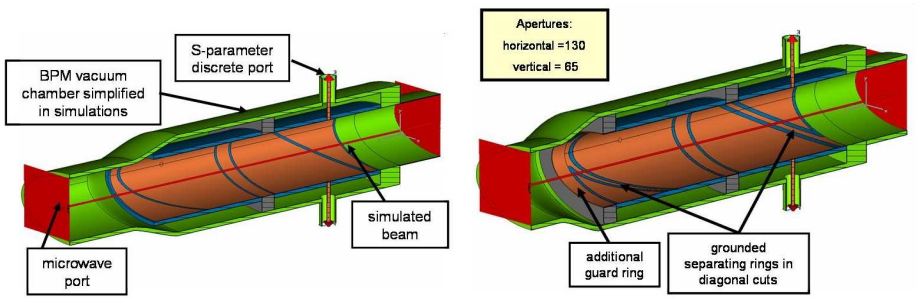

Figure 8: Models of the SIS100 BPMs used in the simulations, see description in text.

In the simulation the two models for SIS100 BPMs shown in Fig. 8 were compared. Both models are based on the ceramic pipe solution but they differ in the separating ground rings positioned in the diagonal cut between the adjacent plates (see Fig. 8 right). Only in the second model an additional massive guard ring is installed at the end of the signal plates. The geometrical design of the investigated BPM was optimizes regarding the following criteria:

- Linearity — high linearity is typical for the diagonal–cut type BPMs, however, it can be strongly spoiled by unhomogenities of the magnetic and/or electric field caused by e.g. too large distance between subsequent electrodes or by structure discountinities. For the BPM under investigation the maximum deviations from the straight line fit shown in Fig. 9 are smaller than ±2% for the BPM without ring, and below ±0.5% for the BPM with ring, over the whole ±50 mm displacement range.

- The position sensitivity, as given by the slope of the curve in Fig. 9 (left), is much higher for the BPM with separating ring as compared to the BPM without ring [1]. This is achieved by insertion of the separating ring that reduces the plate—to—plate cross–talk from -9.5 dB to -21 dB, see Fig. 9 (right).

[1] For the same beam displacement one observe much higher $\frac{\Delta U}{\Sigma U}$

- The offset of the electrical centre of the BPM in respect to its geometrical centre can be reduced from about 13 mm (crossing point with the x-axis of the curve with black circles in Fig. 9 left) to almost zero (curve with the green triangles) by an additional massive guard ring installed at the end of the BPM electrodes (see Fig. 10). It indicates that the geometry of the whole environment (including also the neighbouring guard rings) has to be completely symmetrical for both electrodes belonging of the same electrode pair.

- A very careful treatment of the fringe fields is required in order to achieve a maximum independence of the measurement in vertical and horizontal directions. Particularly, the length of all guard rings has to be large enough to move the fringe fields distortions possibly far away from the electrodes. As it can be seen in Fig. 9 (left, blue squares and red triangles) the horizontal displacement of the beam has no influence on the signal measured in the vertical plates.

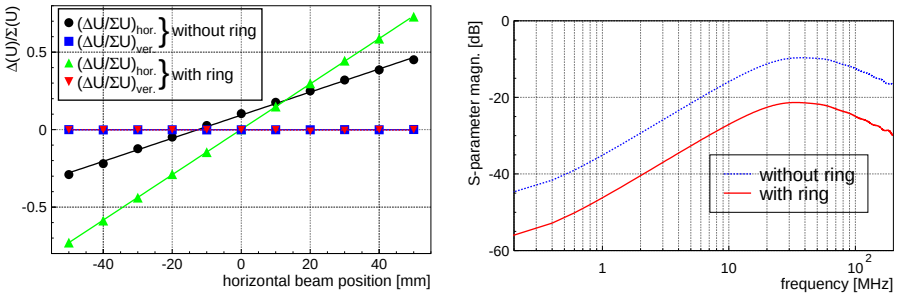

Figure 9: Left: position sensitivity for the BPM without and with separating ring; Right: Separation between two adjacent signal plates (here horizontal) obtained in the simulations of models with (solid line) and without (dashed line) separating ring.

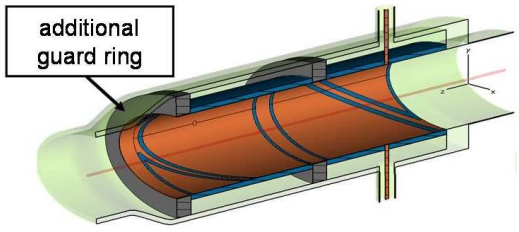

Figure 10: The massive guard ring installed in SIS100 BPM at the end of the ceramic pipe, see description in text.

3.3 Frequency dependence of position sensitivity

The position sensitivity is often frequency dependent, see e.g. Ref. [8]. This is especially important in the case of bunches that are strongly deformed and/or for the bunches that have inconstant longitudinal structure. For those bunches the frequency spectrum varies in time, which effects the beam position estimation. Therefore, the frequency response of the position sensitivity should be

always investigated for the interesting frequency range. The analysis results are presented in Fig. 11 showing only a moderate frequency dependence even at higher frequencies.

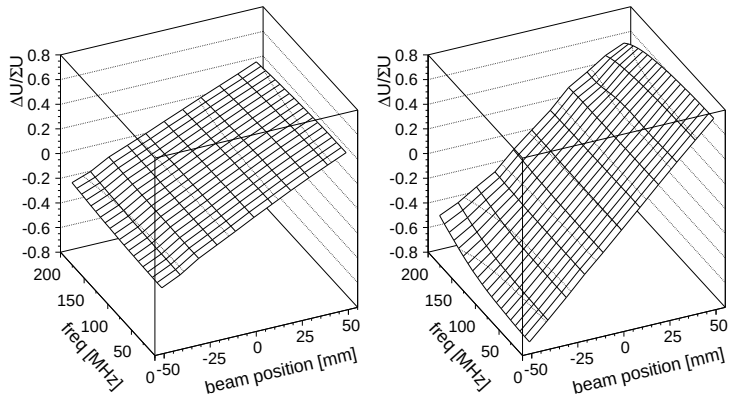

Figure 11: Position sensitivity as a function of frequency for the BPM without (left) and with (right) separating ring.

Least-square fits of a linear function given by Eq. 1 to the data for each frequency value yield the frequency dependencies of both parameters, position sensitivity and offset. These dependencies are shown in Fig.12.

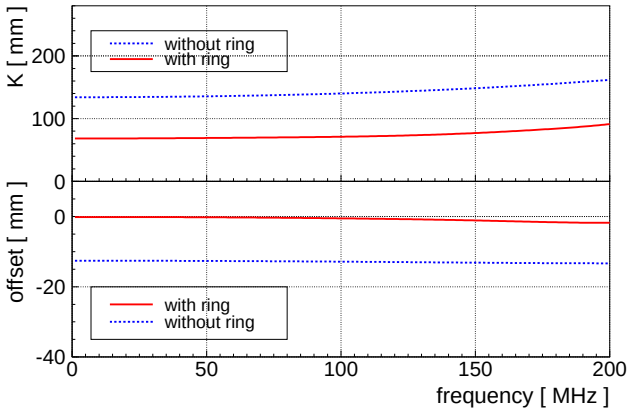

Figure 12: Frequency dependence of *"pickup constant"* K (top) and offset of the BPM electric centre (bottom) for the horizontal beam displacement.

Position sensitivity and offset for both investigated geometries are almost frequency independent in the relevant frequency range. However, the position sensitivity of the BPM with guard ring is a factor of two larger compared to the BPM without ring [2]. The small reduction of the sensitivity at higher frequencies is caused by inductive cross–talk between signal plates and guard rings that is more pronounced at higher frequencies.

[2]The smaller the value of K in the Eq. 1 the larger is the BPM response ($\frac{\Delta U}{\Sigma U}$) for the same beam shift (Δx).

4 Summary and outlook

Simulations performed using CST Suite 2006 are able to reproduce effect observed in the investigated BPMs. It is shown that a BPM design with separating ring provides good linearity and much better position sensitivity than a BPM without ring. Hence, the separating ring should always be considered in the BPM design as long as a ceramic solution is used. In the future signal/field simulations further geometries, like those described in Ref. [10] will be tested and adopted for the elliptic electrode shape.

5 Mechanical problems – open questions

The operation of SIS100 in cryogenic environment and the demands for good mechanical stability require answers on the following questions:

1 Is the metal coated ceramic suitable for low temperatures (see Fig. 13, detail 1)?

2 How should the ceramic pipe be connected with the BPM chassis (see Fig. 13, detail 2)?

3 How to solve the problems concerning connection and positioning of guard rings in the BPM chassis (see Fig. 13, detail 3)? — This connection should guarantee good electrical contact between the guard rings and the BPM body but, on the other hand, should allow contraction compensation of the ceramic pipe.

4 Which solution for the signal feed through could give a stable enough electrical connection with the coating material of the ceramic pipe, that at the same time, is able to compensate relative displacements of the connected elements (see Fig. 13, detail 4)?

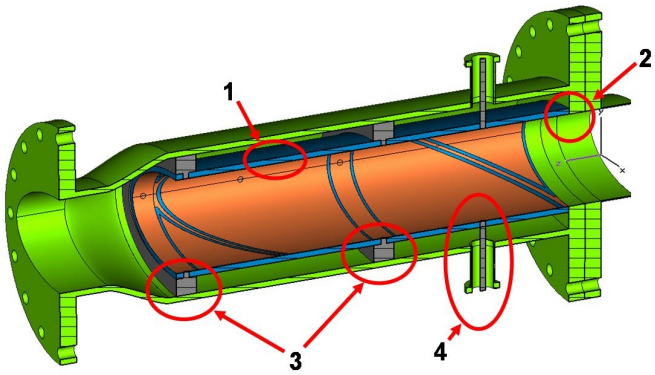

Figure 13: Most challenging detail in the SIS100 design, see description in text.

The first tests of the mechanical features of ceramics at low temperatures and studies based on experiences collected in other institutes allows to prepare preliminary answers on the questions listed above:

ad.1 Two samples of the ceramic–based BPMs shown in Fig. 14 were tested using liquid nitrogen — each sample in 20 thermal cycles. In the last ten cycles the samples were rapidly put into liquid nitrogen to check effects of the thermal shock. The surfaces of the samples were checked for cracks or any other form disintegrations using scanning–electron microscopy. The test samples were:

- CLIC-III BPM: diameter of 50 mm, 2mm wall thickness, coating $5 - -10\mu\mathrm{m}MoMN$, $5\mu\mathrm{m}Ni$ and $\sim 1\mu\mathrm{m}Au$
- GSI-Unilac ring pickup: diameter of 58 mm, 4mm wall thickness, coating metal: $10 - -50\mu\mathrm{m}MoMN$, $1 - -3\mu\mathrm{m}Ni$

  In all tests no changes were found neither in the ceramics nor in the metal coating. That indicates that the ceramics can be used under the cryogenic conditions.

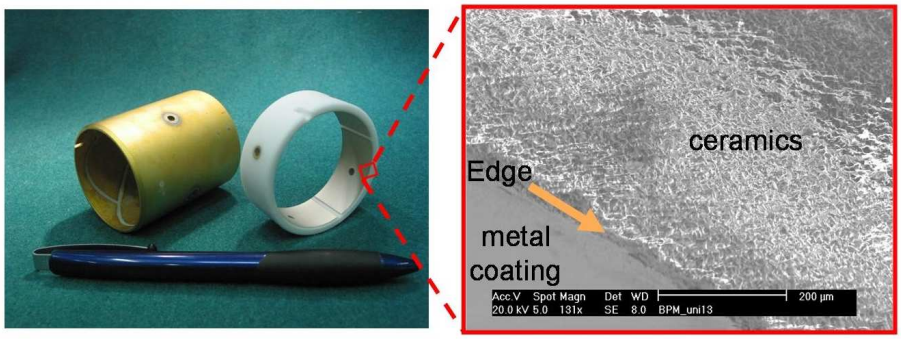

Figure 14: Samples use in the cryogenic tests (left) and an example of the surface picture taken using electron microscope (right).

ad.2 The ceramic–metal interconnection was already tested under cryogenic conditions for many element types in hundreds of locations in superconducting Nuclotron synchrotron in Dubna, see Fig. 15. This interconnections remain tight and not destroyed even after several tens of thermal cycles. To solve particularly the problem marked in Fig. 13 with number (2) one can use analogical solution as for the ceramic beam pipe insertion marked in Fig. 15 with arrow. However, first the mechanical stability of this connection have to be tested.

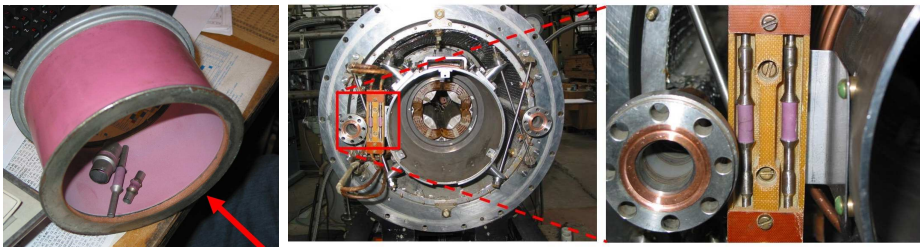

Figure 15: Left: Different examples of the metal–ceramics interconnections used in Nuclotron in Dubna. Middle and right: Ceramic insertion used as an isolator in the superconduction coils in Nuclotron quadrupole.

ad.3 For the good positioning and proper RF connection of the guard rings to the BPM chassis one can use a multi-contact band positioned in the groove formed on the outer side of the guard ring, see Fig. 16. This solution, used already e.g. for CLIC-III BPMs [11], provide good connection for the whole frequency range and leaves enough room for contraction compensation.

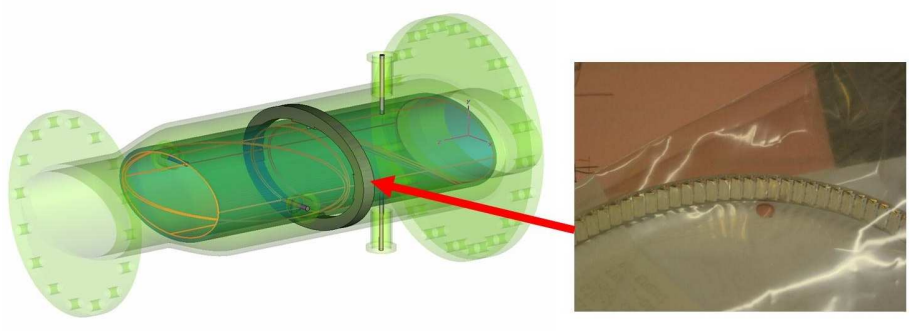

Figure 16: Possible solution for the guard ring positioning in BPM chassis: multi-contact band inserted in the groove formed in the outer part of the guard ring.

ad.4 The question concerning the signal feed–through remains open. There is a number of different possibilities like mini bellows used at DESY [12] or a special membrane connection used at RHIC BPMs, but it is not tested yet if those solutions can be applied in SIS100 BPMs.

5.1 Next steps

Further mechanical tests are foreseen for all crucial BPM components. The samples of feed–through ceramics–metal interconnections etc. will be prepared. All samples will be tested in liquid helium in several tens of thermal cycles. A possible degradation of the sample structure will be investigated in between subsequent thermal cycles. The tests will be performed at GSI in a helium cryostat especially build for this purpose.

References

[1] FAIR Technical Report available on:
http://www.gsi.de/fair/reports/techrep_e.html

[2] J. Stadlmann et al., *Proc. EPAC06*, p.214, Edinburgh (2006).

[3] V. Mikhaylov et al., *Proc. EPAC06*, p.240, Edinburgh (2006).

[4] A. Galatis et al., *Proc. EPAC06*, p.1019, Edinburgh (2006).

[5] see e.g. H. Koziol, Beam Diagnostic for Accelerators, *Proc. Cern Acc. School CAS,* p.565, UNI. Jyväskylä, Finland **CERN 94-01**

[6] J. Schölles and W. Kaufmann, *Proc. DIPAC05*, p.190, Lyon (2005).

[7] http://www.cst.com

[8] P. Kowina et al., *Proc. DIPAC05*, p.114 Lyon (2005).

[9] see e.g. B. C. Wadell, *Transmission Line Design Handbook*, Artech House Boston (1991), ISBN 0-89006-436-9.

[10] E. Schulte, *Beam Instrumentation*, CERN-PE-ED001-92, Rev. Nov 1994, p.129 and references therein.

[11] L. Søby, CERN, Geneve, Private communication.

[12] S. Vilkins–Czvitkovits, DESY, Hamburg, Private communication.

Electromagnetic Simulations for the PETRA III BPMs

N. Baboi, DESY, Hamburg

1. Introduction

1.1. PETRA III:

PETRA III is a new high-brilliance synchrotron radiation source to be built at DESY, Hamburg [1]. Planned to start operation in 2009, the facility will have 14 beam lines spread along one eighth of its circumference. 40 to 960 bunches with a current of 100 mA and an emittance of 1 nm·rad will be circulated at 6 GeV. The topping up operation will ensure a stable beam.

235 beam position monitors (BPM) of button type with several different designs will be built in the various chamber sections of the accelerator. These monitors have been studied through various methods, such as measurements on button models, analytical calculations and simulations of the electromagnetic fields. This report presents simulations made with two electromagnetic field codes, MAFIA [2] and Microwave Studio [3], on the characteristics of these BPMs. The results for a few types of monitors are shown.

1.2. BPM characteristics

Most of the vacuum chamber along the PETRA III circumference has elliptical cross-section of various dimensions. The pickups of the BPMs are placed up-right (UR), up-left (UL), down-right (DR) and down-left (DL) (see Fig. 1).

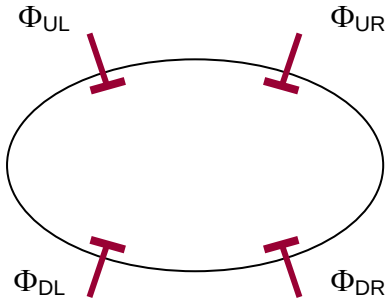

Figure 1: Schematic of a typical BPM for PETRA III

Through combination of the signals Φ at these buttons, excited by the beam, one gets signals, Φ_H and Φ_V, proportional to the horizontal and vertical beam offsets from the chamber center (eqs. (1)):

$$\Phi_H = \frac{\Phi_R - \Phi_L}{\Phi_R + \Phi_L} = \frac{(\Phi_{UR} + \Phi_{DR}) - (\Phi_{UL} + \Phi_{DL})}{\Phi_{UR} + \Phi_{DR} + \Phi_{UL} + \Phi_{DL}}$$
$$\Phi_V = \frac{\Phi_U - \Phi_D}{\Phi_U + \Phi_D} = \frac{(\Phi_{UR} + \Phi_{UL}) - (\Phi_{DR} + \Phi_{DL})}{\Phi_{UR} + \Phi_{UL} + \Phi_{DR} + \Phi_{DL}} \quad (1)$$

The monitor constant is defined as the slope of Φ_H and Φ_V at the chamber center:

$$\frac{1}{\mathbf{K_H}} = \frac{\partial}{\partial \mathbf{x}} \Phi_{\mathbf{H}}(\mathbf{x}=0, \mathbf{y}=0), \qquad \frac{1}{\mathbf{K_V}} = \frac{\partial}{\partial \mathbf{y}} \Phi_{\mathbf{V}}(\mathbf{x}=0, \mathbf{y}=0) \tag{2}$$

From here one can calculate the measured beam offset with a good approximation over a certain range as:

$$\mathbf{x} = \mathbf{K_H}\Phi_{\mathbf{H}}, \qquad \mathbf{y} = \mathbf{K_V}\Phi_{\mathbf{V}} \tag{3}$$

In conjunction with the characteristic of the electronics used with a BPM, K gives the resolution of the monitor.

Another characteristic of a BPM is the coupling of the beam to the pickups, which tells how much signal is delivered by a pickup for a given beam.

2. Electrostatic Simulations

Although they cannot give a full picture of the signals from a BPM, electrostatic simulations can lead to the monitor constant and information on the coupling factor. We use MAFIA for such simulations [2].

2.1. Method

In most cases a 2D model is sufficient to calculate the monitor constant and a relative coupling factor. Fig. 2 shows the model of a BPM for the damping wiggler section of PETRA III. The chamber profile is flat with rounded ends, with dimensions 120mm×30mm. The background is defined as perfect conducting, while the chamber is defined as vacuum. The four pickups are defined as being of different materials, all perfect conductors, but with the possibility to define a different potential applied to each of them.

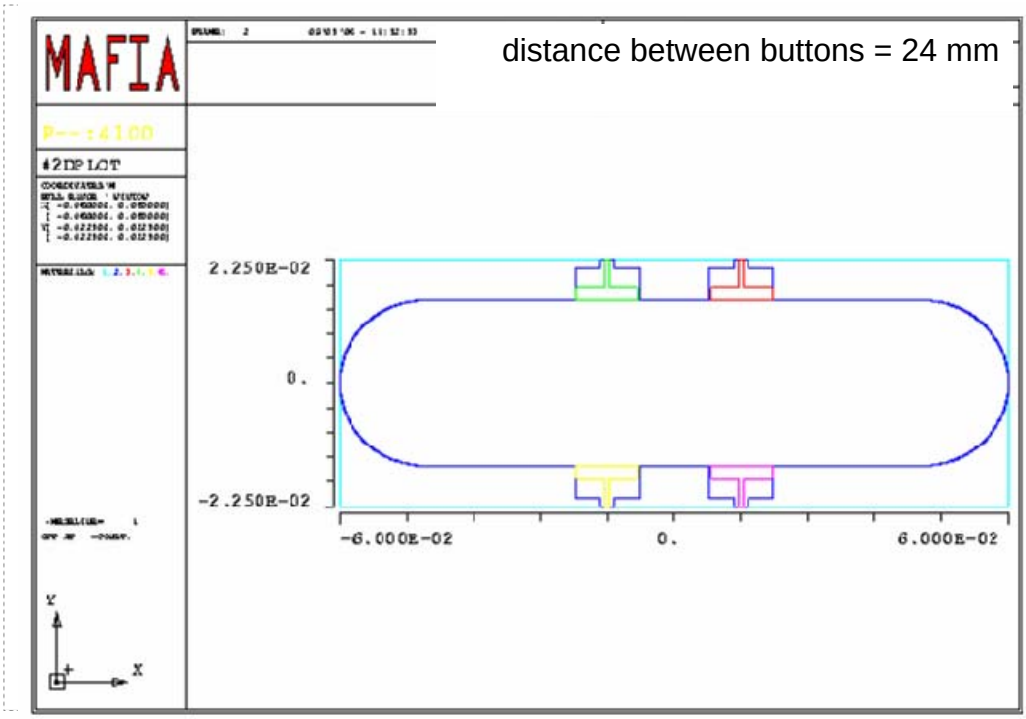

Figure 2: 2D model of a BPM for the damping wiggler section

We apply 1V at one of the buttons, while we keep the others at 0V, and calculate the electric field distribution. By considering the symmetry of the model, one can then calculate the field for the case of applying 1V at each of the pickups individually. By combining the

four results, based on reciprocity, one can then calculate Φ_H and Φ_V, and from here the monitor constants, K_H and K_V.

We define the coupling factor between the beam and the pickups, as the voltage at the middle of the vacuum chamber when applying 1V at one of the pickups. Although this number will not give us the signal amplitude for a real beam, one can compare in this way the signals for various monitors. For example, based on experience, 10 % indicates a strong coupling for the PETRA III monitors [4].

2.2. BPM for the damping wiggler section

Fig. 3 shows results for the BPM for the damping wiggler section. The equipotential electric field lines when applying 1V at the UR-pickup are shown in plot a, as well as the voltage along the vertical and horizontal cross-sections through the chamber center (plots b and c respectively). At the chamber middle one obtains 0.1V, or a coupling of 10 %. The locations where 0.01V is found delimit approximately the range where a signal can still be measured. A more relaxed range for voltage above 0.02V still indicates a rather large position range.

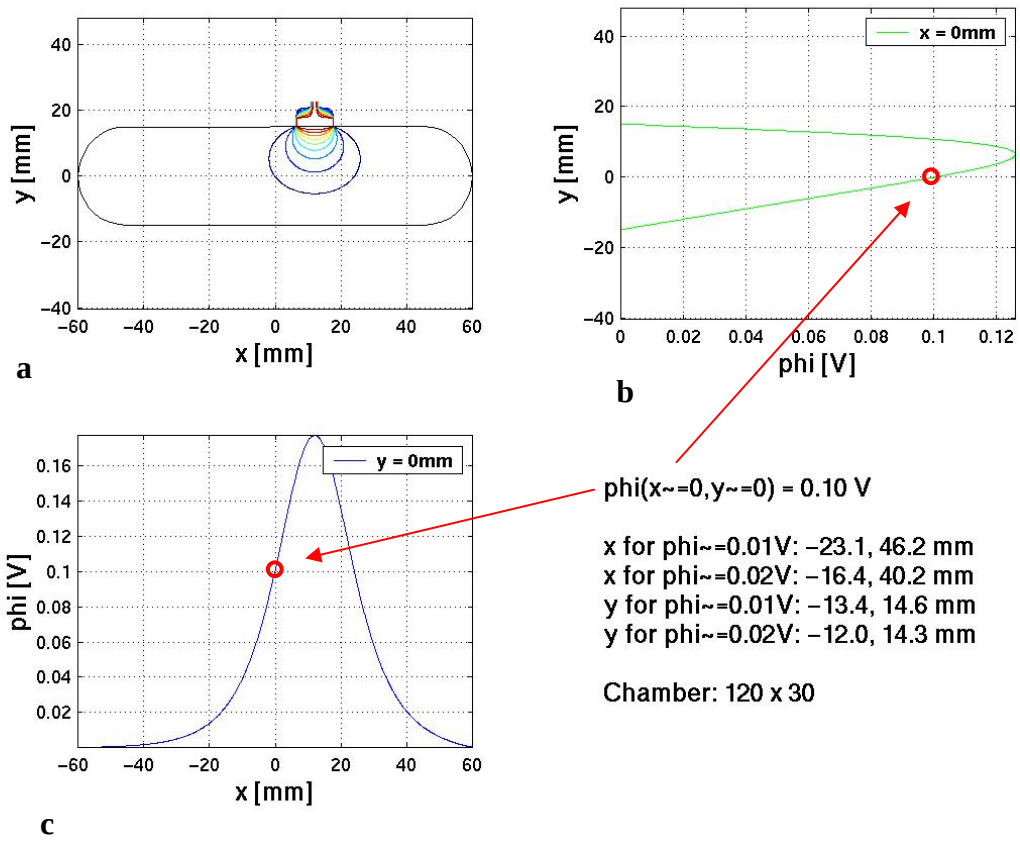

Figure 3: Potential of the electric field when applying 1 V on the UR pickup. a: equipotential field lines; b: potential along vertical cross-section and c: potential along horizontal cross-section of vacuum chamber

Fig. 4 shows Φ_H and Φ_V in the chamber cross-section, while Fig. 5 plots the same quantities along the horizontal and vertical axes. The monitor constants are: $1/K_H = 0.08$ mm^{-1} and $1/K_V = 0.06$ mm^{-1}. For a horizontal beam position resolution of 1 μm one needs $8 \cdot 10^{-5}$ resolution in Φ_V, (given by the electronics).

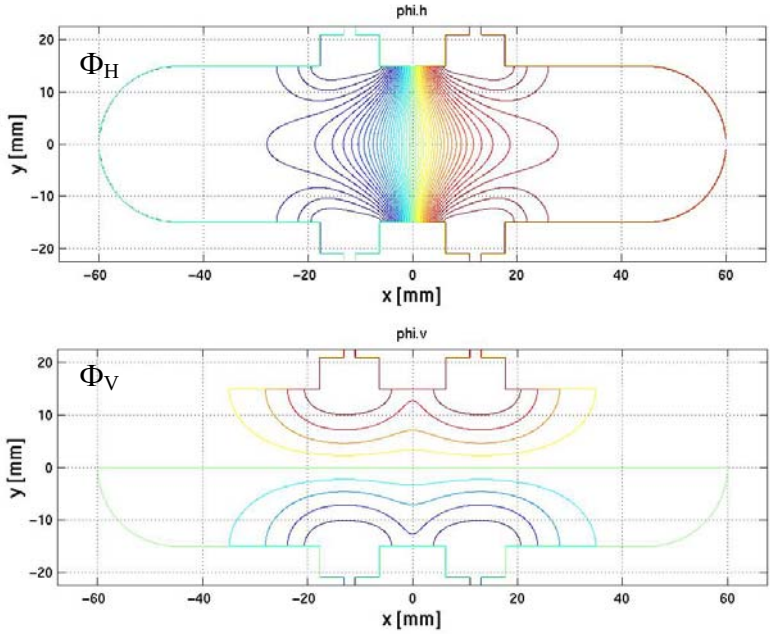

Figure 4: Φ_H and Φ_V in the transverse section of the vacuum chamber.

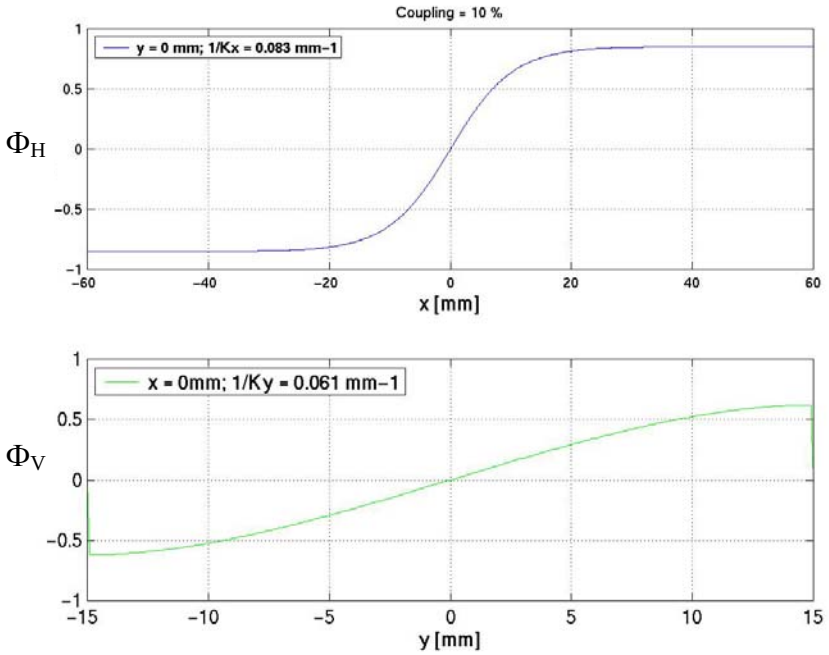

Figure 5: Φ_H and Φ_V along the horizontal and vertical cross-sections through the center of the vacuum chamber.

Various horizontal distances between the two upper and lower pickups have been considered. Table 1 shows the results for several values. A distance of 31 mm gives a somewhat low coupling, with very different monitor constants for the 2 transverse directions. While a distance of 20 mm gives equilibrated monitor constants in both directions, it is harder to realize mechanically. Therefore a distance of 24 mm has been chosen for this monitor.

Table 1: Monitor constants and coupling factors for various distances between the pickups

Pickup distance	1/Kx [mm-1]	1/Ky [mm-1]	Coupling [%]
20	0.074	0.070	12
24	**0.083**	**0.061**	**10**
31	0.093	0.045	7

2.3. Coupling between pickups

Another concern with button type BPMs is the coupling between the pickups. A strong coupling may lead to the mixture of reflections from one pickup into the signal of another pickup. This is particularly critical for the BPM in the narrow undulator chamber with dimensions 66mm×11mm. In this chamber the pickups have to be longitudinally displaced with respect to each other due to mechanical reasons.

We attempt to extract information about the coupling between the button with a MAFIA electrostatic simulation. For this we look at a 2D model of a section through the 4 pickups. Note that the width of the model is therefore larger than the chamber width. We apply 1V at the UR pickup and define the UL pickup as vacuum (Fig. 6-a). Then we look at the field profile along vertical sections through the chamber middle (Fig. 6-b) and through the left pickups (Fig. 6-c). The field through the left buttons suggests a coupling of the UR pickup to the UL one of ca. 0.009 %, which is negligible, as compared to the coupling for this monitor of the pickup to the beam of 23 %.

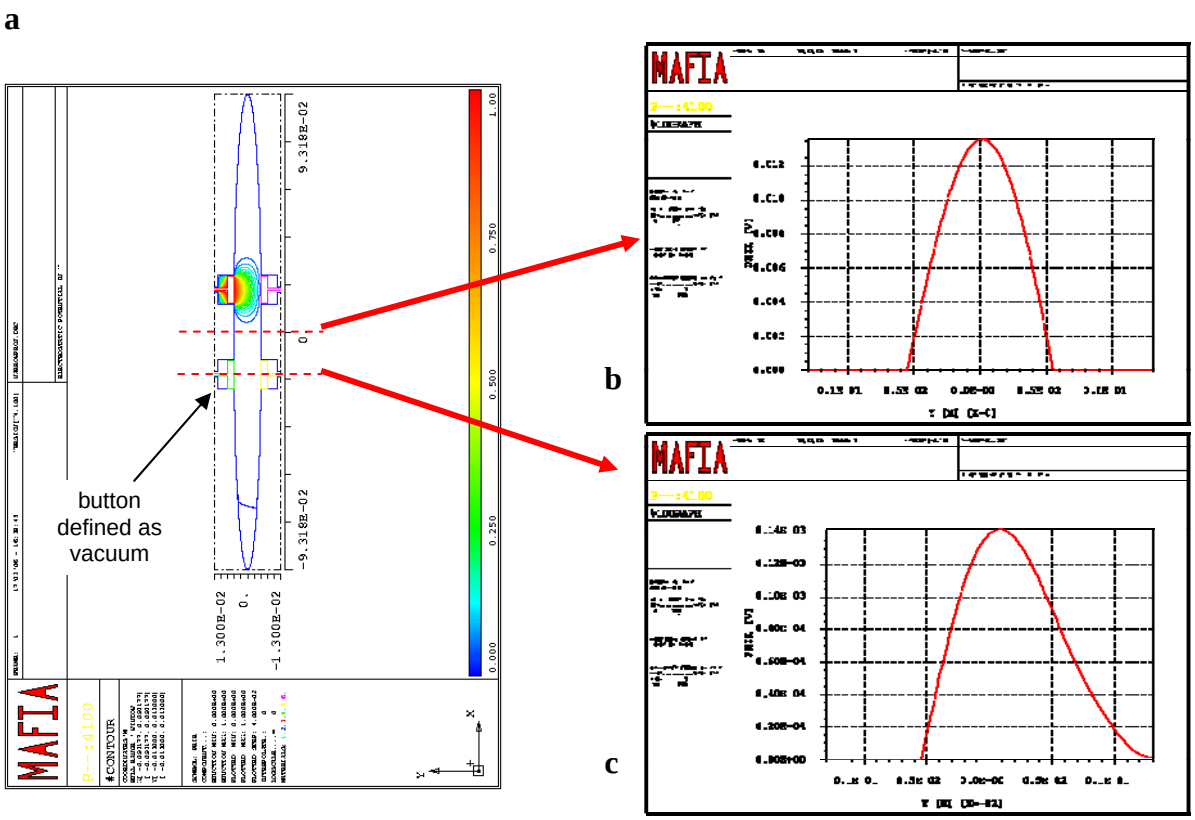

Figure 6: Coupling between UR and UL pickups of a BPM for the undulator chamber. Potential for 1V applied at the UR button: a: in 2D monitor cross- section; b: along vertical cross-section through chamber middle and c: along vertical cross-section through UL pickup.

A similar reasoning leads us to a coupling of the UR to the DR button of 10 %, (Fig. 7) comparable to the coupling to the beam, which seems unreasonable. Moreover, RF measurements on a model with 4 real pickups show a coupling between the UR and DR buttons of -45 dB, or 0.6 % at 500 MHz [5].

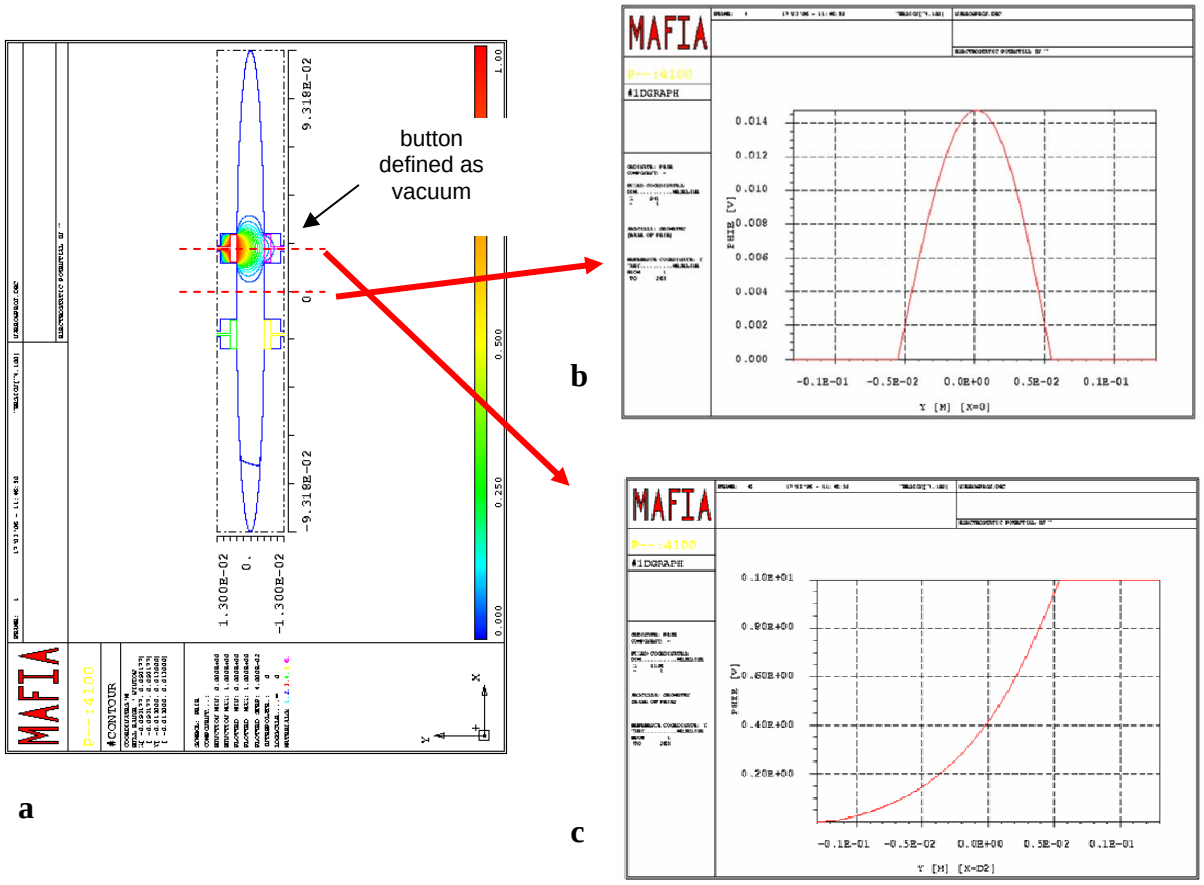

Figure 7: Coupling between UR and DR pickups of a BPM for the undulator chamber. Potential for 1V applied at the UR button: a: in 2D monitor cross- section; b: along vertical cross-section through chamber middle and c: along vertical cross-section through DR pickup.

Therefore another simulation, taking into account the RF character of the system, has been made with Microwave Studio.

3. RF Simulations

3.1. Frequency domain simulation: S-parameters

In order to calculate the coupling between two opposite buttons in the narrow undulator chamber described in section 2.3, we model first in Microwave Studio (MWS) [3] two pickups in a flat vacuum chamber (Fig. 8-a). We define a waveguide port at the end of each antenna.

The S-parameter for these two ports can then be obtained directly from the simulation. The results are shown in Fig. 8-b. S21 at 500 MHz is about -50 dB, in relatively good agreement to the RF measurements.

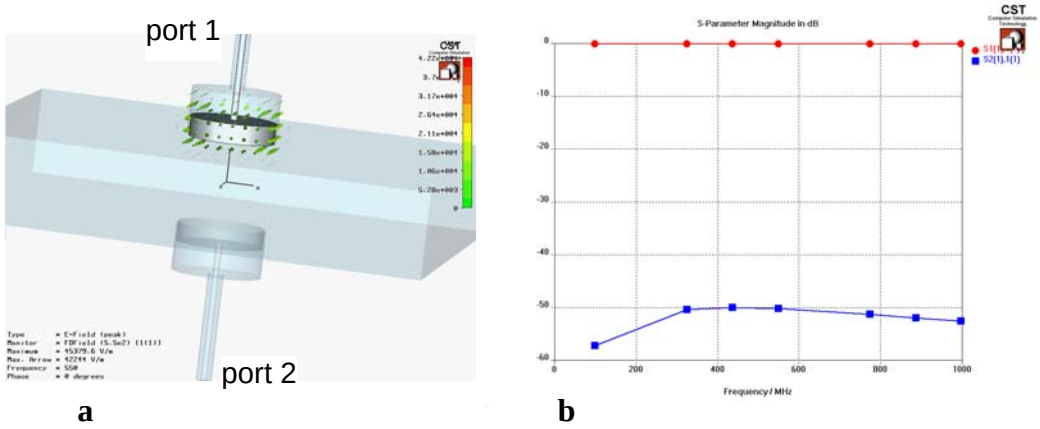

Figure 8: a: MWS model of 2 opposite pickups for the BPM for undulator chamber; b: S-parameters between the two pickups (normalized to 50 Ohm)

A more complex simulation of the BPM for the undulator chamber in time domain is shown in the next section.

3.2. Time domain simulation

3.2.1. Coupling between buttons

Fig. 9 shows a 3D model of the undulator vacuum chamber with the four BPM pickups. The ends of the pickups are defined as ports, while the two ends of the vacuum chamber are assigned either electric or magnetic boundary conditions. A Gaussian source is considered at port 1. The response at the other ports is then calculated.

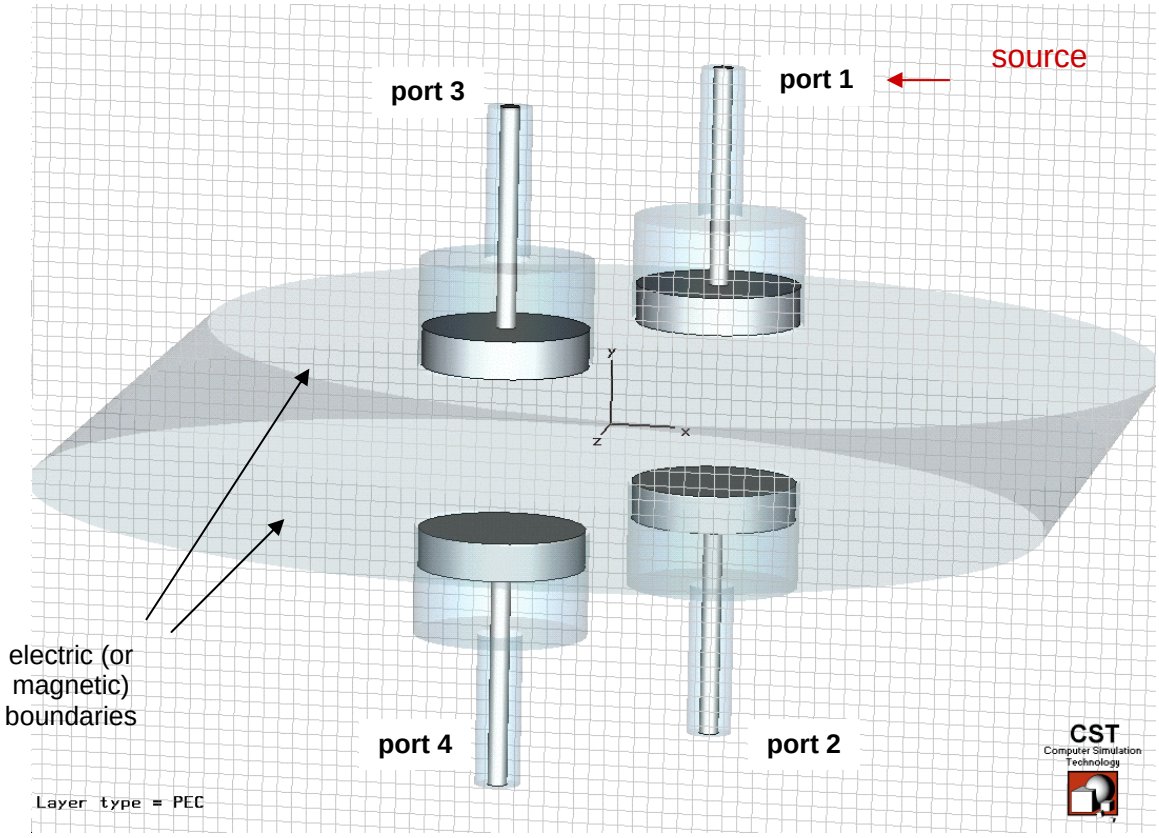

Figure 9: MWS model of the BPM for the undulator chamber for time domain simulations. Each pickup ends with a port. A Gaussian source is applied at port 1 (UR).

The results of the time domain simulation are shown in Fig. 10. The upper plots (a and b) show the transmission parameters to each of the 3 ports, in linear and logarithmic scale. S21, the transmission to the opposite pickup, is -45 dB at 500 MHz, in very good agreement to the RF measurement. Fig. 10-c shows the exciting current (i1, in red) and the reflection at port 1 (green). The response at the other ports is shown in plot d.

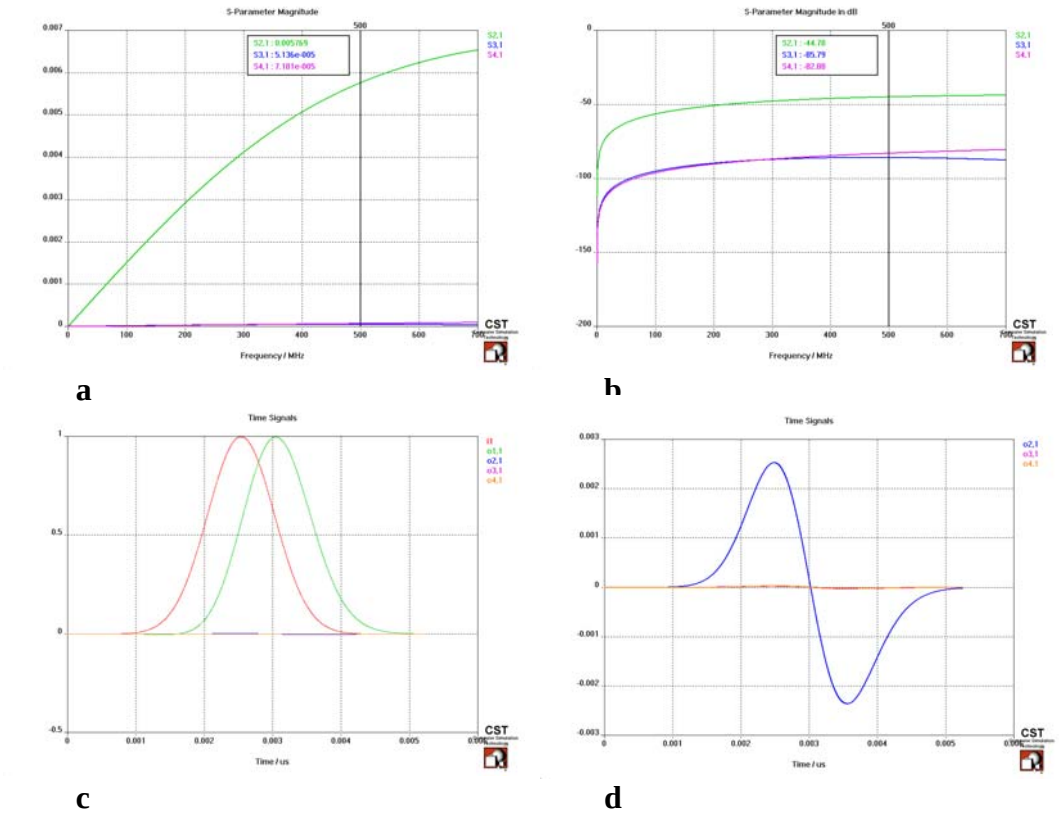

Figure 10: Results of the time domain simulation in Fig. 9. a: S-parameters between each of the ports in linear scale; b: same in dB; c: exciting current and reflection at port 1; d: response at ports 2-4.

3.2.2. "Beam" simulation

A simulation of an electron bunch with Gaussian profile is attempted by using a discrete port along a line on the axis of the vacuum chamber (port 5 in Fig. 11). A current source with a Gaussian time profile (with amplitude equal to 1) is defined on this line. Note that, unlike for a real bunched beam, in the model the current rises and decays at the same time in all points of the line.

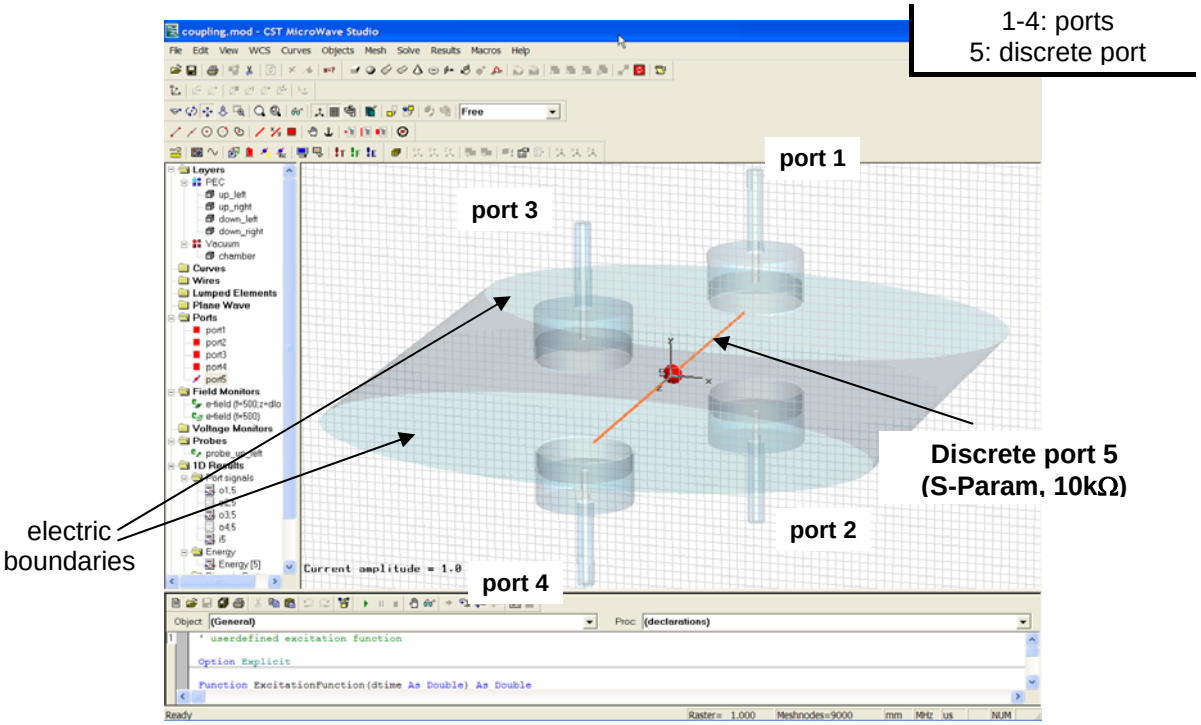

Figure 11: "Beam" simulation with MWS. The "beam" is simulated by a discrete port along the axis of the vacuum chamber.

Fig. 12 shows the results of the simulation. The time response at the 4 pickups is shown in the left graph (a), while the S-parameters are shown in plot b. Note that the time response is not as expected from a real bunch, due to the fact that in our model the current does not propagate along the axis. The meanwhile available Particle Studio [6] simulation code can overcome this difficulty in future simulations.

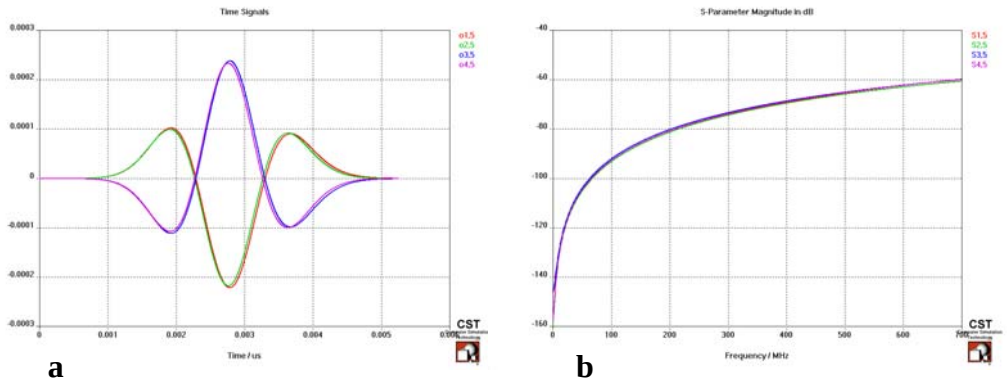

Figure 12: Results of the "beam" simulation. a: time signals at the 4 ports at the pickups; b: S-parameters.

4. Summary

Various BPMs for PETRA3 have been simulated with electromagnetic field codes in order to study their behavior. Relatively simple 2D electrostatic simulations with MAFIA deliver the monitor constants, and can be used to optimize the geometry of the position monitors. The same type of simulations also gives information on the coupling of the button pickups to the beam.

In order to study the coupling between buttons and to simulate the signals generated at the pickups by a particle beam, a simulation of the electromagnetic fields has to be made. A 3D model of a BPM in a narrow vacuum chamber has been built in Microwave Studio for this purpose. The S-parameters between the ports of various pickups have been obtained. A very good agreement with RF measurements has been obtained.

The attempt to simulate a beam by using a current source on a discrete port along the axis of the model gave unrealistic result for a propagating bunch. For a more realistic simulation of the beam, Particle Studio will be used in future simulation.

5. Acknowledgements

I thank my colleagues for the fruitful discussions and ideas: K. Balewski, M. Dohlus, R. Wanzenberg, M. Wendt, K. Wittenburg and many others.

6. References

[1] K. Balewski et al. (eds.), "*PETRA3 – Technical Design Report*", DESY 2004-035 (2004); petra3.desy.de

[2] http://www.cst.com/Content/Products/MAFIA/Overview.aspx

[3] http://www.cst.com/Content/Products/MWS/Overview.aspx

[4] M. Wendt, Private communication

[5] R. Neumann, Private communication

[6] http://www.cst.com/Content/Products/PS/Overview.aspx

POSITION MONITORING ON THE ISIS SYNCHROTRON

B. G. Pine, Rutherford Appleton Laboratory, Oxfordshire, UK

Abstract

The ISIS Facility at the Rutherford Appleton Laboratory in the UK produces intense neutron and muon beams for condensed matter research. It is based on a 50 Hz proton synchrotron which, once the commissioning of a new dual harmonic RF system is complete, will accelerate about 3.5E13 protons per pulse from 70 to 800 MeV, corresponding to mean beam powers of ~ 0.2 MW. Transverse space charge is a key issue for both present and proposed upgrades to the machine, and is the focus of current R&D studies. Experiments on the ISIS ring are central to this work, therefore understanding and quantifying limitations in diagnostics is essential. This paper presents work studying and modelling the ISIS synchrotron beam position monitors.

INTRODUCTION

The ISIS synchrotron has a circumference of 163 m. The vacuum vessels are rectangular and have a varying aperture, averaging half apertures of roughly 80 by 60 mm. Beam is accumulated over 130 turns using charge-exchange injection, and then formed into two bunches during acceleration. Space charge levels are especially high during injection and bunching, though still have a significant effect when the beam is extracted. The ISIS cylindrical split-electrode beam position monitors have operated successfully for many years, but higher intensity operation and related beam studies are motivating a more detailed analysis.

THEORY

Proton bunches in ISIS are relatively long, between 30 and 60 m. With such long bunches, it is assumed that a 2D electrostatic approximation may be used to calculate the position monitor response, as the electromagnetic fields are quasi-steady-state for much of the bunch passage. The purpose of this work was to test whether a 2D approximation was valid, using a simulated 3D monitor. The effects of high frequency bunch passage, and bunch edge effects are likely to also have an effect, but are not considered in this paper.

Laplace's Equation can be solved in 2 dimensions for an off-centre beam in a grounded vacuum vessel [1]. The field can also be calculated using images (*Appendix A*). The surface charge distribution on the inner surface of the grounded vacuum vessel must produce an electric field that cancels this – i.e. is equal to and opposite the beam field at the surface. Therefore the surface charge density can be calculated if the beam field is known. Making the approximation that the electrodes can be treated the same way gives this expression for the total surface charge on one of the electrodes, including the variation of electrode width [2, 3]:

$$Q_1 = -q_b L \int_0^{2\pi} \frac{\left(1+Cos\phi\right)\left(R^2-b^2\right)}{R^2+b^2-2RbCos(\phi-\theta)} d\phi \quad (1)$$

where φ is the polar angle, R is the electrode radius, b is the radial displacement of the beam and θ is the angular displacement of the beam, q_b is the beam charge density and L is the electrode half length, as in Figure 1.

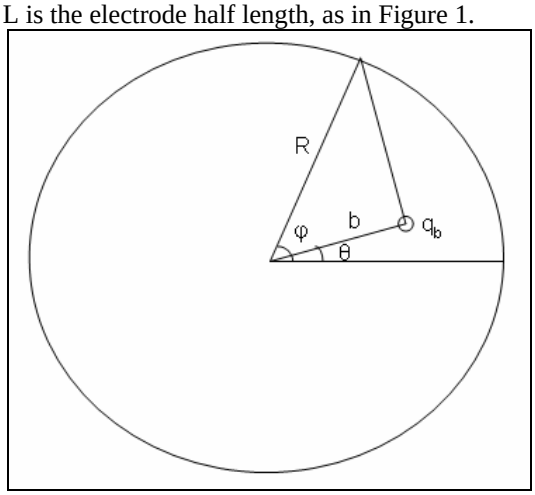

Figure 1: Beampipe geometry.

The solution to this integral is (not obvious, see *Appendix B*):

$$Q_1 = -2\pi q_B L\left(1+\frac{b}{R}Cos[\theta]\right)$$

And as $x = bCos[\theta]$,

$$Q_1 = -2\pi q_B L\left(1+\frac{x}{R}\right)$$

The opposing electrode will have

$$Q_2 = -2\pi q_B L\left(1-\frac{x}{R}\right)$$

This 2D electrostatic theory predicts that the individual electrode signals will be proportional to the position.
The normalised difference:

$$\frac{Q_1-Q_2}{Q_1+Q_2} = \frac{\Delta Q}{\Sigma Q} = \frac{x}{R}. \quad (2)$$

$\frac{\Delta Q}{\Sigma Q}$ is also linear in the displacement, and the gradient of the difference-over-sum (DoS) curve is equal to *1/R*.

SIMULATIONS

ISIS split-cylinder capacitative position monitors have been modelled with CST Studio Suite [4], and the results compared with the theory discussed above.

Most of the ISIS monitors are centred around the beampipe, and have a rectangular vacuum vessel which cuts into their housing, as can be seen in Figure 2.

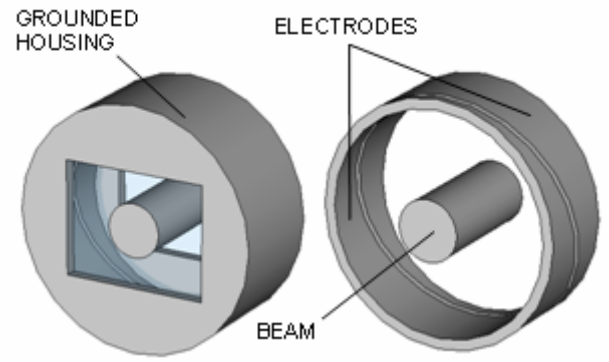

Figure 2: ISIS position monitor.

There are other designs, for instance in the extraction straight there are larger monitors, which allow for the vertical displacement of the beam during extraction, and measure in both planes; one of these designs is shown in Figure 3.

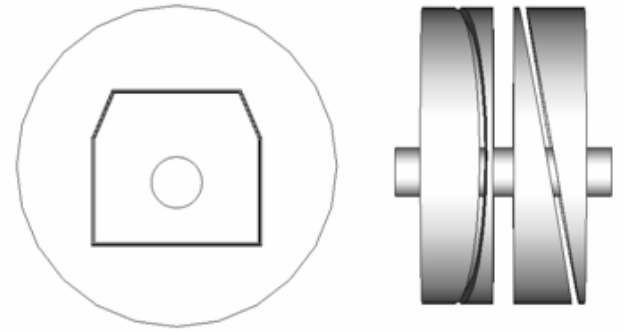

Figure 3: ISIS synchrotron Straight 1 position monitor.

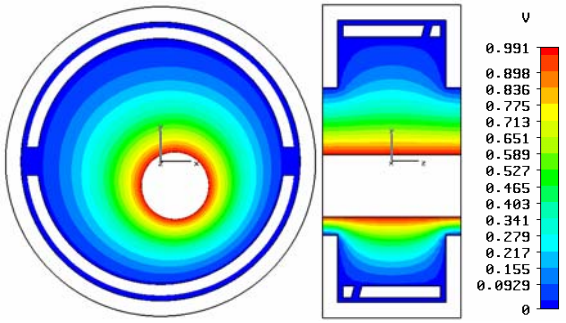

Figure 4: ISIS position monitor potentials with offset beam: surface beam potential normalised to 1V in this case.

These models were created using perfect conductors to form the vacuum vessel and electrodes. The beam was made from perfect conductor with a constant potential on the surface in early models, and later a volume of constant charge density replaced this. The vacuum vessels were fixed at 0 V, and the electrodes given a "floating" potential which allowed them to vary to fit the environment. Electrode potentials calculated by the CST Electrostatic Solver were recorded as the beam was moved around the transverse plane. Electric boundary conditions were used around the vacuum vessel, and magnetic at the open end ends of the beampipe. The potential distribution for an offset beam with one of the standard monitors is shown in Figure 4.

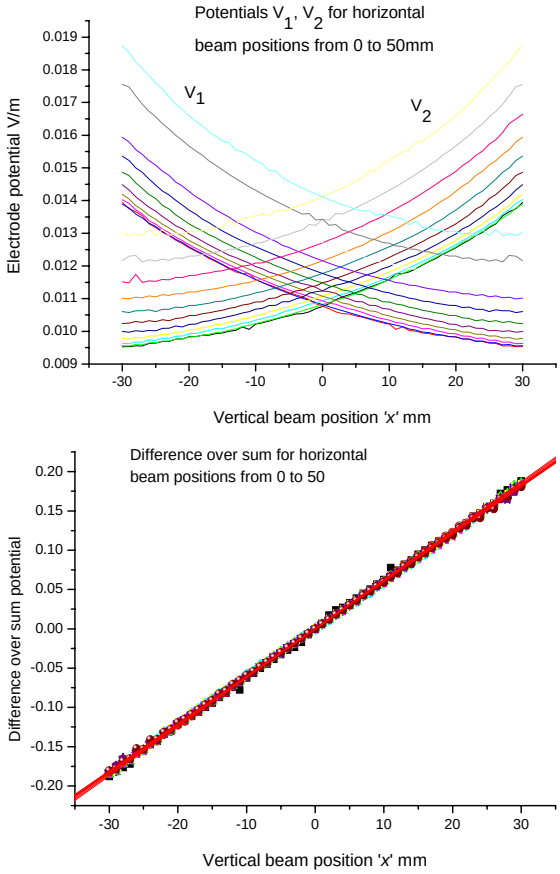

Figure 5: (a) Electrode potentials and (b) Difference over sum for a vertical monitor.

A set of results obtained from the CST model determined the electrode potential as the beam was scanned over both transverse dimensions. Figure 5(a) shows the electrode potentials V_1 and V_2, and Figure 5(b) shows the DoS for those potentials.

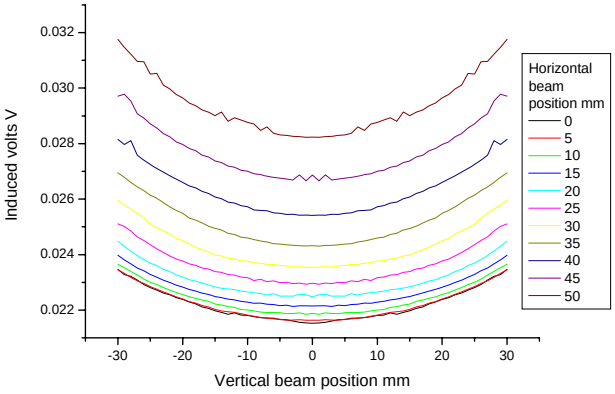

Figure 6: Electrode sum signal for beam position varying in both horizontal and vertical planes.

As can be seen, the DoS is linear across the whole aperture of the monitor, though the individual electrode signals are not linear. It was found that the value of the

DoS gradient deviated significantly from *1/R*. The 2D theory assumes that the total charge induced on the electrodes (the sum signal) is constant, whereas the simulations show that the sum potential of the two electrodes also varies with beam position, Figure 6.

Another feature was explored by taking one of the standard synchrotron monitor models, and stretching the longitudinal dimension of the monitor. As the monitor was stretched, it's behaviour grew asymptotically closer to the simple theory – the inverse constant of proportionality tended to the electrode radius. If a position monitor were created infinitely long it would act the same way as the 2D theory predicts, see Figure 7.

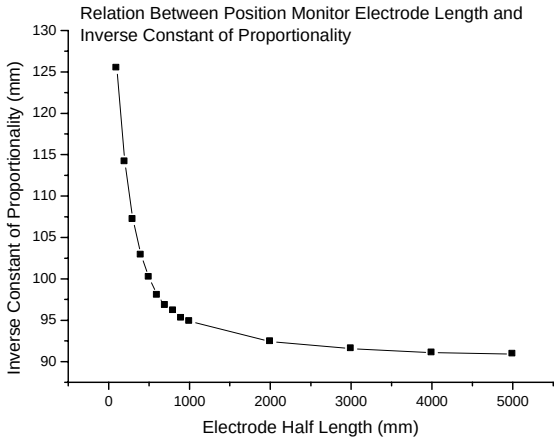

Figure 7: Inverse DoS gradient (R) versus electrode half-length for a model with electrode radius = 90 mm.

BEYOND 2D

Simple 2D theory describes some of the features that the simulations display, such as DoS linearity, but not others. Is there some way of extending the simple theory so that it is sufficient to describe the monitor fully without resorting to simulation? In 1977, J. H. Cuperus wrote a paper 'Edge Effect in Beam Monitors' [5], in which the non-linearities contributed by transitions in the beampipe are studied. He concluded that additional grounded electrodes should be added at the front and back of the monitor. If these guard electrodes are sufficiently long then they counter the effect of a transition near the monitor, and 2D theory is sufficient to describe the beam behaviour, examples can be seen in Figure 8.

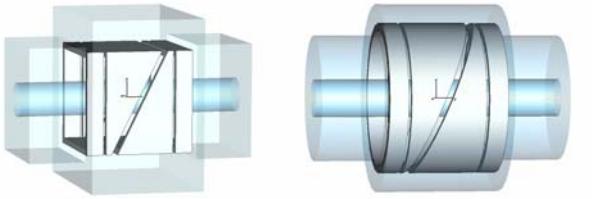

Figure 8: Monitors with guard electrodes.

His paper uses a form of perturbation theory, to iterate through improvements for a guessed shape of perturbed potential at the beampipe transition. He discovered that the answers came in an infinite series, but that most elements in the series could be discarded if the guard electrodes were sufficiently long.

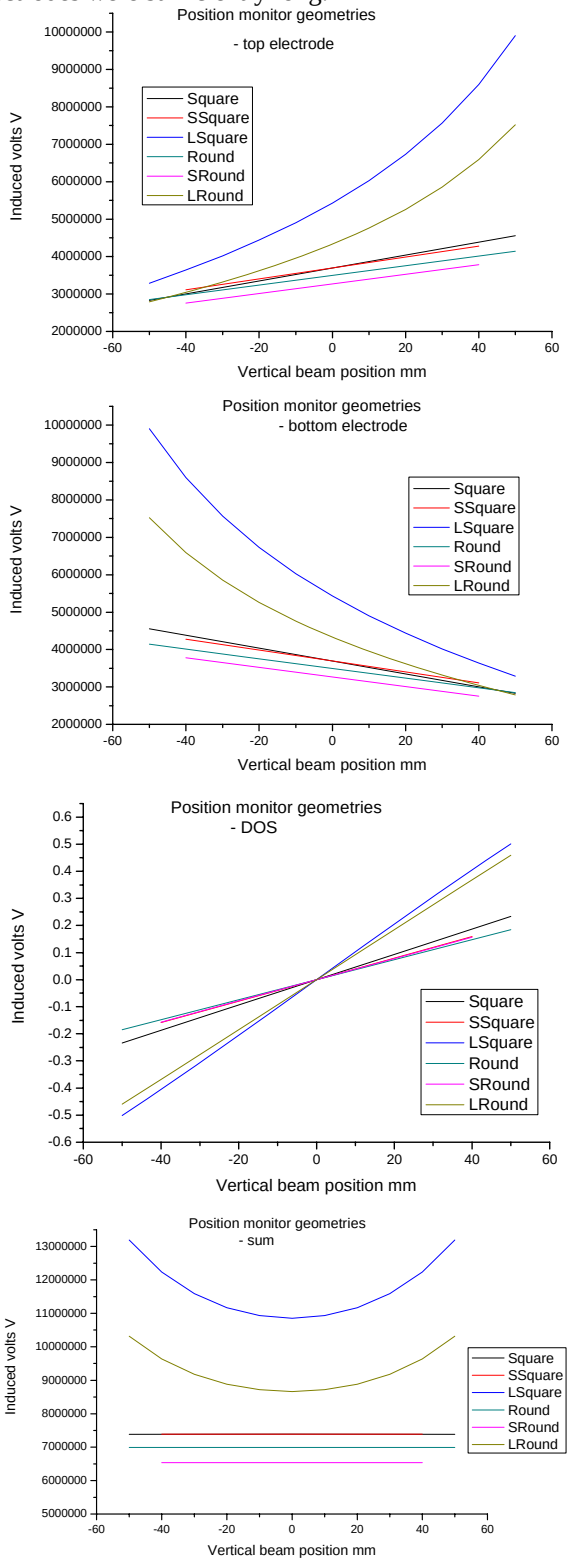

Figure 9: Effect of guard electrodes: Square and Round have electrodes the same size as the beampipe, which are square and round in shape respectively; SSquare and SRound have electrodes smaller than the beampipe; LSquare and LRound have electrodes larger than the beampipe.

Figure 9 shows the simulated response of a set of monitors with guard electrodes. There are 6 variations: square monitor in square beampipe with electrodes bigger, equal and smaller than the beampipe; and the same for a round monitor in a round beampipe. As can be seen, the electrode responses are linear for both shapes if the electrodes are smaller than or equal to the size of the beampipe. Further work could be done here, as it is seems possible that longer guard electrodes would make even the larger monitors linear.

ISIS monitors do not have guard electrodes, and it would be troublesome to install them now. There are also difficulties repeating Cuperus's calculation: ISIS monitors have a rectangular beampipe going into a larger cylinder housing the cylindrical electrodes, which makes the geometry more complex. As there is no guard, higher order elements in the infinite series solution must be considered, and this makes the perturbations very difficult to calculate. Still this is an interesting area for further study.

CONCLUSION

It has become clear that 2D theory is not sufficient to account for the behaviour of the ISIS synchrotron position monitors. While the behaviour of the difference over sum output may well still be linear, the gradient of this line is different from that predicted by theory.

It is apparent that this difference is primarily due to transitions in the beampipe shape and size near to the electrodes, and could be factored out by including sufficiently long guard electrodes in the monitor design. As this would be difficult to achieve for the current monitors, a possible correction is being considered using theory, simulations and experimental verification.

However, monitors built in the future for ISIS or ISIS upgrades would certainly be planned with guard electrodes from the beginning.

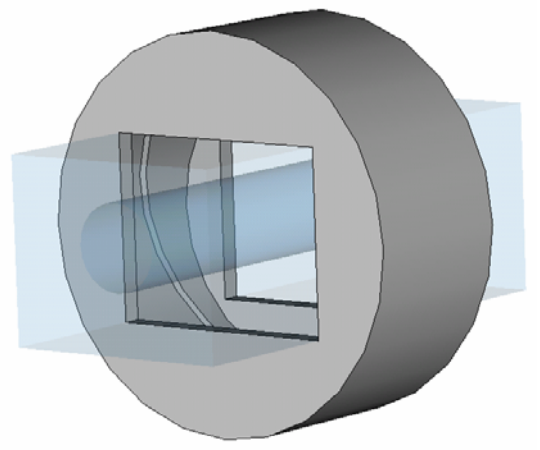

Figure 10: Monitor simulated with beampipe.

FUTURE WORK

At time of writing the iteration cycle that Cuperus used has been recreated, but there is still a great deal of uncertainty about applying the method to the ISIS monitors. Simultaneously then, another set of simulations are running in CST, to take more account of the beampipe environment near the monitors, see Figure 10.

Work studying the effects of high frequency bunch passage through the monitors is also anticipated, both using CST Microwave Studio, and with further analysis.

REFERENCES

[1] E. Regenstreif, "Electrostatic beam potential created by a uniform round beam coasting off centre in a circular vacuum chamber", CERN Report, 1976.

[2] R. E. Shafer, "Beam Position Monitoring", AIP Conference Proceedings Vol 212, (1989).

[3] A. Hofmann, CAS 1992 Proceedings, CERN 94-01, p342 (1994).

[4] www.cst.com.

[5] J. H. Cuperus, "Edge Effect in Beam Monitors", Nuclear Instruments and Methods 145 (1977) 233-243.

[6] C. R. Prior, private correspondence.

APPENDIX A: IMAGE METHOD

The electric field parallel to the beam pipe boundary must be zero, and the electric field perpendicular to it must be proportional to the surface charge. Assume there is another line charge with the opposite charge to the beam, situated outside the cylinder, a distance *l* from the axis, see Figure 11.

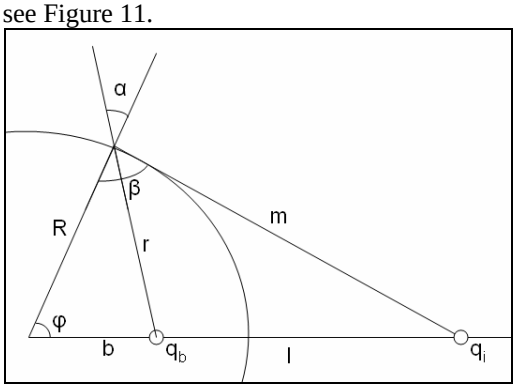

Figure 11: Beampipe geometry with images.

We try to satisfy the boundary condition on the surface such that $E_{//} = E_\phi = 0$.

The beam field:

$$E_{\phi b} = \frac{\lambda}{2\pi\varepsilon_0}\frac{1}{r}Sin\alpha$$

And the image field:

$$E_{\phi i} = -\frac{\lambda}{2\pi\varepsilon_0}\frac{1}{m}Cos(\beta - 90)$$

$$= -\frac{\lambda}{2\pi\varepsilon_0}\frac{1}{m}Sin\beta$$

Beam and image fields parallel to boundary cancel:

$$E_{\phi b} + E_{\phi i} = 0 = \frac{\lambda}{2\pi\varepsilon_0}\frac{1}{r}Sin\alpha - \frac{\lambda}{2\pi\varepsilon_0}\frac{1}{m}Sin\beta$$

$$= \frac{\lambda}{2\pi\varepsilon_0}\left(\frac{1}{r}\frac{bSin\phi}{r} - \frac{1}{m}\frac{lSin\phi}{m}\right)$$

$$b(R^2 + l^2 - 2RlCos\phi) = l(R^2 + b^2 - 2RbCos\phi)$$

$$= bl^2 - (R^2 + b^2)l + bR^2$$

Solving this last equation leads to either $l = b$ or $l = \frac{R^2}{b}$.

Then using this result, we find the field perpendicular to the vacuum vessel:

$$E_{\rho b} + E_{\rho i} = \frac{\lambda}{2\pi\varepsilon_0}\frac{1}{r}Cos\alpha - \frac{\lambda}{2\pi\varepsilon_0}\frac{1}{m}Cos\beta$$

$$= \frac{\lambda}{2\pi\varepsilon_0}\left(\frac{1}{r}\frac{R^2 + r^2 - b^2}{2Rr} - \frac{1}{m}\frac{R^2 + r^2 - l^2}{2Rm}\right)$$

$$= \frac{\lambda}{4\pi\varepsilon_0 R}\left(\frac{R^2 - b^2}{r^2} - \frac{R^2 - l^2}{m^2}\right)$$

$$= \frac{\lambda}{4\pi\varepsilon_0 R}\left(\frac{2R^2 - 2b^2}{R^2 + b^2 - 2RbCos\phi}\right)$$

Which is equal to the surface charge distribution on the inside of the cylinder. This equation for the total surface charge is called the Poisson Integral:

$$Q = \frac{\lambda}{2\pi\varepsilon_0 R}\int_0^{2\pi}\frac{R^2 - b^2}{R^2 + b^2 - 2RbCos\phi}d\phi$$

APPENDIX B: SOLUTION TO EQUATION [1]

Equation (1) combines the Poisson equation with the electrode width and can be solved using complex analysis. Many thanks to C. R. Prior for the solution [6].

$$Q = -q_b L\int_0^{2\pi}\frac{(1+Cos\phi)\left(R^2 - b^2\right)}{R^2 + b^2 - 2RbCos(\phi - \theta)}d\phi$$

Let $\overline{R} = \mathrm{R}e^{i\phi}$ and $\overline{b} = b\,\mathrm{e}^{i\theta}$,

then $\overline{R}\overline{R}^* = \mathrm{R}^2$, $Cos\phi = \frac{\overline{R} + \overline{R}^*}{2R}$,

$R^2 + b^2 - 2RbCos(\phi - \theta) = \left|\overline{R} - \overline{b}\right|\left|\overline{R}^* - \overline{b}^*\right|$,

and $d\overline{R} = i\,\mathrm{R}e^{i\phi}\,d\phi = i\overline{R}d\phi$

$$Q = -q_b L\left(R^2 - b^2\right)\oint\frac{\left(1 + \frac{\overline{R} + \overline{R}^*}{2R}\right)}{\left|\overline{R} - \overline{b}\right|\left|\overline{R}^* - \overline{b}^*\right|}\frac{d\overline{R}}{i\overline{R}}$$

$$= -\frac{q_b L\left(R^2 - b^2\right)}{2R}\oint\frac{\left(2R + \overline{R} + \frac{R^2}{\overline{R}}\right)}{\left|\overline{R} - \overline{b}\right|\left|\frac{R^2}{\overline{R}} - \overline{b}^*\right|}\frac{d\overline{R}}{i\overline{R}}$$

$$= -\frac{q_b L\left(R^2 - b^2\right)}{i2R}\oint\frac{\left(2R\overline{R} + \overline{R}^2 + R^2\right)}{\overline{R}\left|\overline{R} - \overline{b}\right|\left|R^2 - \overline{b}^*\overline{R}\right|}d\overline{R}$$

This equation has poles at $\overline{R} = 0$, $\overline{R} = \overline{b}$ and $\overline{R} = \frac{\mathrm{R}^2}{b}$, but only the first two are correct as $\frac{\mathrm{R}^2}{b}$ is always greater than *R*, for *b* < *R*.

Residue for $\overline{R} = 0$,

$$R[0] = \frac{q_b L\left(R^2 - b^2\right)}{i2R}\frac{R^2}{\overline{b}R^2} = \frac{q_b L\left(R^2 - b^2\right)}{i2R\overline{b}}$$

Residue for $\overline{R} = \overline{b}$,

$$R[\overline{b}] = -\frac{q_b L\left(R^2 - b^2\right)}{i2R}\frac{\left(2R\overline{b} + \overline{b}^2 + R^2\right)}{\overline{b}\left|R^2 - \overline{b}^*\overline{b}\right|}$$

$$= -\frac{q_b L\left(R^2 - b^2\right)}{i2R}\frac{\left(2R\overline{b} + \overline{b}^2 + R^2\right)}{\overline{b}(R^2 - b^2)}$$

$Q = 2\pi i \times$ Sum of residues

$$= 2\pi i \times \frac{q_b L\left(R^2 - b^2\right)}{i2R}\left[\frac{1}{\overline{b}} - \frac{\left(2R\overline{b} + \overline{b}^2 + R^2\right)}{\overline{b}(R^2 - b^2)}\right]$$

$$= -\frac{\pi q_b L}{R}\left[\frac{b^2}{\overline{b}} + \overline{b} + 2R\right]$$

$$= -\frac{\pi q_b L}{R}\left[2R + \overline{b} + \overline{b}^*\right]$$

$$= -2\pi q_b L[1 + \frac{b}{R}Cos\theta]$$

HIGH RESOLUTION RE-ENTRANT BPM FOR LINEAR COLLIDERS

C. Simon#, S. Chel, M. Luong, O. Napoly, J. Novo, D. Roudier, CEA-Saclay, Gif sur Yvette, France
N. Baboi, D. Noelle, N. Mildner, DESY, D-22603 Hamburg, Germany
N. Rouvière, CNRS-IN2P3-IPN, Orsay, France

Abstract

A high resolution beam position monitor (BPM) is necessary for the beam-based alignment systems of high energy and low emittance electron linacs. Two monitors with a large aperture (78 mm) are installed in the FLASH linac at DESY: one inside a cryomodule and the other at room temperature in a clean environment. The mechanical and signal processing designs of this BPM were determined to get a high position resolution and the possibility to perform bunch to bunch measurements. Methodology, simulations and experimental results will be discussed in this paper.

INTRODUCTION

A BPM based on a radio-frequency re-entrant cavity is developed in the framework of the European CARE/SRF programme, in a close collaboration between DESY and CEA/Saclay. A first prototype of a re-entrant BPM installed inside a cryomodule in the FLASH linac has already delivered measurements [1]. A second system is installed at room temperature to confirm the theoretical analysis. The RF simulations carried out with the software HFSS and the development of a Mathcad model determined the mechanical design and signal processing of this BPM.

CAVITY BPM

Mechanical design

The re-entrant cavity BPM is composed of a mechanical structure with four orthogonal feedthroughs. It is arranged around the beam tube and forms a coaxial line which is short-circuited at one end [2]. The cavity (Fig. 1) is fabricated with stainless steel, its aperture has a diameter of 78 mm and its length of 170 mm is minimized to satisfy the constraints imposed by the cryomodule.

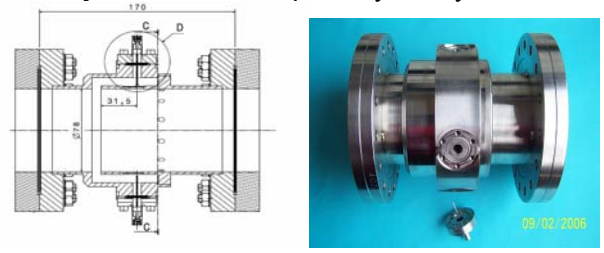

Figure 1: Re-entrant cavity BPM installed in the FLASH linac.

Twelve holes of 5 mm diameter were drilled at the end of the re-entrant part for a more effective cleaning. The position of feedthroughs was determined by simulations with the software HFSS, to reduce the magnetic loop coupling and separate the main RF modes (monopole and dipole modes). Several cryogenic and vacuum tests were, successfully, applied to feedthroughs. For each antenna, a CuBe RF contact is welded in the inner cylinder of the cavity to ensure electrical conduction between the feedthrough and the cavity, providing a magnetic coupling loop.

RF characteristics of the cavity BPM

The resonant cavity was, first, simulated with the software HFSS (Ansoft) in eigen solver mode to determine its frequencies and coupling. The simulations were carried out with HFSS on a half of the cavity. The electrical and magnetic fields are high in the re-entrant part. With Matlab and the HFSS calculator, the R/Q ratio was computed in using the following equation (R: the Shunt impedance and Q: quality factor).

$$\frac{R}{Q} = \frac{V^2}{2*\pi*f*W} \qquad (1)$$

With $V = \left| \int E(z)*e^{jkz}\,dz \right|$ and $W = \frac{\varepsilon_0}{2} \iiint \left| E*E^* \right| d\tau$

where k= w/c and W is the stored energy in the mode. Q factors were determined by HFSS with matched feedthroughs in eigen solver mode. The RF measurements, presented in Table 1, compare some computed quantities to measured values. The frequencies and coupling measurements of the main RF modes (monopole and dipole modes) were carried out to check the proper mounting of feedthrough on the cavity. The difference on Q factors can be explained by the boundary conditions which are not the same during the measurements in laboratory and in the tunnel.

Due to the finite tolerances in machining, welding and mounting, some small distortions of cavity symmetry are generated. The dipole mode orthogonal polarizations show slightly different eigenfrequencies; the relative difference was measured and is, however, less than 2 per 1000. Furthermore, a displacement of the beam in the 'x' direction gives not only a reading in that direction but also a non zero reading in the orthogonal direction 'y'. This asymmetry is called cross talk. Cross-talk isolation measurements are performed on the cavity with a network analyzer [3]. The crosstalk was measured in the FLASH tunnel to be around 33 dB instead of 41 dB measured in laboratory. This difference is not yet understood but it may be explained by the fact that the BPM has a rotation/tilt (11.25 degrees) with a button BPM which is very close.

Eigen modes	F (MHz)			Q_{ext}			R/Q_l (Ω) at 5 mm	R/Q_l (Ω) at 10 mm
	Calculated	Measured in lab.	Measured in the tunnel	Calculated	Measured in lab.	Measured in the tunnel		
Monopole mode	1250	1254	1255	22.95	22.74	23.8	12.9	12.9
Dipole mode	1719	1725	1724	50.96	48.13	59	0.27	1.15

Table 1: RF characteristics of the re-entrant BPM.

The transmission measurement on two opposite antennas was completed in the 1 to 4 GHz range (Fig. 2).

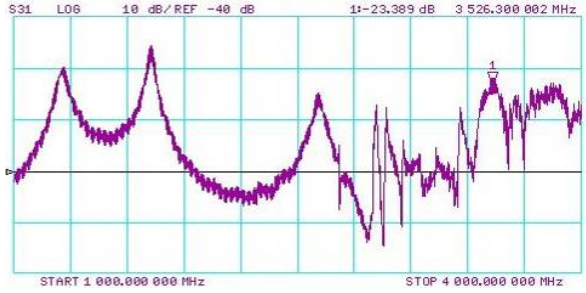

Figure 2: Transmission measurement on the opposite antennas without beam

The first and second peaks are the monopole and dipole modes. Others peaks are higher order modes which can propagate out of the cavity through the beam pipe. Those 'higher order modes' should be well rejected by a 1.72 GHz band pass filter used in the signal processing. This filter was measured in laboratory, at 3 GHz, its attenuation is around -70 dB and around -60 dB at 4 GHz.

SIMULATION

Mathcad Model

To assess the performance of the system, a model (cavity+signal processing) is elaborated with a Mathcad code based on Fourier transforms. The simulation covers a span from 0 to 20 GHz. Each mode of the cavity is modelled as a resonant RLC circuit. The delivered time domain signal is therefore determined by the RF characteristics of each mode (Equation 3). The single bunch response of the cavity depends on frequency w_i and external coupling Q_i of the modes. The signal from a pickup is the sum of all resonant modes excited by the beam.

$$S_{pickup} = \Sigma S_i \quad (2)$$

$$S_i = \Phi(t)\left[V_i \exp\left(-\frac{w_i.t}{2.Q_i}\right)\left(\cos\left(a_i.t - \frac{w_i.\sin(a_i.t)}{2.Q_i.a_i} \right)\right)\right] \quad (3)$$

With $a_i = w_i\sqrt{1-\frac{1}{4{Q_i}^2}}$ and $V_i = \sqrt{\frac{{w_i}^2.(R/Q)_i.q^2.R_o}{\zeta_i.Q_i}}$

where $\Phi(t)$ is the heaviside function, q the bunch charge, R_0 the 50 Ω cable impedance, R/Q_i defines the coupling to the beam and $\zeta_i = 4$ if it is a monopole mode or $\zeta_i = 2$ if it is a dipole mode.

The signal processing uses a single stage down-conversion to obtain Δ/Σ and is shown in Fig 3.

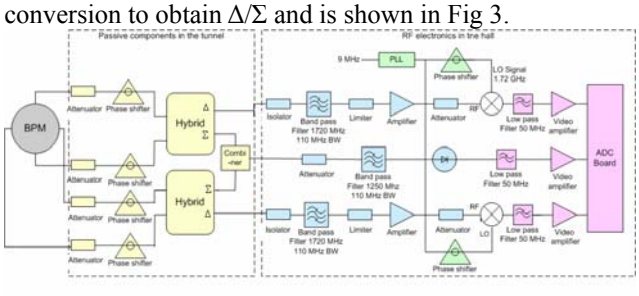

Figure 3: RF signal processing electronics

As the signal from the monopole mode does not depend on the beam position, the rejection of the monopole mode is necessary and is carried out in three steps [3].

To simulate the signal processing, the transfer functions of different components are used.

The model of the 180° hybrid couplers composing the signal processing is derived from the network analyzer measurements [4]. Its isolation is higher than 20 dB in the band 1-2 GHz. A local enhancement of the isolation can be obtained with adjusting of the phase and attenuation to have a better rejection of the monopole mode. The transfer function of cables (H_c) takes into account the effect of attenuation and dispersion. The "sum" signal peak power was measured around 36 dBm and the "sum" peak power simulated with the Mathcad model is around 34 dBm. Those values are close, the Mathcad model can be, therefore, validated.

The band pass filter with a 110 MHz bandwidth centred at 1.72 GHz provides a monopole mode rejection and a noise reduction. Its transfer function is given by a CAD code. The local oscillator (LO) signal is modelled by a sine wave at the dipole frequency with 1 Volt amplitude. To carry out the synchronous detection, a phase shift is added to put in phase the LO signal and the RF signal (without monopole mode) from the Δ channel. Follows a 50 MHz lowpass filter, which the transfer function is given by the same CAD code. The output signal of the signal processing (Fig 4) is, then, sampled at the peak for a significant beam offset, around 1 mm.

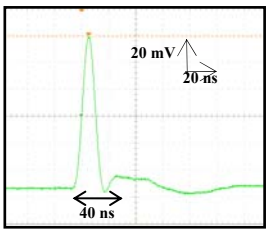

Figure 4: Output signal from the Δ channel.

Results

The position resolution is the rms value related to the minimum position difference that can be statistically resolved. The noise is determined by the thermal noise and the noise from signal processing channel [3]. The signal is given by the model (cavity+signal processing). The gain was adjusted to get an RF signal level around 0 dBm on the Δ channel with 100 µm beam offset. The noise level is about 0.4 mV. In using those parameters, the position resolution is around 350 nm [4].

One of the most important parameters for a BPM is the time resolution. It is usually identified to the damping time which is around 9.5 ns for the re-entrant cavity. Nevertheless, considering the whole system, the time resolution is around 40 ns [3], since the rising time to 95% of a cavity response corresponds to 3τ.

FIRST BEAM TESTS

Summer 2006, the two subsystems, composing the signal processing, were installed and calibrated. The adjustment of phase shifters allows having a high common mode rejection (30 dB at the monopole mode frequency). The synchronous and direct detectors, as well as amplifiers and limiters for protection were adjusted to have a linearity range around +/- 10 mm.

After the electronics calibration, the first tests with beam were carried out. The aim of this first calibration was to know the measurement dynamic range and no to have a high resolution. As the re-entrant BPM is mounted with a tilt angle of 11.25° with respect to the horizontal direction, a frame rotation change, done by software, was necessary. Figure 5 shows that the re-entrant BPM has, on the X and Y channels, a good linearity in a range 15 mm but there is an asymmetry and the linearity is better for a positive deviation. This effect is not yet well understood.

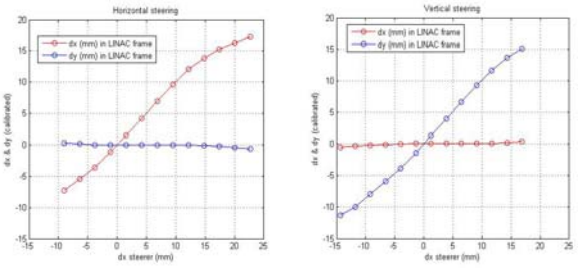

Figure 5: Calibration results in LINAC frame from horizontal (left) and vertical (right) steering

The standard deviation of the calibrated position measurement (fig. 6) was plotted for the horizontal and vertical steering.

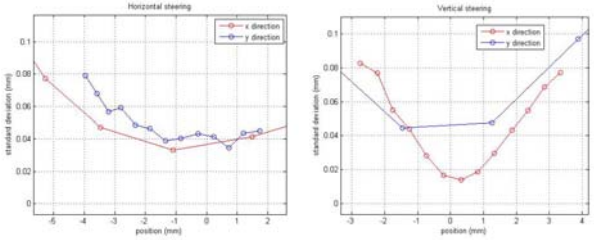

Figure 6: Standard deviation of the position measurement (calibrated)

The raw RMS resolution of the system directly measured by the standard deviation of the readings from the re-entrant BPM can reach 20 µm on the X channel and around 40 µm on the Y channel, at the BPM centre. But those results depend on the beam jitter, too. With simulations, the resolution of this system was determined around 15 µm.

OUTLOOK

For the next beam measurements, the resolution will be studied. The mixer used in the electronics will be replaced by a new one which accepts a high power RF input (around 17 dBm instead of 0 dBm). Some attenuators will be removed to change the gain and improve the resolution. Table 2 shows the re-entrant BPM simulations with the new mixer and 10 mm beam offset.

Table 2: Resolution estimated with the new mixer and 10 mm beam offset.

	Resolution (µm)
75m cables and RF signal level around 12 dBm on the Δ channel	1.3
33m cables and RF signal level around 17 dBm on the Δ channel	0.7

With this layout, the resolution of the re-entrant BPM should be around 1 µm with a measurement dynamics range around +/- 10 mm.

CONCLUSION

This BPM is designed to be used in a clean environment, at cryogenic or room temperature. Its main features are a large aperture (78 mm) and an excellent linearity. The time resolution is around 40 ns and the theoretical resolution is around 1 µm with a measurement dynamics range better than +/- 5 mm. The preliminary measurements on the BPM show a very good agreement with the theoretical analysis. This BPM appears as a good candidate for being installed in the XFEL and ILC cryomodules.

ACKNOWLEDGMENTS

We acknowledge the support of the European Community-Research Infrastructure Activity under the FP6 “Structuring the European Research Area” programme (CARE, contract number RII3-CT-2003-506395).

We thank our colleagues from DESY: the TTF operational team for its support, MDI and MVP teams for their help at TTF site and their advices about on the mechanics.

REFERENCES

[1] C. Magne, et al, “Reentrant cavity BPM for linear colliders”, BIW2000R.

[2] R. Bossart, “High precision beam position monitor using a re-entrant coaxial cavity” Processings of LINAC94, KEK, (1994).

[3] C. Simon, et al., “High Resolution BPM for linear collider”, BIW 2006.

[4] C. Simon, et al., “High Resolution BPM for linear collider”, EPAC 2006.

CERN LINAC4 Stripline signals

by L. Soby, CERN

For the future Linac4 at CERN the measurement of position, intensity and phase of low beta H- beams are foreseen using either button BPMs or shorted stripline BPMs. The very small available space limits the choice of BPM type. At low relativistic beta the transverse sensitivity of a stripline BPM varies with beta and frequency and must be taken into account, as shown by R. Schafer.

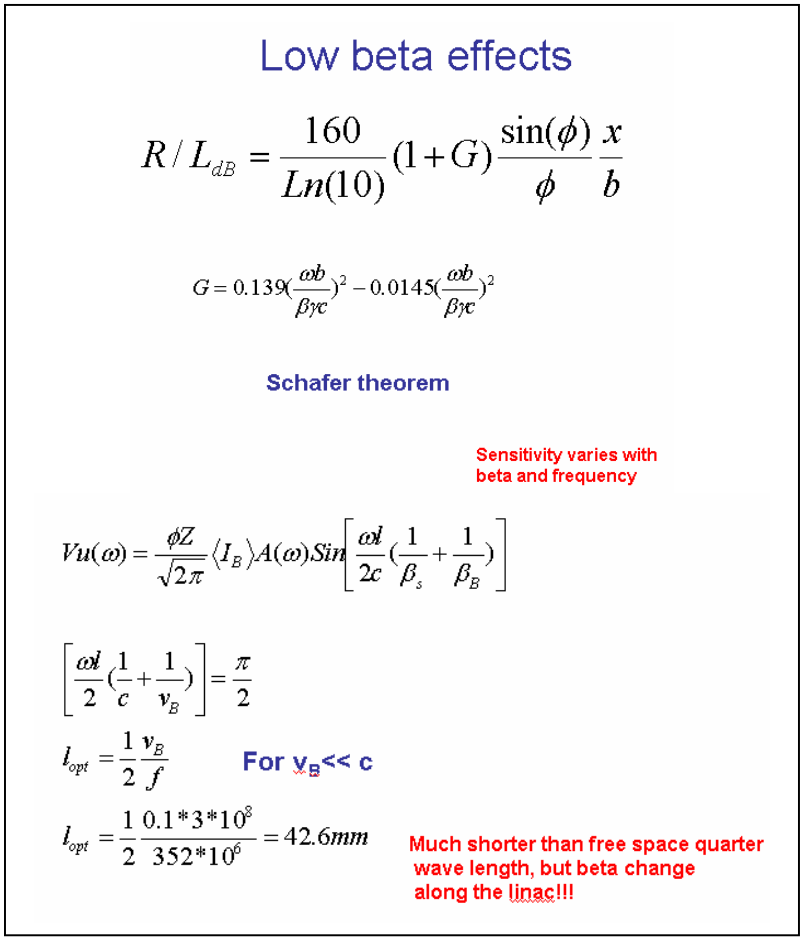

Present 3D electromagnetic field solvers does not consider low beta beams and the question was how to simulate low beta beams. A new Microvawe Studio package now gives the possibility for simulating low beta beams."

4th CARE-Meeting HHH-N3-ABI in Lüneburg, Germany

Simulation of BPM front-end electronics and Special Mechanical Designs

1st half day: **BPM sensor technology – simulation tools and results**
Chair: Andreas Peters, GSI

Invited Talks:

1. BPM simulations for the FAIR SIS100 synchrotron with Microwave Studio
   Piotr Kowina, GSI
2. EM Simulations for PETRA3
   Nicoletta Baboi, DESY
3. ISIS Position Monitoring
   Ben Pine, RAL
4. High resolution BPM for Linear Colliders
   Claire Simon, CEA
5. Cold Cavity BPM R&D for the ILC
   Manfred Wendt, FNAL

Main remarks in the discussions:

- Talk 1: Prevent high voltages by introducing additional capacitance, inductance, respectively low pass filtering
- Talk 1: Justification for the design? Is a stripline an alternative? One reason for the chosen design is the broad shape of the beam causing a lot of problems with non-linearities, which have to be solved.
- Talk 2: Discussion about simulation of beam through a wire with discrete ports in Microwave Studio (problems: reflections at ports), demand of the upcoming Particle Studio, introducing a real particle beam simulation; already implemented in MAFIA T3, but much more complicate to use than Microwave Studio and the needed computer power is very high
- Additional comments from Piotr Kowina and Lars Soby (see their transparencies)
- Talk 3: 2D theory (e.g. by Bob Shafer, 1989) is just good for understanding the basics describing infinite long monitors, but real devices are 3D, causing a lot of differences to 2D theory
- Talk 4: Reasons for asymmetry of the results discussed, additional simulations with (always unavoidable) mechanical tolerances demanded; discrepancy between the simulated resolution and measurement results will be investigated; mechanical set-up and further developments are discussed to enhance the alignment
- Talk 5: Discussion about different coefficients of expansion (copper, ceramics) and danger of breaks in the actual design (in total 8 feed-throughs per cavity BPM), testing in next future is foreseen
- Short summary: Different simulation codes are on the market: MAFIA, Micowave Studio, HFSS, etc., in addition self-written codes in Matlab, MathCAD and others, contact authors for detailed information

Cold Cavity BPM R&D for the ILC

Manfred Wendt

Fermi National Accelerator Laboratory, Batavia, IL 60510, U.S.A.[1]

Abstract. A cold L-Band cavity BPM for installation in a SCRF cryomodule is currently under development at Fermilab. The BPM has to meet the ILC BPM specifications, i.e. < 1 µm single bunch, single pass resolution, going along with sufficient accuracy and reproducibility. Real estate limitations and the superconductive RF environment require some special considerations for this design.

INTRODUCTION

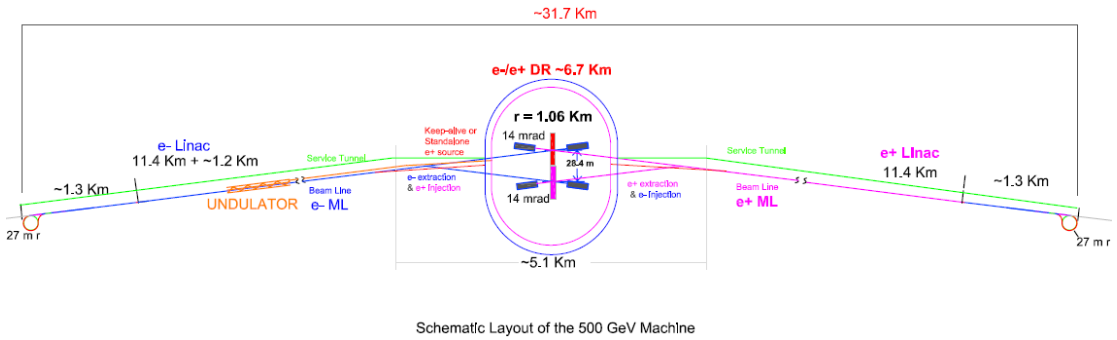

FIGURE 1. Layout of the International Linear Collider (ILC).

A 500 GeV center-of-mass (CM) International Linear Collider (ILC) is currently under study as the next large particle accelerator for high energy physics (HEP) to test "Mother Nature's" laws. Hearts of the machine are two ~ 10 km long superconducting RF main linacs, providing the required beam energy (see Fig. 1).
A crucial point is beam transport through the main linacs, i.e. preserving its low-emittance, in order to achieve the luminosity goal. Table 1 gives an overview of the ILC beam parameters, showing a vertical emittance of ~ 0.04 mm mrad, which is equivalent to a 5 nm (!) vertical beam size at the IP. Particle tracking studies of the main linac lattice, using different orbit correction methods, pointed to the need of a high resolution beam orbit measurement. In order to preserve the emittance, and therefore the luminosity, to a > 90 % level, the resolution requirement of the beam position monitors (BPM) is well below 5 µm. For diagnostics purposes, i.e. to find sources of beam jitter, fluctuations and other problems, we have to be able to detect beam displacements in the order of a fraction of the nominal transverse beam size. Therefore a single bunch (bunch-by-bunch, measurement time < 369 ns) resolution < 1 µm is required for the main linac BPMs.

[1] This work was supported by Fermi National Accelerator Laboratory, operated by Universities Research Association Inc. under contract No. DE-AC02-76CH03000 with the United States Department of Energy

TABLE 1. ILC beam parameters (nominal).		
beam energy	=	2 x 250 GeV
luminosity L	=	2 x 10^{34}
rep. frequency f_{rep}	=	5 Hz
macro pulse length t_{pulse}	=	800 µs
bunch spacing Δt_b	=	369 ns
bunch charge	=	3.2 nC
bunch length σ_z	=	300 µm
vert. emittance $\gamma \varepsilon_y^*$	=	0.04 mm mrad
RMS energy spread	=	0.1 %
β_x^* (IP)	=	21 mm
B_y^* (IP)	=	0.4 mm
hor. beamsize (IP) σ_x	=	500 nm
vert. beamsize (IP) σ_y	=	5 nm

"COLD" BEAM POSITION MONITORS FOR THE ILC

Table 2 shows an overview of the major beam instrumentation systems needed in the different ILC accelerator areas. The beam position monitors (BPM) are the most complex, while also most important distributed beam instrumentation system in the ILC accelerator complex. About 600, of a total of ~ 4000 BPMs, are located inside every 3rd cryomodule, flanged to a superconducting quadrupole magnet package; these "cold" BPMs are used in the Main Linac (ML) and in the Ring-To-Main-Linac (RTML) areas. Along the ~ 10 km Main Linac the BPMs are almost the only beam instrumentation, therefore they are a key component to diagnose problems and errors.

The requirements for the cold BPMs are very specific, also because of their neighborhood to the superconducting 1.3 GHz RF cavities:

- A real estate of ~ 170 mm length and 78 mm circular beam pipe aperture is given.
- The BPM has to operate in a cryogenic environment (~ 4 K).
- A cleanroom class 100 certification is required, because of the nearby superconducting cavities.
- The BPM has to operate in ultra-high vacuum (UHV).
- A single bunch (bunch-by-bunch, i.e. < 350 ns measurement time) resolution of < 1 µm is required to preserve the vertical emittance along the Main Linacs. This high resolution will also enable the use of the BPMs for troubleshooting and diagnostics e.g. spot sources of beam jitter.
- The absolute alignment error between electrical center of the BPM and magnetic center of the corresponding quadrupole should be < 200 µm.

Related issues to the cold BPM pickup are the cold RF feedthroughs, the RF cabling inside the cryostat and the read-out system for the pickup signals.

INSTRUMENT requirements (e.g. resolution)	**ILC ACCLELRATOR AREA**					
	e^--source	**e^+-source**	**DR**	**RTML**	**ML**	**BDS**
Button/stripline BPM 10…30 µm ($e^{-/+}$-source) <0.5 µm averaged (DR)	69	400	2x747			
Cavity BPM (warm) < 0.1…0.5 µm (C, S-Band) 1…5 µm (L-Band)		109 (C)		2x649 (C) 2x27 (L)		42 (L) 14 (S) 262 (C)
Cavity BPM (cold) ~0.5…2 µm (L-Band)				2x28	2x280	
Laserwire ~ 10 % of tr. beam size (0.05…0.5 µm)	8	20	2x1	2x12	2x3	8
DMC dE~0.01% / s_z~100 µm (< 1 µm)	3	4		2x2		2 (cold)
Beam phase monitor 0.01^0(BC)…0.1^0@1.3GHz	4	2		2x3		
Wirescanner	12	8				
Beam current monitors 0.5…1 % of bunch charge	7	11	2x1	2x2	2x3	10
Optical monitors	6	17	2x2	2x8		11
BLM (PMT/IC) < 0.01 % of total beam int.	60/2	400/20	2x40/4	2x25/2	2x325/10	100/10
Feedback systems	5	10	2x2	2x1	2x10	12

Table 2: Counts of beam instrumentation system installations in the ILC accelerator complex, along with some basic requirements (DR: Damping Rings, RTML: Ring-To-Main-Linac areas, ML: Main Linacs, BDS: Beam Delivery System).

A "COLD" CM-FREE CAVITY BPM FOR THE ILC

There are basically two possible ways to approach the cold BPM requirements of the ILC:

- A dedicated, high resolution BPM based on a common mode (CM) free dipole mode cavity BPM pickup (baseline design).
- The use of a simple, button-style BPM pickups of low or moderate single bunch resolution in combination with a signal processing scheme of a beam excited dipole mode on the higher-order mode (HOM) couplers, offering a high resolution BPM measurement (alternative design).

Other ongoing cold BPM developments include a modified re-entrant coaxial cavity BPM (CEA-Saclay), as well as a CM-free S-Band dipole mode cavity BPM with reduced aperture (~ 35 mm) (SLAC).

Cavity BPM Principle

A cylindrical "pillbox" having conductive (metal) wall dimensions of radius R and length l resonates at eigenfrequencies:

$$f_{mnp} = \frac{1}{2\pi\sqrt{\mu_0 \varepsilon_0}} \sqrt{\left(\frac{j_{mn}}{R}\right)^2 + \left(\frac{p\pi}{l}\right)^2}$$

This resonator can be utilized as passive, beam driven cavity BPM by assembling it into the vacuum beam pipe. A subset of these eigenmodes is excited by the beam, for use as BPM the lowest transverse-magnetic dipole mode TM_{110} is of interest. Its

$$E_z = C J_1\left(\frac{j_{11} r}{R}\right) \cos \emptyset \; e^{i\omega t}$$

field component couples to the beam, with almost linear dependence to the beams displacement r, and beam intensity (hidden in the constant C).

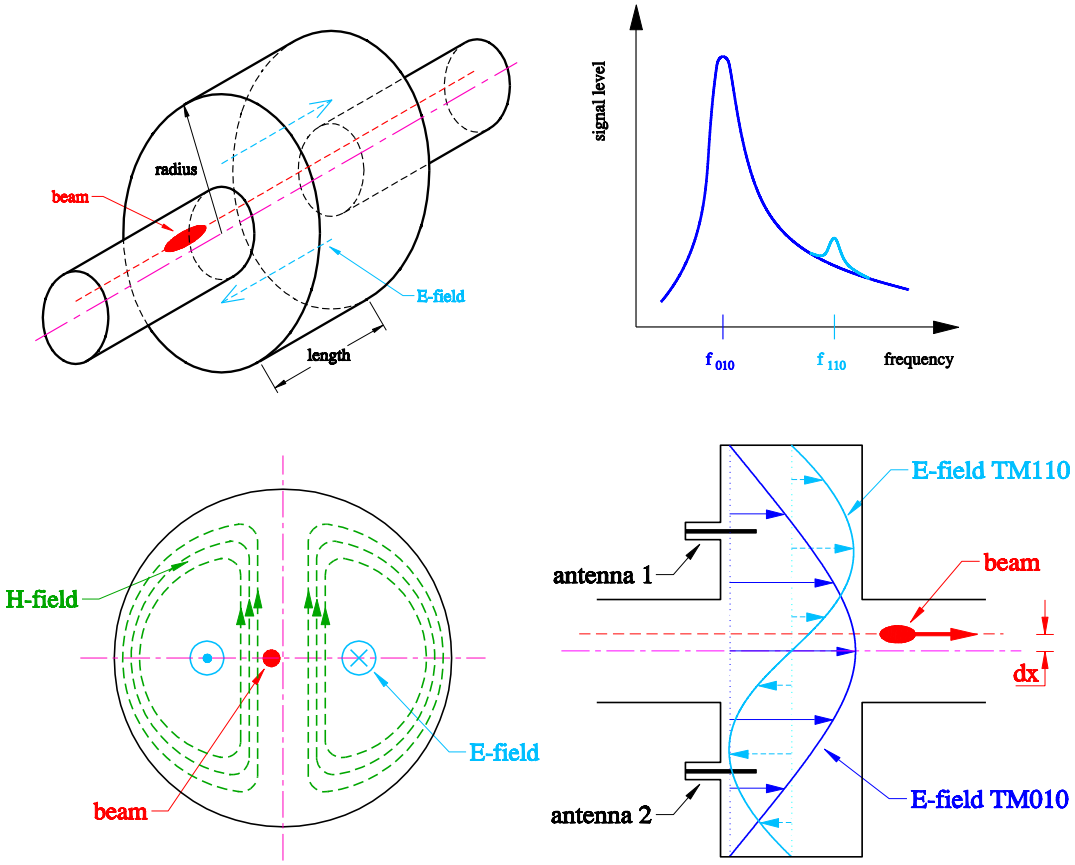

FIGURE 2. Principle of a "pillbox" cavity BPM.

As Fig. 2 illustrates, the TM_{110} dipole mode vanishes as the beam moves exactly through the center of the cavity pickup (r = 0). A set of capacitive coupling pin-antennas can be used to sense this dipole mode displacement signal of frequency f_{110}. Compared to broadband BPM pickups, e.g. button- or stripline style, the strength of the beam excited eigenmode is due to the cavity shape. For a simple cylindrical cavity BPM the corresponding R_{sh}/Q (shunt impedance over Q-value) typically has much higher values, compared to the transfer impedance of a broadband BPM, i.e. has higher beam displacement sensitivity and therefore a much greater potential to work as a high resolution BPM.

Unfortunately this simple, basic pillbox cavity BPM setup has several issues, which have to be addressed for a practical implementation:

- **Common modes:** Fig. 2 further illustrates that monopole modes (in BPM applications often called "common" modes, as they are independent from the beam displacement, thus always present) are also excited by the beam – here shown the fundamental TM_{010} eigenmode. The finite Q-value generates an unwanted contribution of this fundamental, high level TM_{010} monopole mode at f_{110} of the dipole mode. As the ILC BPMs have to time resolve every passing bunch, the Q-value of the resonator has to be chosen in a way that the stored energy doesn't last longer than the bunch-to-bunch time interval (~ 350 ns). In practice this requires rather low Q-values (500…1000), thus would result in a high monopole mode contamination at the dipole mode frequency (Fig. 2 upper-right plot).
- **Cross talk:** In an ideal cylindrical cavity the *polarization axes* of the dipole and other higher modes are undefined. Fig. 2 shows the vertical polarized part of the TM_{110} dipole mode, thus functioning as horizontal BPM. Every dipole mode has two polarization axes, which in practice align to small imperfections of the circular cross-section, or to the feedthrough pin-antennas, etc. In case of larger asymmetries the frequencies of the two polarizations may be not exactly the same. To act as a usable BPM both polarization axes of the cavity BPM have to be aligned to the horizontal/vertical plane within the specified tolerances. Without special considerations a simple pillbox cavity BPM may have somehow undefined polarization axes, which results in so-called "cross talk" effects between horizontal and vertical planes.
- **Transient response:** As already mentioned, the loaded Q-value has to be low enough to time resolve the beam position of every passing bunch, i.e.
  $Q_l \sim 500\ldots1000$. In case of the simple pillbox cavity BPM, made out of copper or equivalent, the unloaded Q-value Q_0 usually is rather high if made out of high. As the pin-antenna loading does not lower the Q-value substantially, either very unusual dimensions have to be realized (very short gap), or a less conductive material has to be used, e.g. stainless steel. Both ways have disadvantages, particular the second:
- **Wakepotetial and heat-load:** All undamped, beam excited modes in the cavity BPM increase the wakepotential. Higher order modes may cause beam breakup and kick effects, trapped monopole and other modes mainly contribute to an unwanted heat load in the cryomodule, which is particular high when using lossy conductors as cavity walls.

Beside these issues the cavity BPM located in the cryomodule has to fulfill special cleanroom and vacuum requirements. Both, magnitude and phase, of the dipole mode signal have to be processed, the magnitude represents the unnormalized beam displacement, the phase gives the sign. To perform a calibrated beam position measurement the dipole mode signal furthermore has to be normalized to the beam current (or bunch charge).

The Common-mode Free Cavity BPM

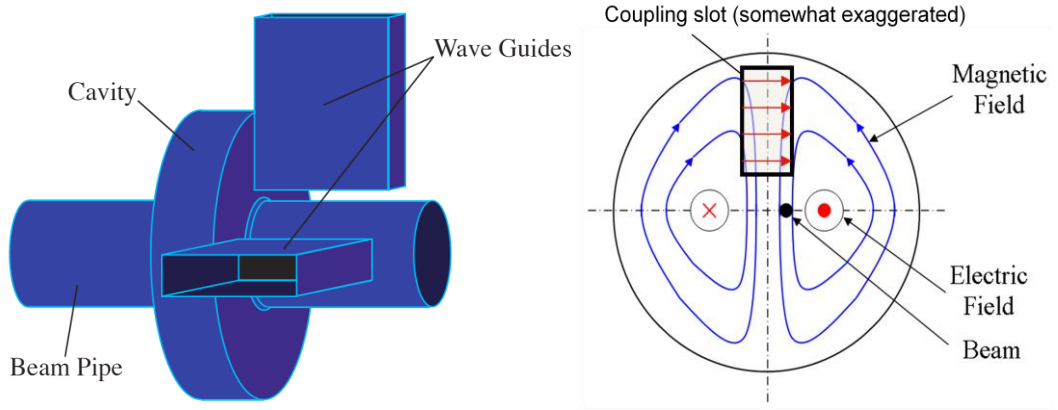

FIGURE 3. Waveguide-loaded CM-free cavity BPM (courtesy of Sean Walston).

The total suppression of the TM_{010} common mode is the key to realize the full resolution potential of a cavity BPM. This can be realized by arranging a set of two or four rectangular waveguides, coupled to the cavity (see Fig. 3). The waveguide acts as a very effective high-pass filter between the cavity and the coaxial output port, utilizing a TE_{10} waveguide-mode cutoff frequency:

$$f_{10} = \frac{1}{2a\sqrt{\varepsilon\mu}}$$

Dimensioning the longer side a of the waveguide's cross-section such that its TE_{10} cutoff frequency is well between the f_{010} monopole mode and the f_{110} dipole mode frequencies of the cavity, will almost vanish the monopole mode contribution at the dipole mode frequency. The coupling slots for the waveguides in the cavity also help to align the polarization axes horizontally and vertically.

CM-free cavity BPM's with various coupling schemas between cavity and waveguides, waveguide arrangements and geometries have been tested at various laboratories. Most impressive results have been demonstrated at the nanoBPM collaboration. By using a set of 3 CM-free C-Band cavity BPMs in a hexapod spaceframe at the KEK Advanced Test Facility (ATF), a resolution < 20 nm could be achieved!

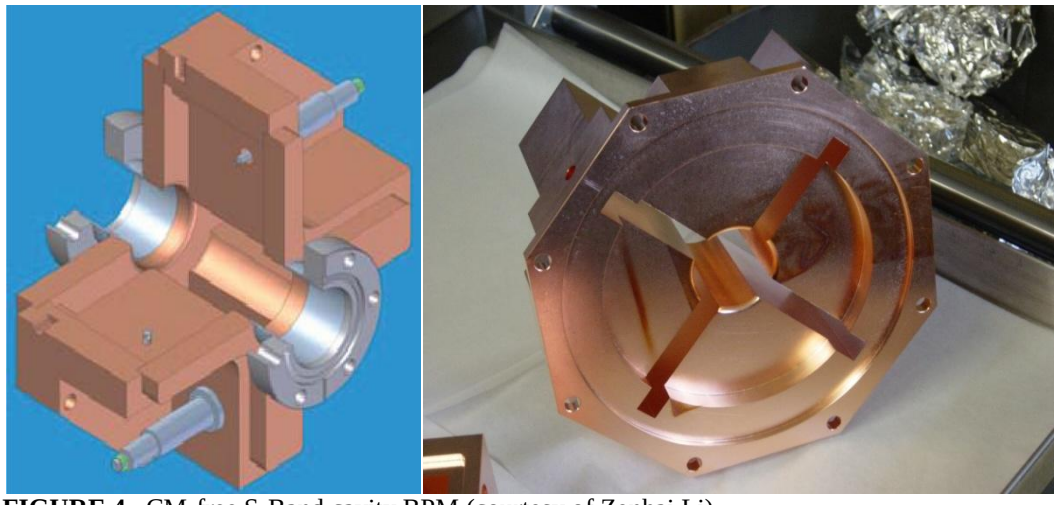

FIGURE 4. CM-free S-Band cavity BPM (courtesy of Zenhai Li).

For the practical realization of a cold cavity BPM in a superconducting RF environment, the additional waveguides appear to be a major problem for the cleaning procedure. Fig. 4 shows a prototype S-Band cavity BPM, addressing this problem by opening the waveguides towards the beam pipe to improve the accessibility for the cleaning procedure. A set of three S-Band cavity BPM's where tested with beam at the SLAC Endstation A (ESA), demonstrating a single bunch resolution < 1 µm. However, a detailed EM analysis shows a strong quadrupole-like parasitic mode below the TM_{010} frequency under certain beam conditions.

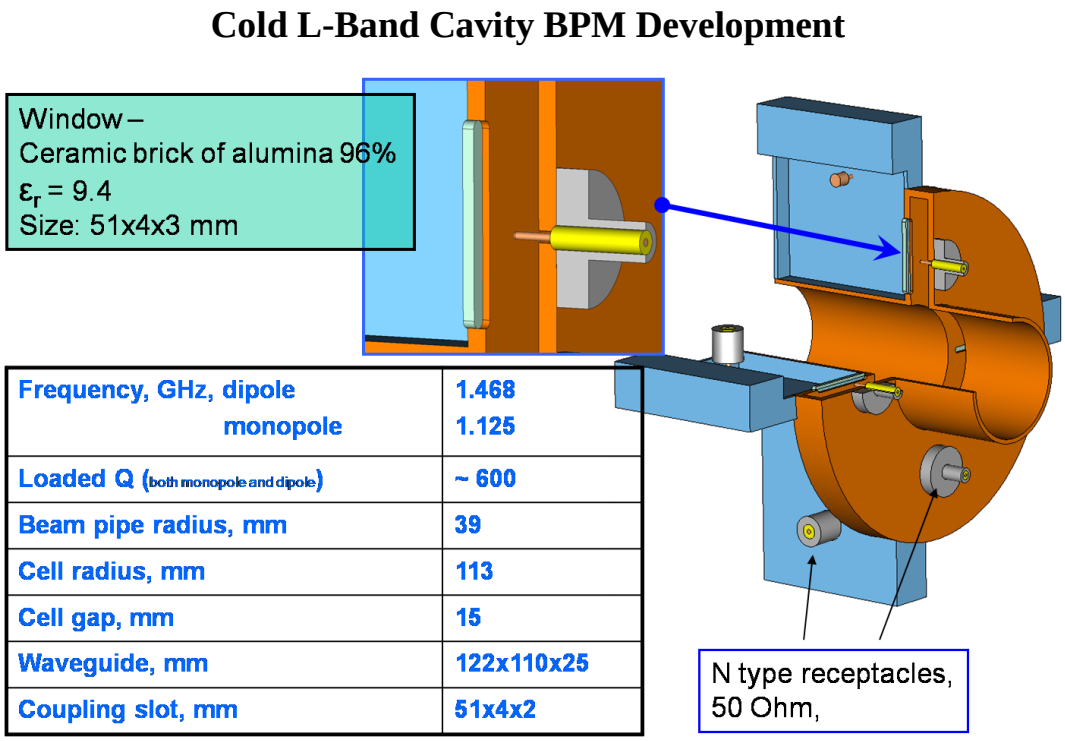

FIGURE 5. Cold L-Band cavity BPM development.

A cold L-Band cavity BPM (Fig. 5), currently at Fermilab under development, tries to address most of the mentioned problems:

- CM-free design using narrow waveguides to couple out the dipole mode signals.
- A ceramic filled slot-window utilizes a $Q_l \sim 600$, and also addresses the cleaning issues.
- Pin-antennas used to couple to the monopole mode signals, used for normalization and phase information. A non-matched signal combiner in combination with transmission-lines realizes an in-phase loading at the monopole mode frequency, while not loading at the anti-phase dipole mode frequency.
- The monopole mode frequency f_{010} and the dipole mode frequency f_{110} are chosen symmetrically to the accelerator frequency f_{RF}, which is foreseen to act as precise, jitter-free LO frequency reference.
- Tuning dimples at the cavity rim allow minimizing the horizontal/vertical cross-talk.

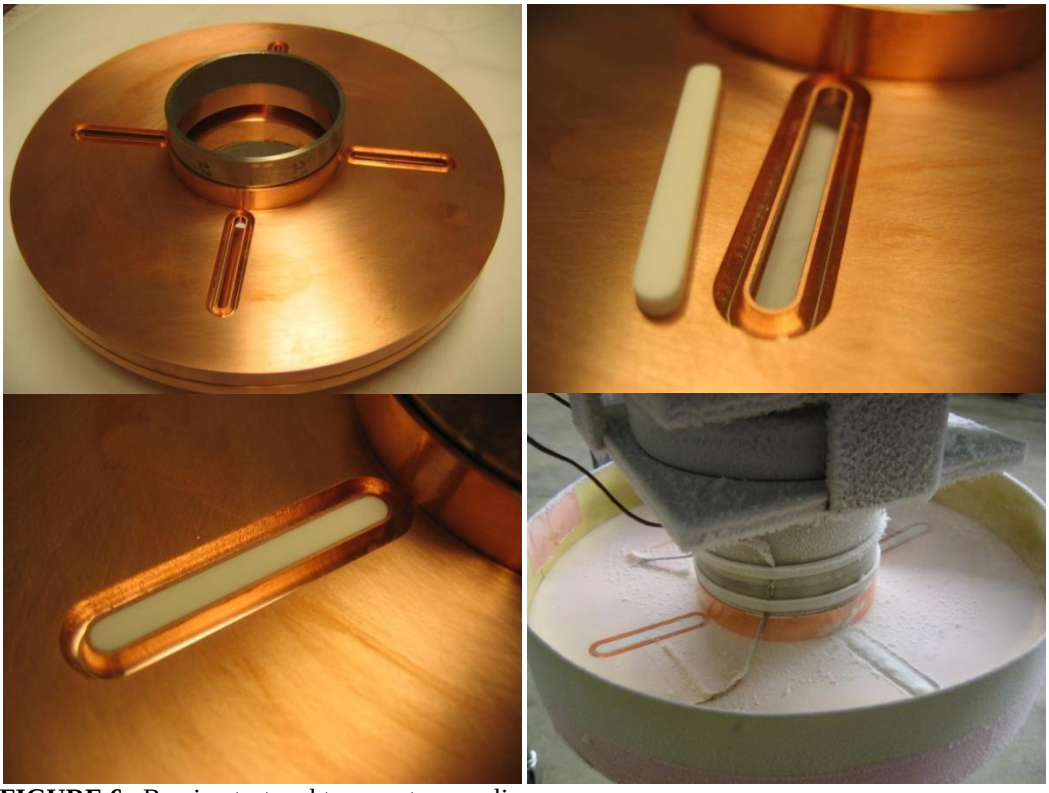

FIGURE 6. Brazing test and temperature cycling.

An experimental setup was used to study the brazing of the ceramic into the slot window, and testing the vacuum certification after several 77 K temperature cycles (Fig. 6). Even though only one of four windows survived all temperature cycles, we could acquire important information and experience with these experiments to further improve and optimize construction details.

From the EM simulations a computed dipole mode shunt impedance $(R_{sh}/Q)_{110} \sim 14\ \Omega$ (for 1 mm beam displacement) promises a sub-micrometer single bunch resolution. Fig. 7 shows a 3D view of the cold L-Band cavity BPM assembly at the current construction status. Most parts will be manufactured using OFHC copper. To reduce the deformation due to the atmospheric pressure a "rip" structure will be used to mechanically strengthen the cavity disks. UHV N-type RF feedthroughs with pin-antennas, mounted under 90^0 on the cavity disk, are used to couple to the monopole mode signals. Higher order mode signals are suppressed with filters in the read-out system. Standard N-type feedthroughs are used on the waveguide as waveguide-to-coaxial transition for the dipole mode signals. Several brazing processes at different temperatures are needed to assemble the complete unit. Next steps in the development are:

- A vacuum experiment to study the eigen-frequency shift due to the deformation of the cavity disks.
- A complete prototype assembly has to be manufactured and undergo a complete test series, including vacuum tests and temperature cycles.
- A network-analyzer based RF characterization and calibration has to be performed.
- The final prototype BPM has to undergo several cleaning procedures to meet the cleanroom class 100 specification.

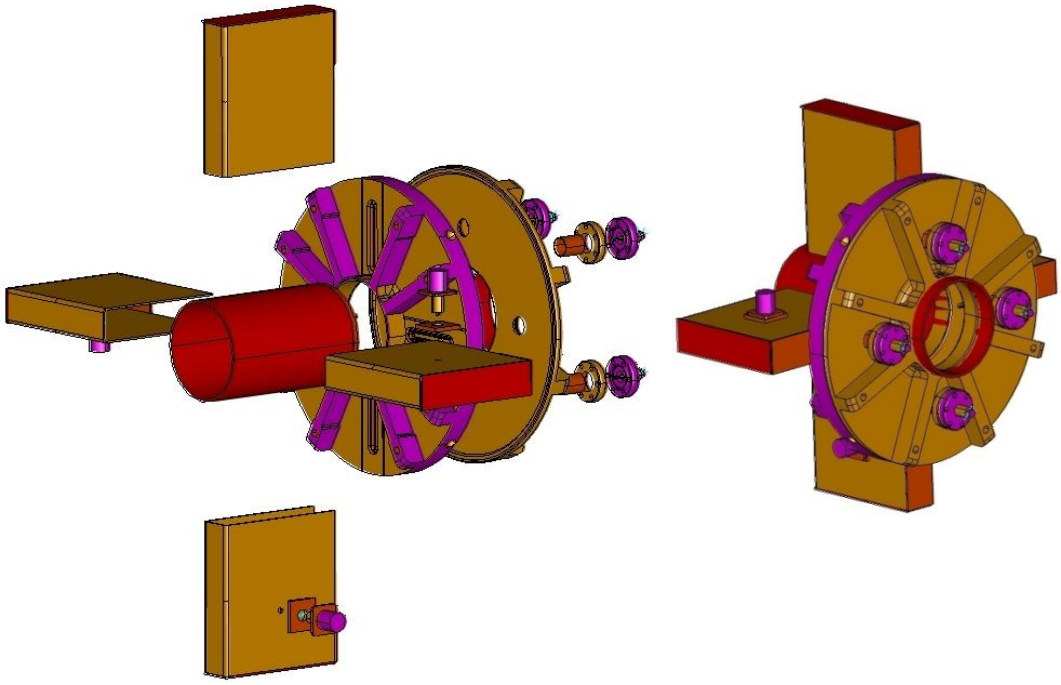

FIGURE 7. Cold L-Band cavity BPM assembly.

Finally the goal is the installation of a prototype cavity BPM in a cryomodule, to be used at the NML linac test facility, currently under construction at Fermilab.

Simulation of BPM Electronics at DESY

Thomas Traber, Rudolf Neumann

March 21, 2007

Abstract

This article is a slightly extended version of the corresponding presentation at the CARE Workshop in November 2006 which describes the first experiences in using the free software simulator Qucs and a Gnucap/Python based simulation system for BPM electronics.

Transient pulse and noise generators are created with python scripts. Simple BPM SNR calculations are done by simulating filters with spice and preprocessing the results with python. Simulations of AM/PM detectors and detectors for the Delay Multiplex Single Path Technique are shown.

1 Which Software to Use?

DESY decided to join the Open Access Movement for Articles and Documentation. There is no essential difference between Articles and Software. The tax payer's money saving argument can be applied to the software selection criteria, too. Although the Free Software Community emphasizes on the philosophical and political aspects of *free*, the economic relevance of *free* should not be neglected at least as far as the tax payers are concerned.

Is there free software available which is suitable for doing efficient simulations?

1.1 Some Free Software Circuit Simulators

1.1.1 Spice based Simulators

Berkeley Spice The mother of circuit simulation. Fully working. [1]

Spice Opus is based on Berkeley Spice 3f4. Fully working.

Ngspice is based on Berkeley Spice 3f4. Full working.

TclSpice is based on Berkley Spice. Uses Tcl/Tk as scripting langugage.

1.1.2 Non spice based simulators

eispice is a ground-up re-write of a simulation enginge similar to Berkeley Spice 3. Aims to be a lot faster than Berkeley Spice. Eispice uses Python as scripting language. Semiconductor Models are still missing.

Gnucap is not based on Berkeley Spice. Interactive use is a bit more comfortable than Berkeley Spice.

Qucs includes a GUI and functionalities similar to ADS, Microwave Office and other contemporary, comercial simulation tools. Qucs is currently in heavy development. The outlook is very promising.

1.2 Other Free Software Tools for Simulation

Python is a universal scripting language for rapid Software prototyping, simulations, signal processing, measurement automation, hardware description language (FPGA programming) ...

Cascade analyzes noise and distortion performance of cascaded elements in electronic systems.

Meep is a finite-difference time-domain simulation software developed at MIT. It uses Scheme as input language.

Camfr Cavity Modelling Framework using Python as input language.

Octave is similar to Matlab.

SciLab is also similar to Matlab - but the syntax is different.

Ptolemy Graphical system simulator[2].

There are much more free simulation tools.

[1] PSpice is based on Berkeley Spice2

[2] ADS is at least partially based on Ptolemy

2 Using Python as Simulation Scripting Language

Python[1] is one of the standard scripting languages. Ports exist for virtually any machine. It is used for:

- Web and Internet Development
- Network Programming
- Database Access
- Desktop GUIs
- Rapid Prototyping
- Signal Processing
- Measurement Automation
- Hardware Description Language
- ...

2.1 Python is frequently used in High Energy Physics

KEKB Injector LINAC GUI and numerical data processing

CERN LHC The webpage says:

> *Python combines remarkable power with very clear syntax. [...] Python is also usable as an extension language for applications that need a programmable interface.*

CERN The EuroPython Conference 2005 and 2006 was held at CERN and an article about it appeared in CERN COURIER.

CERN ROOT The ROOT Data Analysis Framework has a Python interface. [7]

SLAC Data acquisition system for GLAST.

DESY Also at DESY Python is used on some places.

2.2 Python User Interface

Python is in a manner of speaking an interpreter language. It not only interpretes script files but has also an interacitve command line interface to directly type in the commands.

There exists an Python extension called IPython with enhanced functions for interactive use, i.e. intelligent history.

2.3 Python for Numerical Computation

Python has builtin complex number support. Also the easy to use object orientation gleams slightly in the following example.

```
>>> Z=50+30j
>>> print Z
(50+30j)
>>> Z.imag
30.0
>>> Z.real
50.0
>>> A=Z.conjugate()
>>> A
(50-30j)
>>> A*Z
(3400+0j)
```

2.4 Python Addons for Numerical Computation

There exist some libraries for vector and arrays. The **Numeric** library from the **Scipy** project is one of the most used.

```
>>> from Numeric import *
>>> u=array([1.0,1.5,2.0,2.5])
>>> i=u/50
>>> i
array([ 0.02,  0.03,  0.04,  0.05])
```

2.5 Plotting with Python

Matplotlib is one of the most used plotting packages for Python. It provides also interactive graphical user interface.

As ROOT [7] has a Pyton interface it could be used for plotting, too.[3]

```
>>> from pylab import *
>>> t=arange(2*pi,0.1)
>>> u=sin(t)
>>> plot(t,u)
```

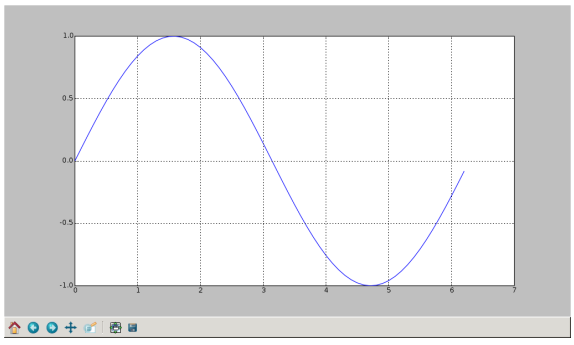

Figure 1: Python Plot Graphics

[3] Unfortunately the authors have no experience using ROOT, yet.

3 Simulation of AM/PM Converter with QUCS

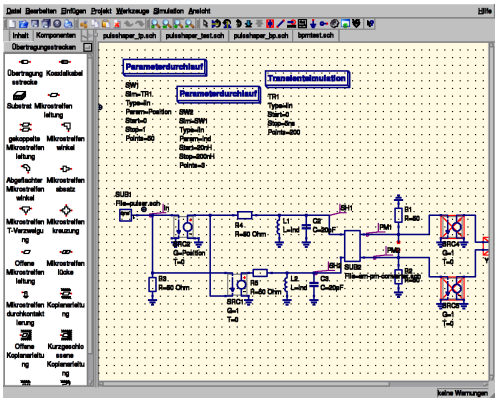

Figure 2: QUCS Graphical User Interface

Qucs [5] is free software simulator consisting of a graphical user interface and an also seperately commandline usable simulator engine.

The graphical user interface of Qucs is similar to ADS, Microwave Office and other contemporary comercial RF simulation tools. Unfortunately it is not possible to export Qucs schematic and import it to those commercial programms.

The pickup cambrel pulse is here simply simulated by combining two narrow pulse voltage sources[4]. Due to limitations in Qucs the position sweep is realized by simply increasing the voltage at one input.

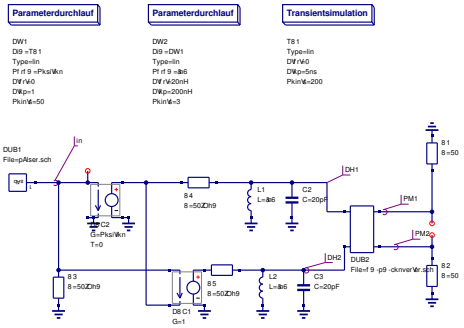

Figure 3: AM/PM Converter Test Circuit

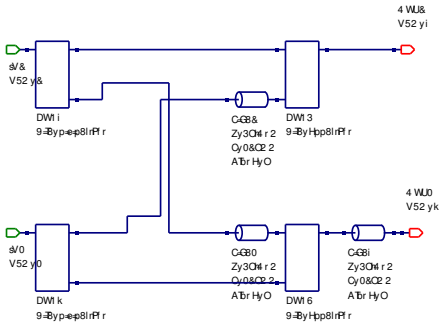

Figure 4: AM/PM-Converter Circuit

3.1 AM/PM-Converter Circuit

3.2 Positionsweep of AM/PM Converter with QUCS

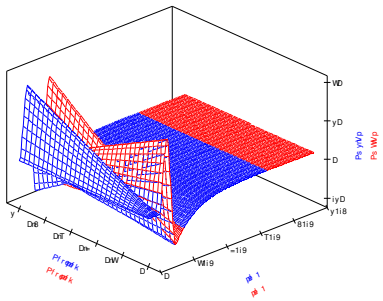

Figure 5: AM/PM Converter Position Sweep

QUCS 3D output looks nice. But at the time of that simulations the plotting code was buggy and documentation rudimentary. Therefore the further plots are done using **Python** and **Matplotlib**.

The spikes in figure 7 are due to bugs in qucsator, the simulation engine of Qucs.

3.3 QUCS Summary

- The current Qucs version (0.09) is a bit buggy. *Newer version behaves much better*
- The GUI has the well-known general drawbacks of GUIs. [6]
- Qucs does not provide a piecewise linear source.

[4] Qucs 0.09 does not provide a piecewise linear voltage source

[5] Disadvantage of GUIs: You need to fiddle with positioning of a lot of items on the canvas.

[6] GUIs are bad to your health.

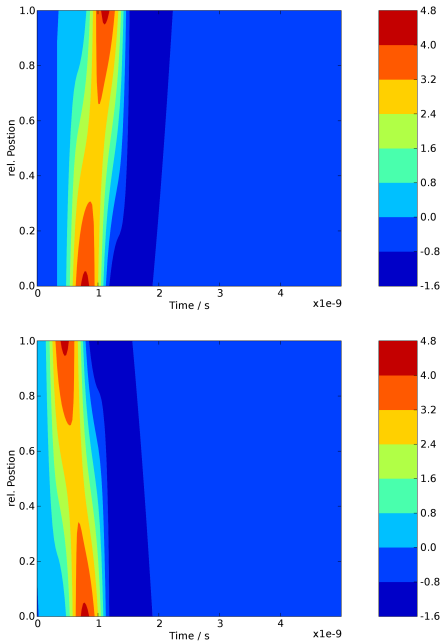

Figure 6: AM/PM Converter Output Voltage vs. Position and Time

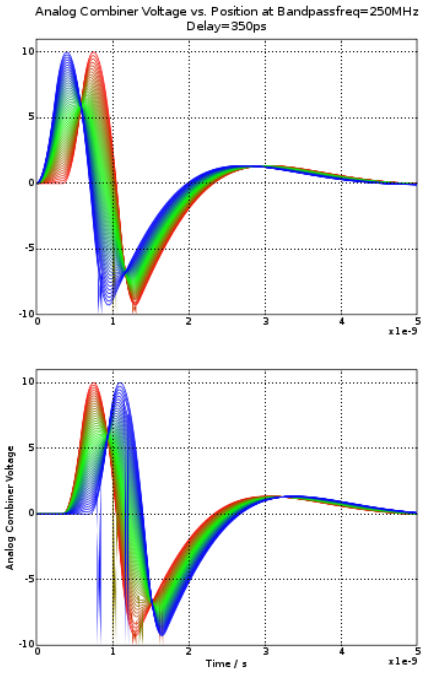

Figure 7: AM/PM Converter Output Voltage vs. Position and Time

4 BPM Circuit Simulation with Spice/Gnucap and Python

4.1 Spice or Gnucap, which is better ?

Pro Spice - contra Gnucap

- Spice3f allows alphanumeric netnames - Gnucap like Spice2 accpets only numeric netnames
- Spice is more frequently used and hopefully less buggy

Pro Gnucap - contra Spice

- Gnucap has a better user interface
- Gnucap has additional features

4.2 Python Wrapper for Gnucap

`gnucap.py` provides interactive and batch mode control of gnucap within python. The advantages are:

- on the fly automated circuit building and modification
- processing the gnucap simulation output allows "mixed mode" simulation
- together with myHDL it would be possible to simulate hardware and FPGA code together

4.3 The Pulse Source

Transient mode pulse source is realized by a Peace Wise Linar Voltage Source (PWL). The voltage values for the PWL are calculated by Python scripts.

We use two scripts:

- `pulse_gen.py` creates a rather simple model of the real pulse using only a view samples for fast evaluation of the circuits.
- For the final simulation we use the script `scope2pwl.py`. This script takes scope data of the actual BPM signal to create the simulation model.

4.4 Using Scope Data in Transient Simulation

Figure 4.4 and **??** show the output of a gnucap voltage source simulation using scope data.

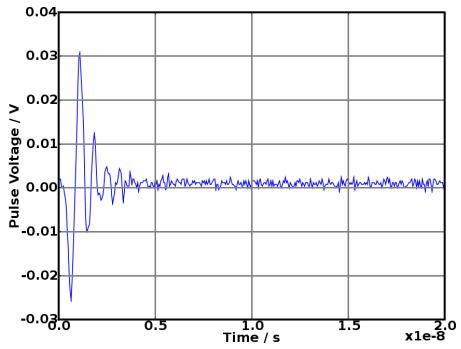

Figure 8: Simulated Output of Gnucap Voltage Source created from Scope Data of Large Button BPM

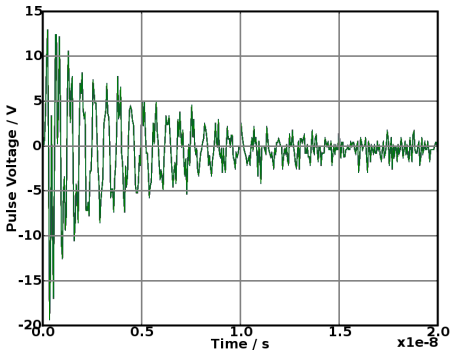

Figure 9: Simulated Output of Gnucap Voltage Source created from Scope Datai of PSI Resonant Stripline BPM

4.5 The Noise Source

Transient mode noise source is accomplished by a Piece Wise Linear Voltage source (PWL). The voltage values for the PWL are caluclated by a Python script.

Python has a module `random` with a function `gauss`which calculates the voltage steps of our PWL source.

```
from python import gauss
for t in time:
    v.append(gauss(DC-Value,RMS-Value))
```

The script outputs a file noise.ckt containing a subcircuit definition with the PWL code.

```
.subckt noise 1
vnoise 1 0 tran pwl
+0.000e+00,8.215e-01,
+5.000e-10,-1.801e+00,
+1.000e-09,4.519e-01,
...
```

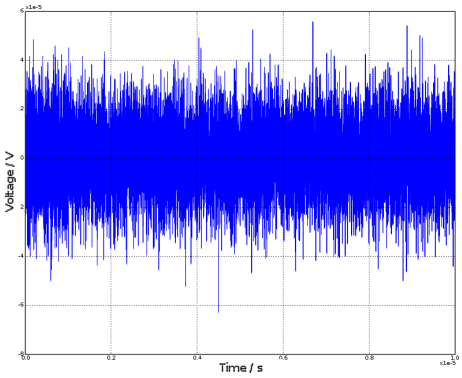

(a) Time Domain

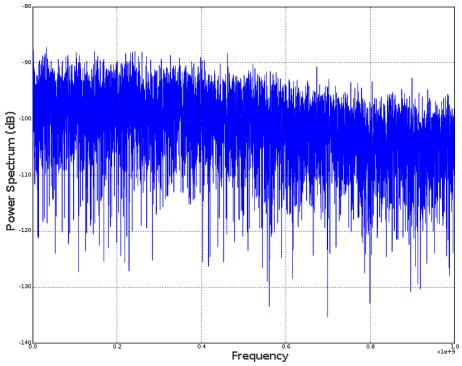

(b) Frequency Spectrum

Figure 10: Output Voltage of Noise Source

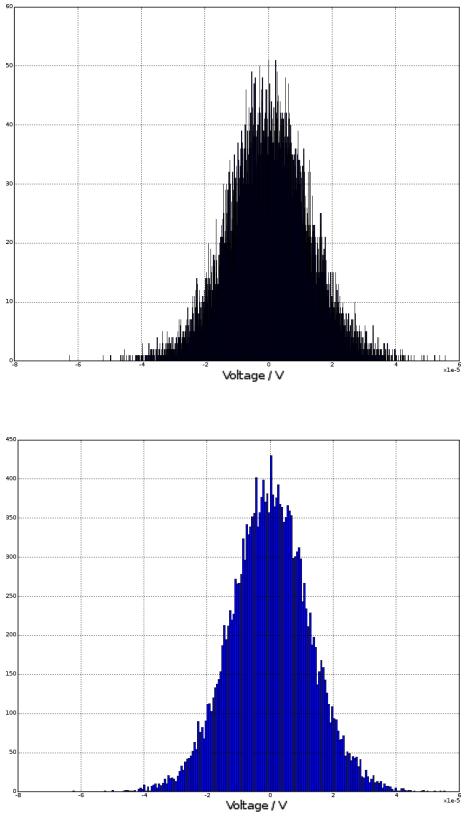

Figure 11: Histogram of simulated Noise Voltage

This subcircuit can be merged or included into the circuit simulation code and used in the following way.

```
.include noise.ckt
...
Xnoise 1 0 noise
```

The power slope towards higher frequencies is due to the large timesteps of 0.5 ns here.[7]

[7] Internally gnucap might use smaller timesteps but the timesteps of the output data were set to 0.5ns to reduce the data size.

4.6 Gnucap Simulation of the AM/PM Principle

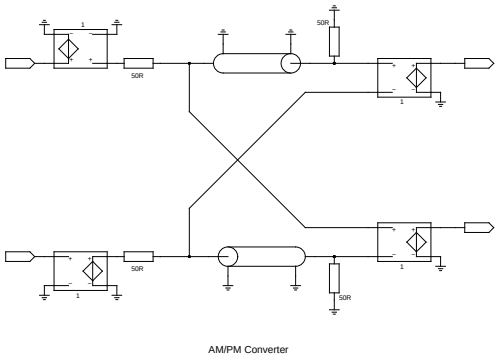

Figure 12: AM/PM Converter Circuit

The AM/PM-Converter is simulated as a circuit. The phase detector and the low pass filter are currently simulated in python using the results of the gnucap circit simulation of the AM/PM-Converter.

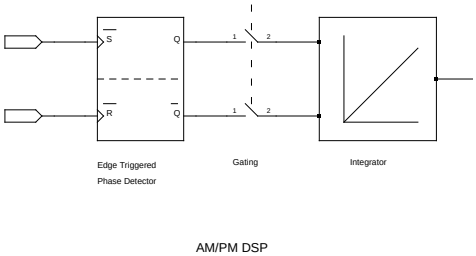

Figure 13: AM/PM Detector Schematic

The edge triggered RS flipflop with gated outputs perform better than other PD types.

4.7 Gnucap Simulation AM/PM Testcircuit

The beam position is sweept by running multiple simulations with different pulse generator voltages. Currently the voltages are calculated with the well known Δ/Σ formulae.

$$x = \frac{u_r - u_l}{u_r + u_l} \tag{1}$$

The noise generators are two independant[8] noise circuit files which where generated by noisegen.py.

[8] Using the same noise source for both inputs gives wrong results. In reality these two sources are uncorrelated.

4.8 Simulated Position Sweep of AM/PM BPM System

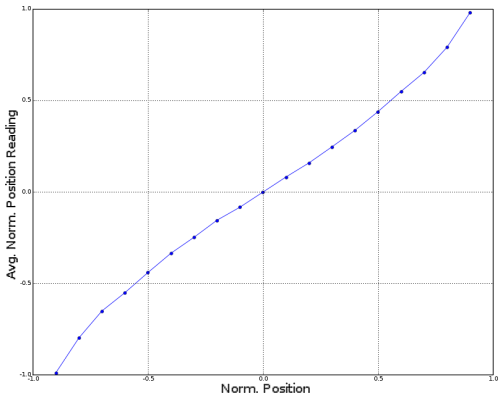

Figure 15: AM/PM converter Output at simulated Position Sweep

The monitor voltages are calculated by the simplified Δ/Σ-Method. Therefore the indicated normalized position is wrong for large offsets. Thus measurement results can not be directly compared to this plot. To be able to simulate the nonlinearities of the readout electronics and get a good comparison to the reality the position sweep generator must be updated to a more exact model.[2]

But for optimizing the circuit nonlinearities the via Δ/Σ calculated position sweep is sufficient.

According to Cocq [4] the output phase and therefore also the output voltage should follow the following formula:

$$\varphi = \arctan \frac{V_a}{V_b} \tag{2}$$

As this is only the phase of one signal, but we are using phase difference between the two the formula for the output phase is:

$$\varphi = \arctan \frac{V_a}{V_b} - \arctan \frac{V_b}{V_a} \tag{3}$$

This gives a detector characteristic as shown in figure 16.

At large positon offsets the simulation and theory are different. The reason for this is probably the following.

The theoretically formula is achieved by considering one frequency and a phase shift of 90 degrees. But the simulation as the real system uses a broadband signal. The transmission line has no constant phase shift but a constant time delay. So the phase shift increases with frequency.

$$\begin{aligned} \varphi = & \, arccos \frac{u_l - u_r \cos \omega t}{\sqrt{u_l^2 + u_r^2 + 2u_l u_r \cos \omega t}} \\ & - arccos \frac{u_r - u_l \cos \omega t}{\sqrt{u_l^2 + u_r^2 + 2u_l u_r \cos \omega t}} \end{aligned} \tag{4}$$

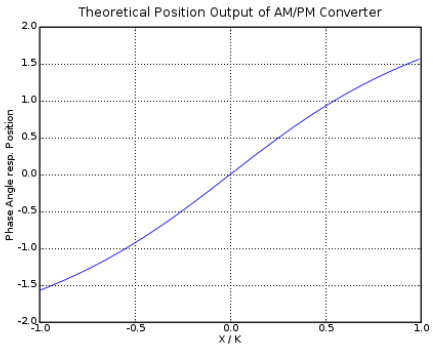

Figure 16: Theoretical AM/PM Detector Characteristic

Figure 17 shows this graphically for transmission line lengths of 0.5ns.

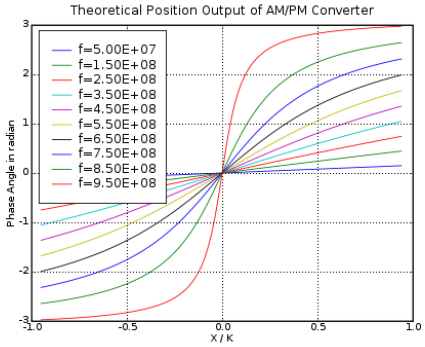

Figure 17: Theoretical Position Ouput of AM/PM Converter at various frequncies

It depends on the phase detector characteristic and the powerdensity vs. frequency how much influence this has on the linearity of the position measurement.

4.9 Difficulties in the Simulation of the AM/PM-BPM System

Due to the small time differences of the output pulse of the AM/PM-Converter the simulation step size needs to be quite small. This results in a large simulation time and a lot of memory consumption.[9]

[9]The actual simulation time step size is controlled by Gnucap resp. Spice.

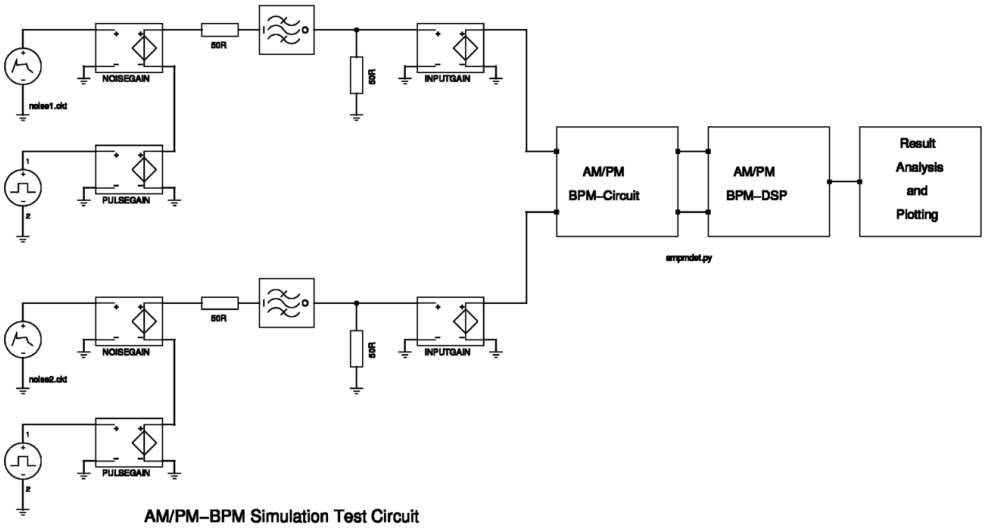

Figure 14: AM/PM Test Circuit

4.10 Calculating the Signal to Noise Ratio of the BPM

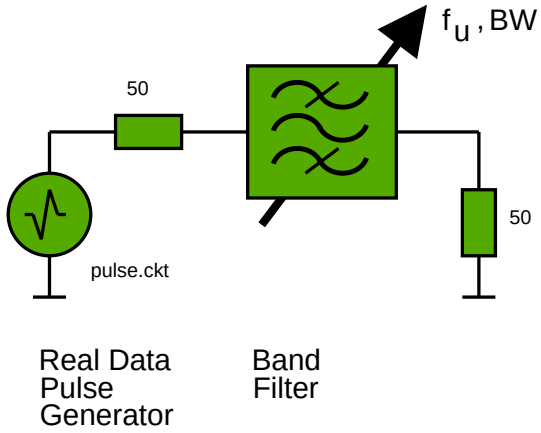

Figure 18: Pulse Filtering

`pulse.ckt` is created using data acquired with a 20GSps Tektronix Scope from BPMs installed at FLASH. The noise power is caluclated by

$$P_N = kTf_{BW} \tag{5}$$

This is the worst case assuming matching between source and load.

4.11 Large Button BPM

The BPM from which this signals are acquired is an experimental BPM intended for installation in the cold section of XFEL. It is currently installed at FLASH at 13ACC7. The pipe diameter is 78 mm and the button diameter 8 mm.

Using the Neumann electronics described in section 5 a resolution of 20um was acchieved. Due to level mismatch a 6 dB attenuator had to be used. With better level matching (ajusted amplifier gain) a resolution of 10um is to be expected. This means the SNR was around 66 dB. According to figure 4.11 with an upper frequency limit of 300 MHz we should get 83 dB.

Several reasons account for this mismtach. First, the SNR of the ADC board used, is limited. Also the band-filter used in this simulation is a simple resonant circuit. Thus the suppression of the high frequency components is rather weak, so this components will still contribute to the signal power. The electronics we used also has only a simple resonant ciruit for filtering. But the active components have their frequency limits also in the range of 300 to 600 MHz. Finally the SNR depends on the detector circuit which is shown in section 5.4.

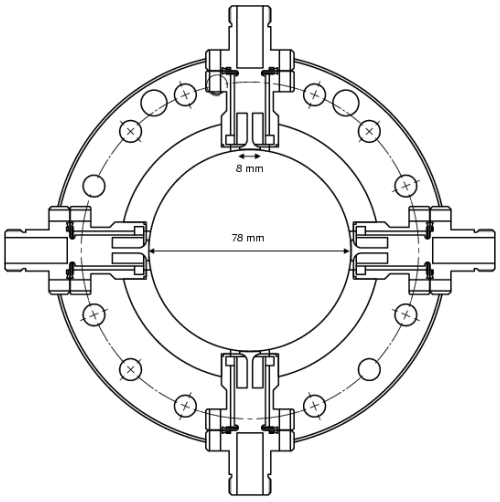

Figure 19: Large Button BPM Mechanical Drawing

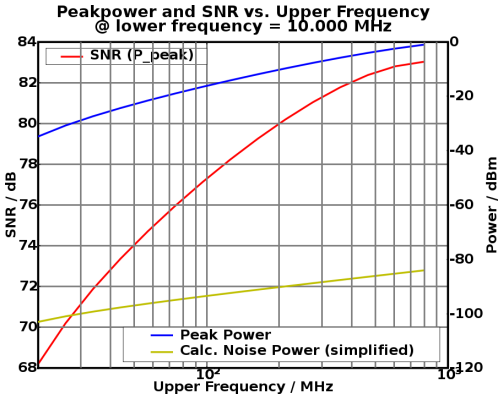

Figure 20: Upper Frequency Sweep at Large Button BPM

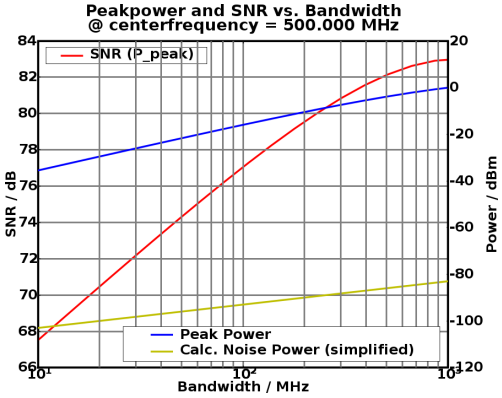

Figure 21: Bandwidth Sweep at Large Button BPM

4.12 Small Button BPM

The signals of the following diagrams are taken from BPM used at many places in FLASH. The data are taken

from 21SEED. It has a pipe diameter of 9 mm and a button diameter of 1.6 mm.

As we use here an ADC with only 8 bit our measurement results are clearly limited by the ADC.

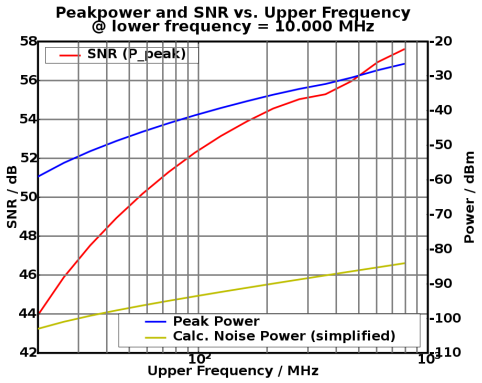

(a) Upper Frequency Sweep

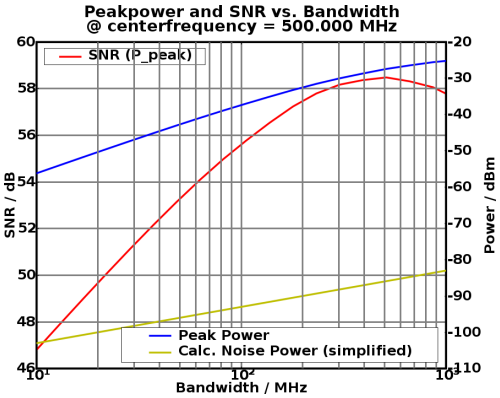

(b) Bandwidth Sweep

Figure 22: Small Button BPM

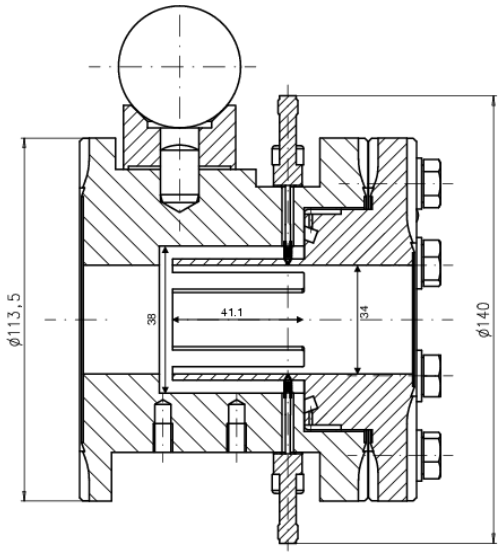

Figure 23: Resonant Stripline BPM Mechanical Drawing

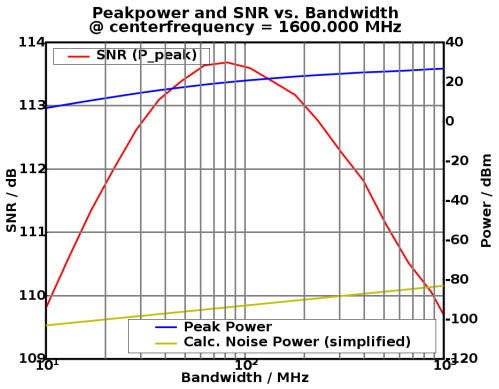

Figure 24: Resonant Stripline BPM Bandwidth Sweep

At low frequencies the SNR increases with approx. 2dB/Octave. The decrease above 80MHz is due to the bandlimiting of the stripline resonator.

Increasing bandwidth increases SNR.

4.13 Resonant Stripline BPM

The resonant stripline BPM is a new BPM design developed by PSI to be used at XFEL in the fast feedback system. It consists of four resonant striplines with a length of 41.1mm. The beam pipe diameter is 34mm.

No electronics is installed at this BPM yet.

5 Delay Multiplex Single Path Technique

The Delay Multiplex Single Path Technique[10] developed by Rudolf Neumann is used at HERA quite a long time without any troubles. First evaluations at FLASH with only minor modifications of the electronics show very good results - even on the small pulses there.

Further simulations concentrate on this technique.

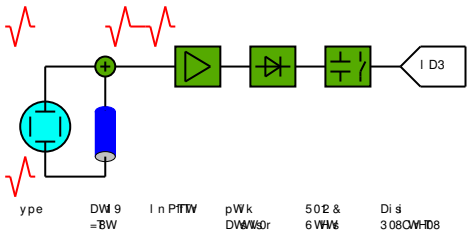

Figure 25: Delay Multiplex Single Path Technique

5.1 How the Delay Multiplex Single Path Technique works

The Delay Multiplex Single Path Technique (Neumann Prinzip) serializes two or more pickup buttons on one processing channel. Thus channel parameters (attenuation, frequency response, phase shift, ...) are the same for all pulses and resulting in increased accuracy and reduced drifts.

The serialization is done by a simple passive network consisting of a delay line and a power combiner. One of the pulses travels through the delayline before it is added to the processing channel. There are no mechnical or electrical switches required.

The serialization also gives good low frequency interference suppression because taking the difference of the two pulses cancels out slowly variing interferences.

This article does not cover the simulation of the delayline properties, but concentrates on the second feature of the Neumann Prinzip: the peak (hold) detector.

5.2 Peak (Hold) Detector

As the bunch length at FLASH and XFEL is much shorter than the button diameter. The time distance between the two edges of the pulse and therefore also the time distance between the two differentiated output pulses depends mainly on the button dimensions and is therefore quite small. The spectral power maximum is thus located in the microwave frequency range. There are several ways to downconvert this signal to lower frequencies for further processing. One can use a mixer (voltage multiplier) and an local oscillator to move the high energy high frequency range to DC or a intermediate frequencies. There are some issues to take care of, e.g. phase stability compared to the input signal.

The simplest way to downconvert the high frequency signal is a diode detector. Clipping the negative pulse results in a DC offset which can be sampled - after low pass filtering - by an ADC. The diode detector can be considered as a mixer, which uses its own input signal as LO (no phase problems with the LO).

The diode detector can also be viewed as a self triggered sample and hold circuit. The peak *opens* the diode channel (i.e. *connecting* the switch) and the hold capacitor is charged. When the pulse decays the diode channel *closes* (the switch *interrupts*) and the hold capacitor holds the peak voltage for sampling with an ADC. There is no jitter problem as at other sample and hold circuits.

5.3 A Short History of Delay Multiplex Single Path Technique at DESY

For the realization of PETRA in 1978 the serial BPM signal processing was used for the first time. When HERA was built around 1986 the ESPM-ADC was developed. The four pickup signals of the BPM are serialized by a four channel delay line system. The amplitudes of those serialized signals are then captured by a fast peak detector circuit with self triggered reset. The output of this peak detector is converted by a FLASH ADC. At HERA there are about 300 BPM electronics of this type installed. Around 1988 120 units of this system were installed at PETRA and by and by a lot of other places on the DESY site were equipped with this technique. Around 450 units totally are running on the DESY site.

In 2002 six units of the Neumann electronic were installed at the A0 photoinjector at Fermilab [1].

At the start of operation of the TESLA Test Facility TTF in 1997 the first working BPM system was the Neumann electronics.

In the year 2006 experiments for increased resolution of Neumann electronics at FLASH targeting XFEL were started. The current results of this experiments are pretty good and match simulations and theory mostly well.

[10] This technique was formerly called Time Multiplex BPM Technique. As the Bergoz System is sometimes also refered to as Time Multiplex Technique we changed the name to avoid ambiguities.

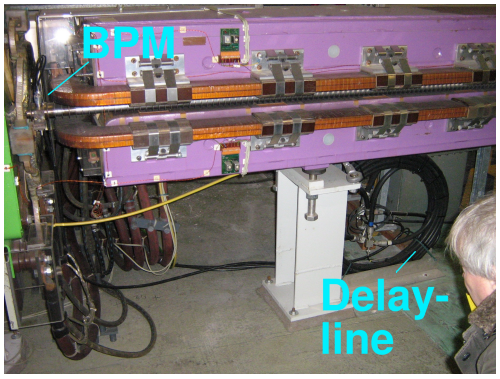

Figure 26: Neumann BPM at DESY

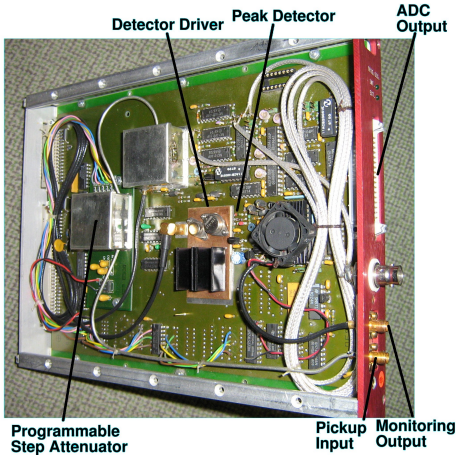

Figure 27: Neumann BPM Electronics

5.4 Comparing various *Ideal* Detectors

To evaulate more or less real detector circuits or their simulations one needs to find out how much a real detector degrades the noise performance of the system compared to an ideal e.g. optimal BPM detector.

How does the optimal BPM detector looks like?[11]

The following pseudo-ideal detectors were compared:

Pulse Energie Detector	$U_{out} = \int u_t^2 dt$
Absolute Voltage Integrator	$U_{out} = \int \lvert u_t \rvert dt$
Peak Voltage Detector	$U_{out} = \hat{u}_t$
Double Peak Voltage Detector	$U_{out} = \hat{u}_t - \check{u}_t$

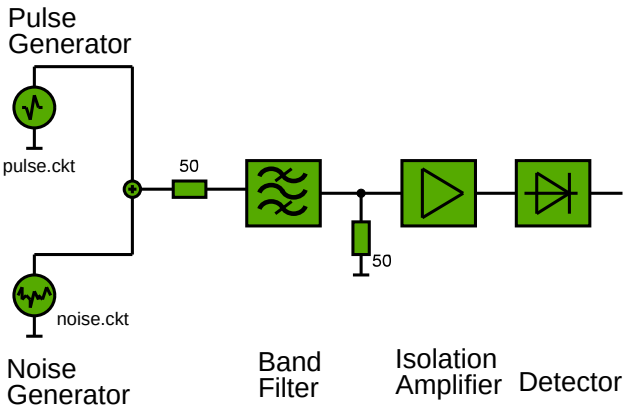

Figure 28: Noise Detector Test Circuit

5.5 Simulation Results

Detector Type	Relative RMS Noise
Pulse Energie Detector	$116 \cdot 10^{-6}$
Absolute Voltage Integrator	$67 \cdot 10^{-6}$
Peak Voltage Detector	$65 \cdot 10^{-6}$
Double Peak Voltage Detector	$49 \cdot 10^{-6}$

The peak voltage detector and the double peak voltage detector take the measurements at the point, where the SNR is at its optimum. While the two integrators take measurements also at the points of lower SNR.

5.6 Noise Performance of Real Detectors

A peak detector circuit and double peak detector circuit with a HSMS 2850 diode are simulated in the same way as the previous ideal detectors.

[11] The **ideal** detector is probably something like a matched filter using every bit of the pulse but weighting it against the expected amplitude e.g. SNR

5.6.1 Double Peak Detector

The peak detector as described in section 5.2 uses only one peak of the input pulse. Figure 29 shows a double peak detector which uses the positive and the negative peak of the input pulse. As we are taking the difference between the two peaks, i.e. measuring the peak-to-peak voltage, low frequency interferences are canceled out[12]. This cancellation not only works for artifical interferers but also on thermal noise.

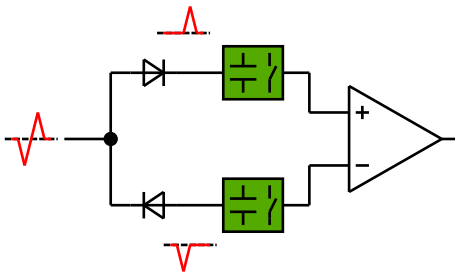

Figure 29: Double Peak Detector Schematic

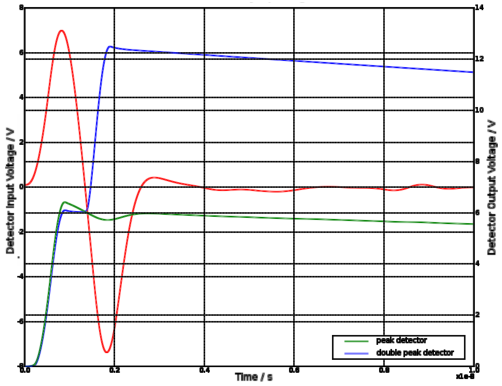

Figure 30: Comparison of Detector Voltages

5.7 Simulation Description

The peak detector and the double peak detector are compared by applying idealized pulse source. The subsequent pulses represent the a sequence of output pulses of a button pickup excited by a zero offset beam. The output voltage of a noise source as described in section 4.5 is added to the pulse voltage.

[12] The Neumann Prinzip already includes such an cancelling mechanism by serializing the pulses on one line and caluclating difference over sum. But the double peak detector shifts the range to higher frequencies.

5.7.1 Simulation Results

Detector Type	Relative RMS Noise of simulated Circuit	Relative RMS Noise of Ideal Detector
Peak Voltage Detector	$94 \cdot 10^{-6}$	$65 \cdot 10^{-6}$
Double Peak Voltage Detector	$64 \cdot 10^{-6}$	$49 \cdot 10^{-6}$

The ratio of the output noise of double peak detector and peak detector is 1.47 which is nearby $\sqrt{2}$, which is the theoretically expected improvement factor[13]. The *real* detectors behave worse than the *ideal* ideal detectors. Possible reasons are:

- Coupling of noise power across the diode capacitance.
- Nonlinearity of the diode.

5.7.2 Comparing Diodes

The diode capacitance and resistances influence the detector performance. Also the $i(v)$ curve might have an impact on the noise performance. This must be evaluated by further simulations at beam positions other than zero.

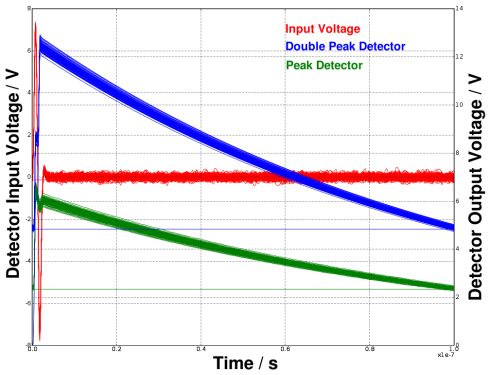

Figure 31: Detector with Diode BAT 17

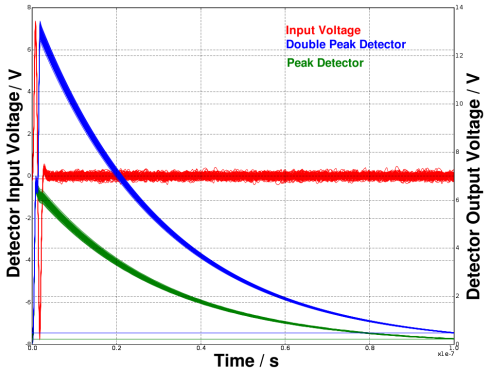

[13]Thanks to Hermann Schmickler for this hint at the workshop

Figure 32: Detector with Diode HSMS 2850

5.7.3 Diode Comparison Results

RMS Error of Normlized Position Reading

Detector - Diode	BAT 17	HSMS 2850
Peak Detector	$10.7 \cdot 10^{-3}$	$10.5 \cdot 10^{-3}$
Double Peak Detector	$8.11 \cdot 10^{-3}$	$7.97 \cdot 10^{-3}$

- The double peak detector shows a better noise performance.
- Diode influence must be further invesitgated.

5.8 Charge and Position Sweep Simulations

These simulations are done with a pure voltage source.

Due to the nonlinearities[14] of the detector diodes, the position reading error increases with decreasing input voltage i.e. beam charge.

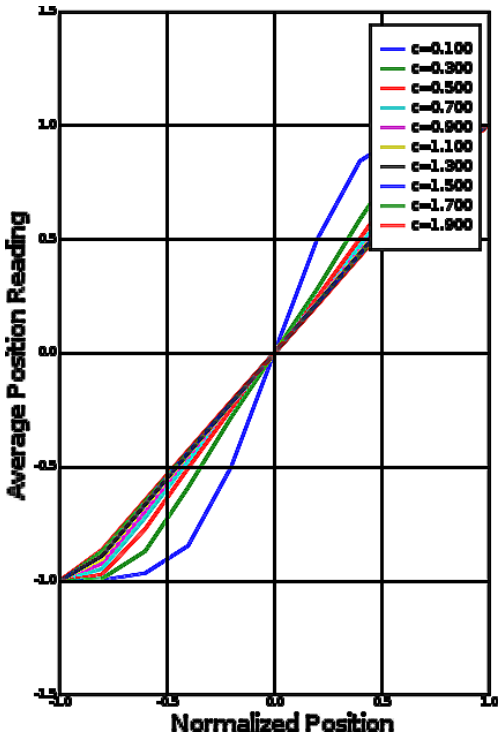

Figure 33: Position Reading versus simulated Position and Charge

5.9 Nonlinearities of Peak Detectors

The source impedance of the detector driver is a critcal design issue due to nonlinearities of the diodes. Amplitude nonlinearity and possibly the sensitivity of the system depend on it.

The intention of the BPM electronic is to measure the voltage of the pickup pulse, U_0 in figure 35. As we are interested in the ratio of the two pickup voltages a constant scaling factor does not concern us.

$$x = \frac{\not{S}u_r - \not{S}u_l}{\not{S}u_r + \not{S}u_l} \tag{6}$$

A subtraction of a constant voltage is more critical.

$$x = \frac{(u_r - \Delta u_r) - (u_l - \Delta u_l)}{(u_r - \Delta u_r) + (u_l - \Delta u_l)} \tag{7}$$

If $\Delta u_l = \Delta u_r = \Delta u$ the equation reduces to

[14]Here the diode voltage itself

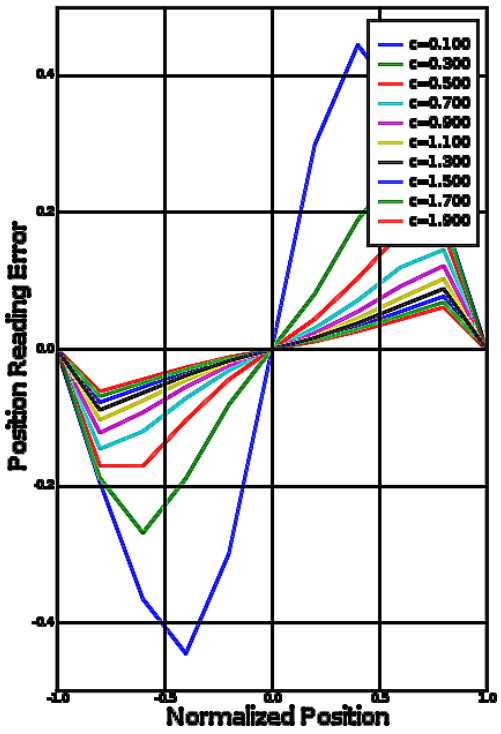

Figure 34: Position Reading Error versus Position and Charge

$$x = \frac{u_r - \Delta u - u_l + \Delta u}{u_r + u_l - 2\Delta u} \tag{8}$$

$$x = \frac{u_r - u_l}{u_r + u_l - 2\Delta u} \tag{9}$$

The different denominator causes a different slope of detector characteristic. Also the the slope is now charge dependent.

This charge dependency caused by the voltage drop across the diode can be seen around the center position in figure 33.

At very large offsets in that figure the slope rapidly decreases, especially at low charges. This is caused by the diode nonlinearity. The voltage drop across the diode depends on the input signal strength. Due that fact the voltage drops accross the diodes are now different: $\Delta u_l \neq \Delta u_r$.

To avoid the charge dependency one can simply add the diode voltage u_D to the read voltage, here u_C, like it is done in the HERA BPM electronics. But due to the hard requirements for XFEL care must be taken.

Obviously a centered beam is not affected by the diode voltage drop at all. Due to the single path processing this drop influences both pulses in the same way. Note that figures 38 and 40 show no errors at zero offset beam position.[15]

[15]With a two channel processing we might have different voltage

The proposed cold BPM for XFEL (figure 4.11) has a monitor constant of approx. K = 18 mm. A beam offset of 6 mm produces a pickup voltage ratio of 2. Assuming 2.3V peak voltage of the larger pulse at the detector input a change in temperature of only one degree causes a diode voltage drift of 2.3K. This results in an readout error of 8um, which seems not to be acceptable for XFEL[16]. Therefore the prototype electronic will have a second thermally coupled diode driven by a DC current source where the diode voltage will be measured to calculate a more accurate position reading. Due to the dynamic properties of the diode the actual voltage drop across the diode will differ from the reference diode. Further simulations should show the difference between these two voltages and also its dependency to temperature and input signal variations.

As shown above the voltage drop of the diode is not only dependent on temperature but also on diode current. As this current is dependent on the input voltage the position readout error varies with beam charge and beam position offset. This nonlinearity can be compensated by digital postdistortion of the pulse voltages.

The complete system will not have only the detector diode as a nonlinear element. There are also various amplifiers (LNA, detector driver, buffer amplifier...) which distort the input pulses, i.e. the gain depends on the input voltage and thus the input/ouput of the amplifier is nonlinear and the position reading varies with input voltage, i.e beam charge and beam offset. These nonlinearities can also be corrected by digital postdistortion of the read pulse voltages.

Due to discharging of the hold capacitor by diode parallel resistance and buffer amplifier resistance resp. bias current the roof of the detector output voltage is not flat but drops down with time (figure **??** and 5.7.2). When more than one ADC samples are used to measure the pulse voltage the postdistortion factor applied to the current sample must not be calculated from this sample but from the first sample of the recent pulse. Maybe it is possible to use the average voltage of all pulse samples to calculate the correction factor. This correction factor must then be applied to each individual sample of the pulse.

5.10 Source Impedance affects the Detector Linearity

In order to reduce the influence of the diode voltage drop the input source can be transformed up to higher impedances. This increases the voltage U_D in figure 35 therewith reducing the relative portion of the diode voltage drop.

In this simulations the generator voltage and resistance are sweept providing a constant maximum output power.

drops on each channel.

[16] Approved specifications are not available yet

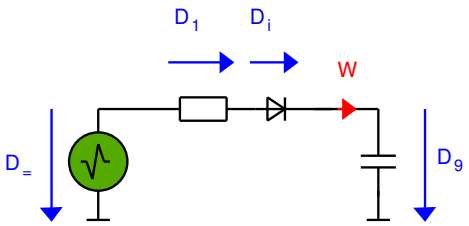

Figure 35: Voltages at the Diode Detector

5.11 Diode Currents at different Source Impedances

Driving the detector circuit with a current source instead of a voltage source removes the diode voltage dependencies described in section 5.9. If i_{src} is proportional to the pickup signal the capacitor voltage ist the integral of this input.

$$u_C = \frac{1}{C}\int i_{src} \quad \text{for} \quad i_{src} > 0 \tag{10}$$

This detector then is very similar to the absolute voltage detector simulated in section 5.4. In this case we are not concerned by any nonlinear effects or voltage drops of the diode.

The practical use of this current charge detector is limited by the stray capacitances of components and PCB. Even when there is no pulse the current source would charge the hold capacitor with noise and reflected pulses. It is one of the advantages of the peak detector that reflected portions of the pulse, which are lower than the original pulse do not charge the capacitor and therefore do not interfere the position reading.

For this reasons the simulations where limited to source impedances up to 500 Ω.

The diode currents for different source impedances but with constant input power are shown in figure 36. The black triangle forming lines show the input voltage prior to the transformer, i.e. the pickup voltage - idealized of course to clearly show the effects. The simulation object was a double peak detector. Both diode currents are shown.

The bent peak of the diode current at low impedances is not caused by diode nonlinearity but by the decreasing voltage difference between source and capacitor. The effect of the voltage drop is visible at the beginning of the first slope of i(D1). While the source voltage is low the current does not follow that voltage directly. At that time i(D2) is the reverse current of D2. It consists of a hunch caused by the diode capacitance and flat shoulder caused

by the diode resistance. Both effects increase with rising impedance.

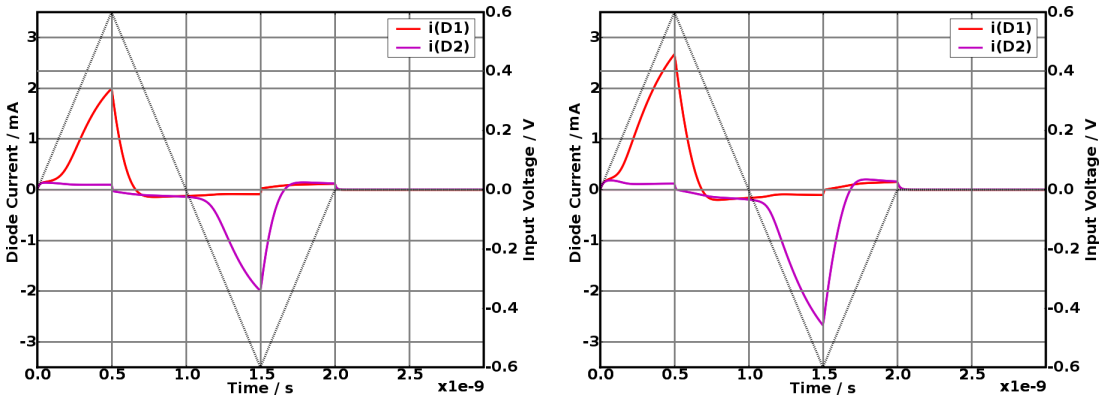

(a) $R_s = 25\Omega, V_s = 0.71V$

(b) $R_s = 50\Omega, V_s = 1.0V$

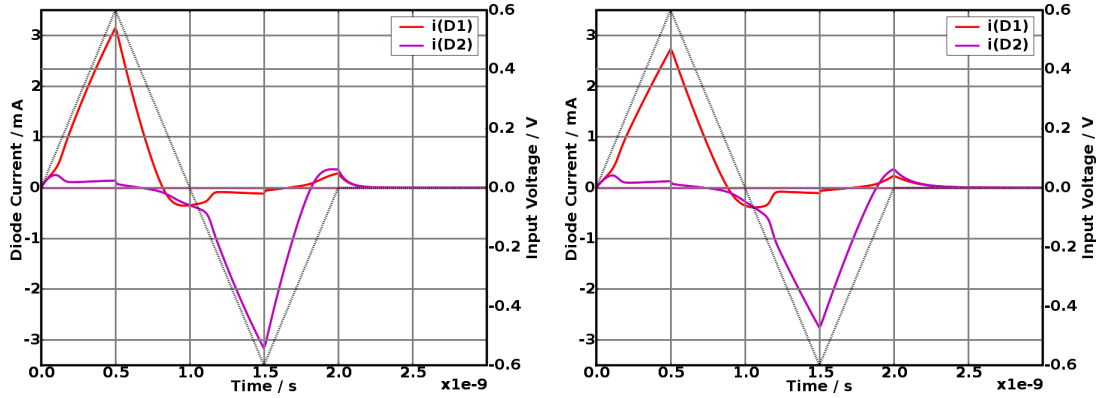

(c) $R_s = 250\Omega, V_s = 2.24V$

(d) $R_s = 500\Omega, V_s = 3.16V$

Figure 36: Diode Currents at different Source Impedances

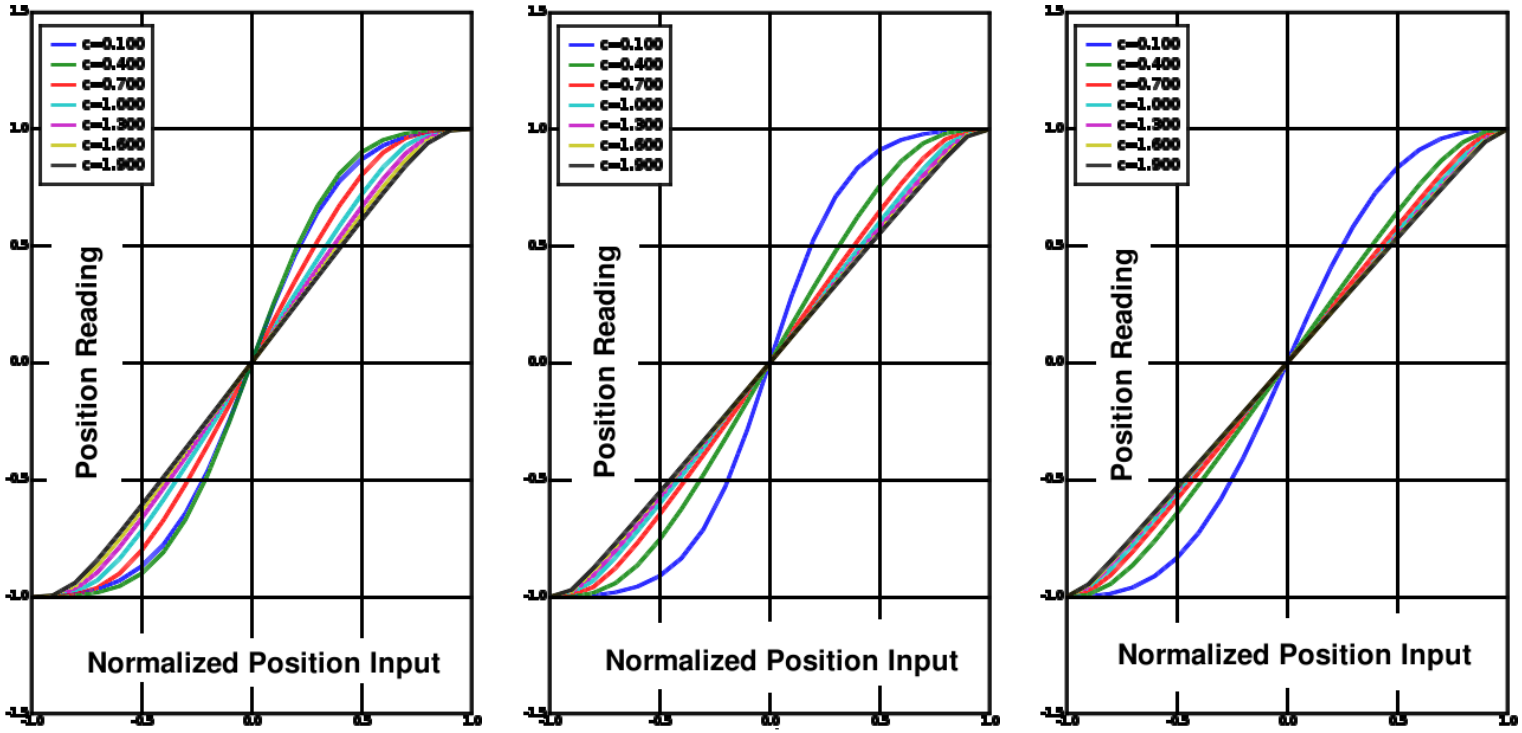

(a) $R_s = 10\Omega, V_s = 0.45V$ (b) $R_s = 50\Omega, V_s = 1.0V$ (c) $R_s = 250\Omega, V_s = 2.24V$

Figure 37: Position Reading for Position and Charge Sweeps with various Driver Impedances

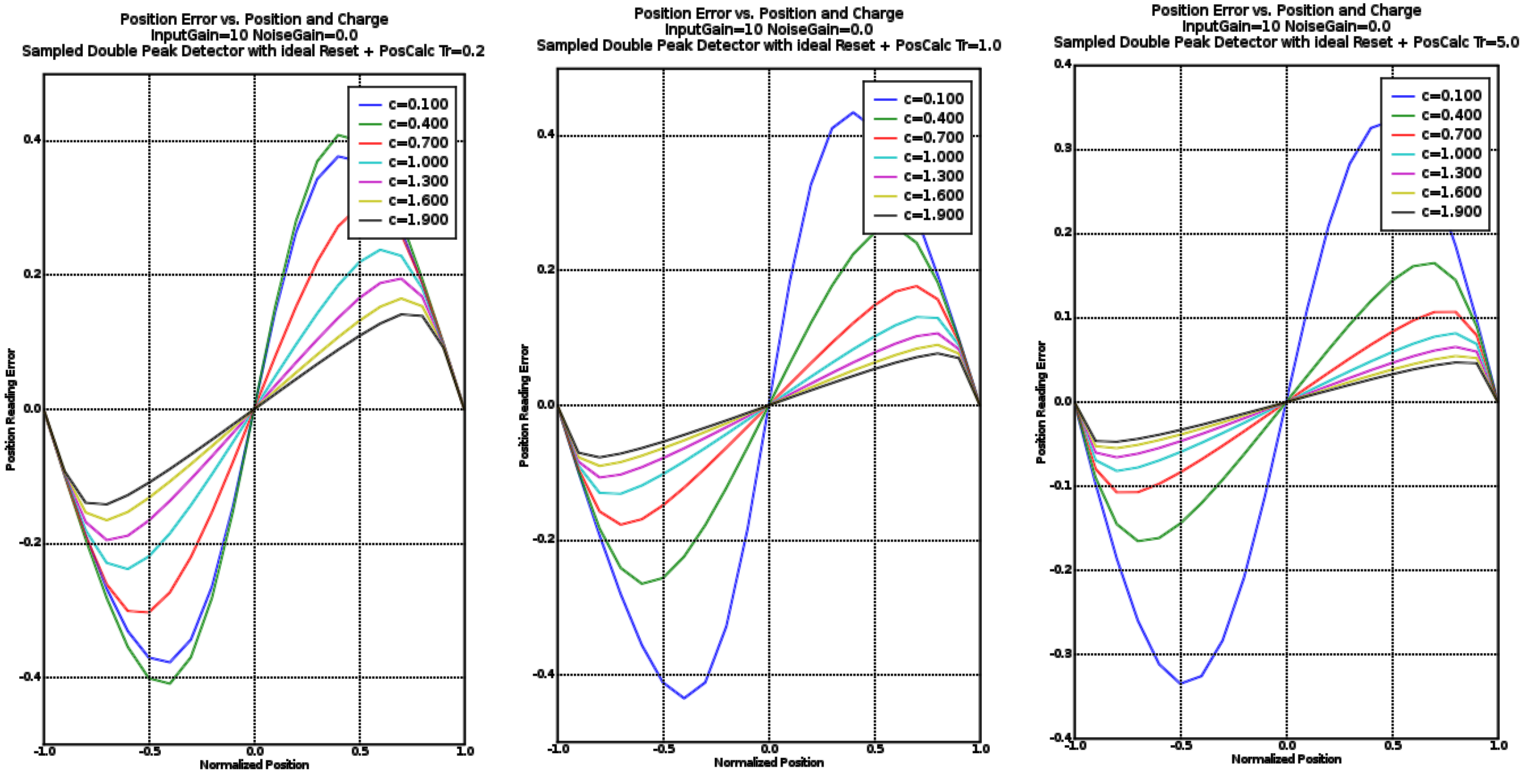

(a) $R_s = 10\Omega, V_s = 0.45V$

(b) $R_s = 50\Omega, V_s = 1.0V$

(c) $R_s = 250\Omega, V_s = 2.24V$

Figure 38: Position Reading Errors for Position and Charge Sweeps with various Driver Impedances

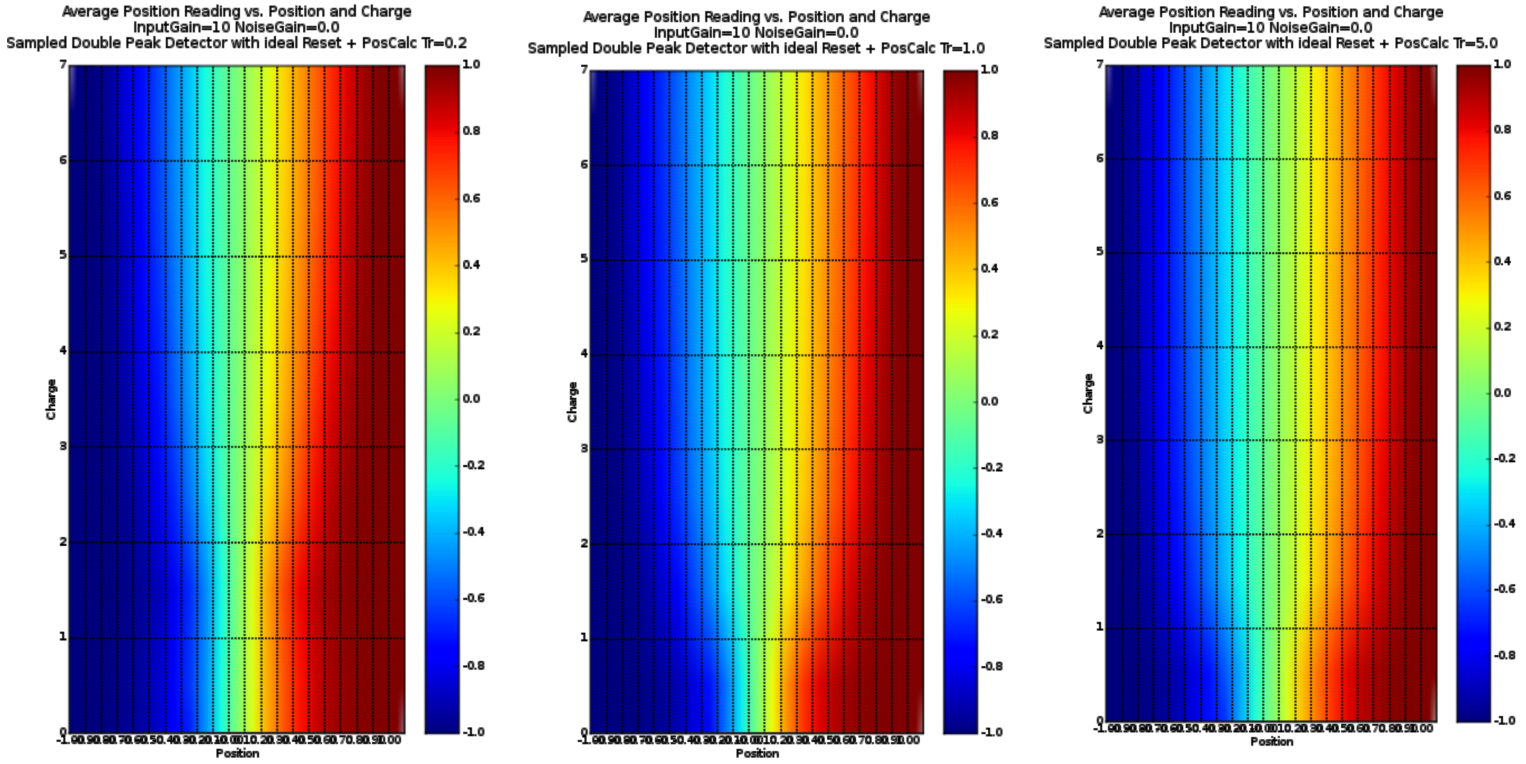

(a) $R_s = 10\Omega, V_s = 0.45V$

(b) $R_s = 50\Omega, V_s = 1.0V$

(c) $R_s = 250\Omega, V_s = 2.24V$

Figure 39: Position Reading for Position and Charge Sweeps with various Driver Impedances

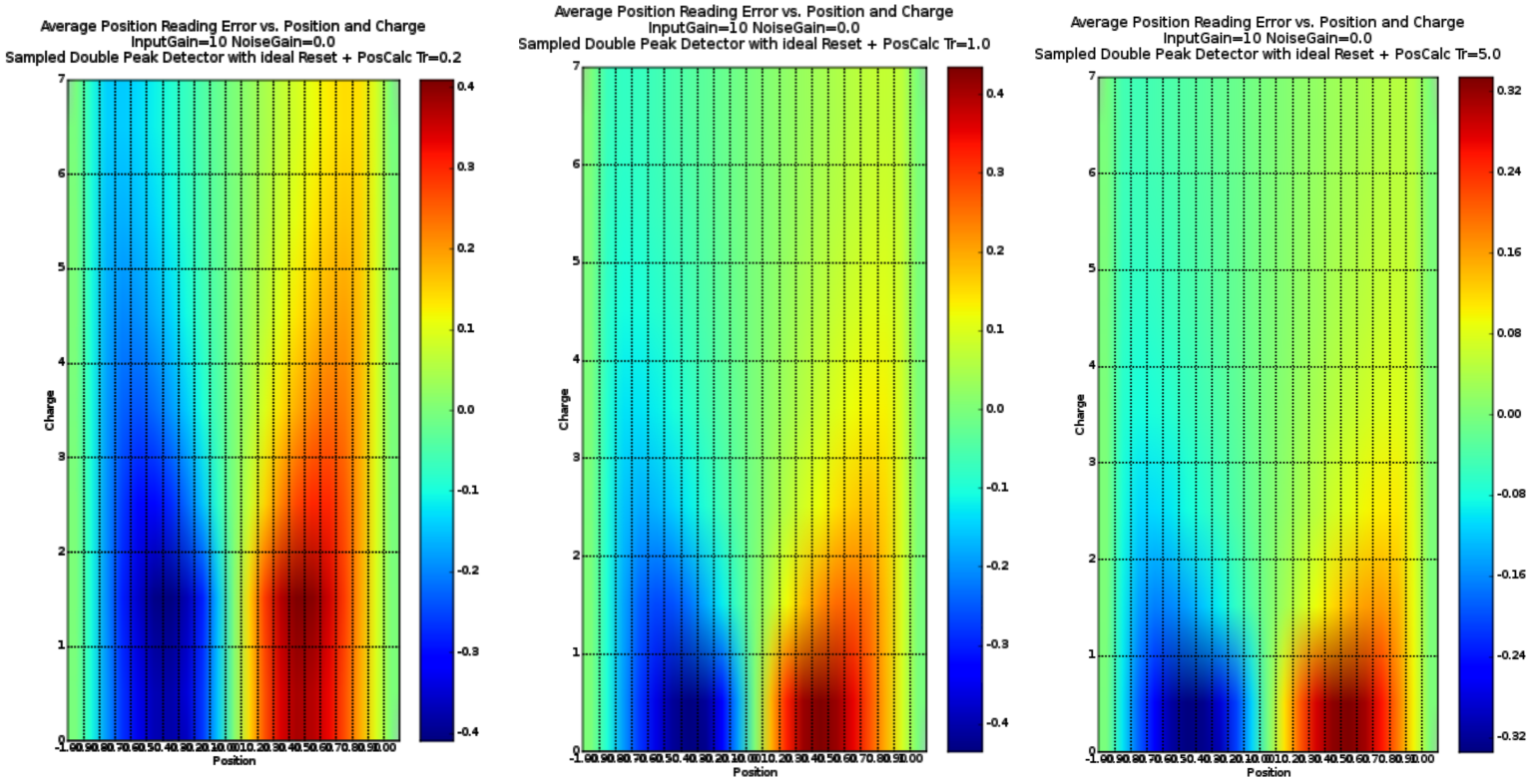

(a) $R_s = 10\Omega, V_s = 0.45V$ (b) $R_s = 50\Omega, V_s = 1.0V$ (c) $R_s = 250\Omega, V_s = 2.24V$

Figure 40: Position Reading Errors for Position and Charge Sweeps with various Driver Impedances

5.12 Using Peak Detectors for Ringing Pulses

Driving a peak detector with an high impedance source changes the properties of a peak detector from *absolute* to *relative* or *local* peak detector. As described in the previous section the current source driven diode detector also integrates the subsequent pulses to the hold capacitor. This was considered bad for button type BPMs. In case of ringing BPMs this is a wanted feature. Figure 41 shows the diode currents for a ringing input signal at different source impedances. The plot show that the subsequent ringing pulses force additional charging currents. Which increase the capacitor voltage, i.e. the output voltage shown in figure 42. Figure 43 shows the same curves including the decay when the charge current falls below the discharge current.

An increasing output voltage does not necessarily mean an increasing SNR. As the level of the subsequent pulses are lower, the SNR there is worse. There must exist a certain integration time length for optimum SNR. Also the reflections on the cables should be taken into account.

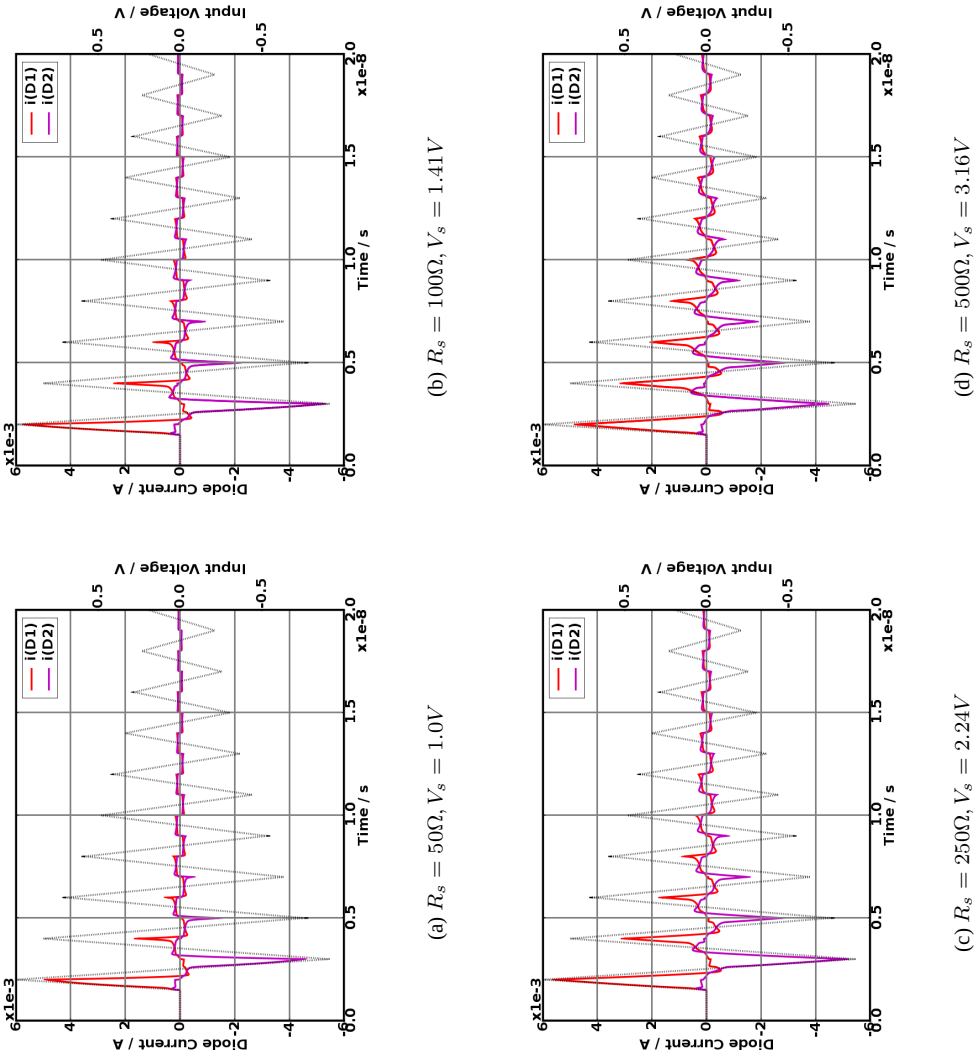

(a) $R_s = 50\Omega, V_s = 1.0V$

(b) $R_s = 100\Omega, V_s = 1.41V$

(c) $R_s = 250\Omega, V_s = 2.24V$

(d) $R_s = 500\Omega, V_s = 3.16V$

Figure 41: Diode Currents with Input Pulse Ringing

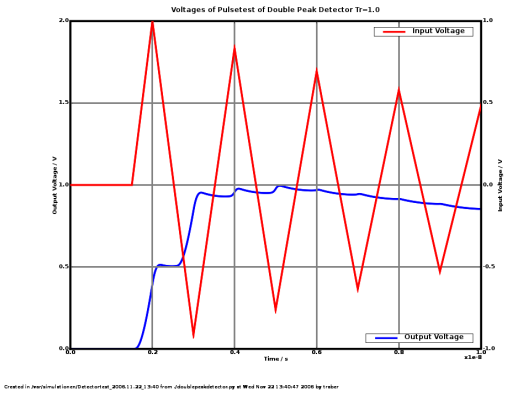

(a) $R_s = 50\Omega, V_s = 1.0V$

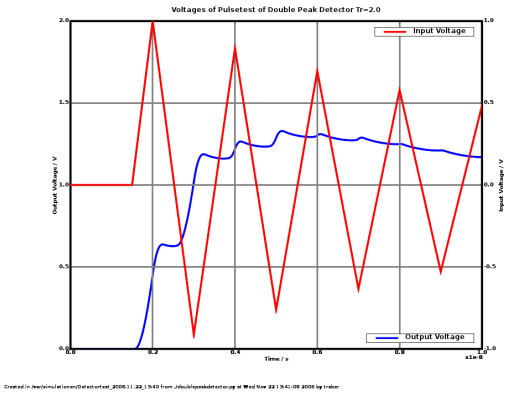

(b) $R_s = 100\Omega, V_s = 1.41V$

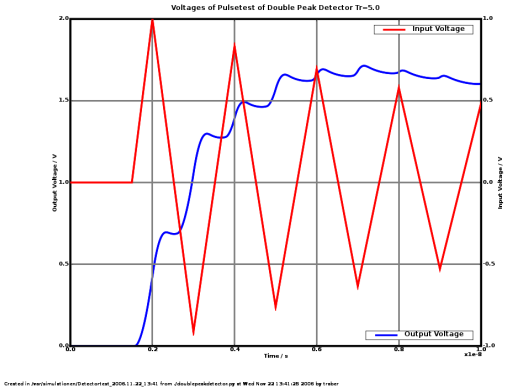

(c) $R_s = 250\Omega, V_s = 2.24V$

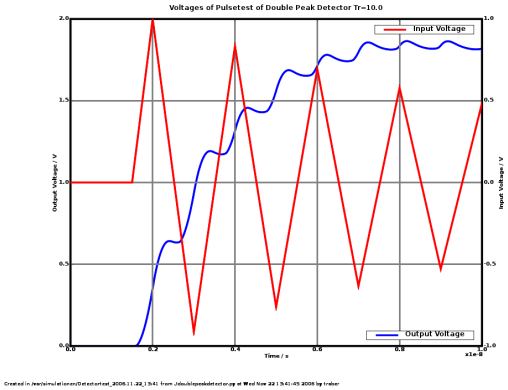

(d) $R_s = 500\Omega, V_s = 3.16V$

Figure 42: Output Voltages with Input Pulse Ringing

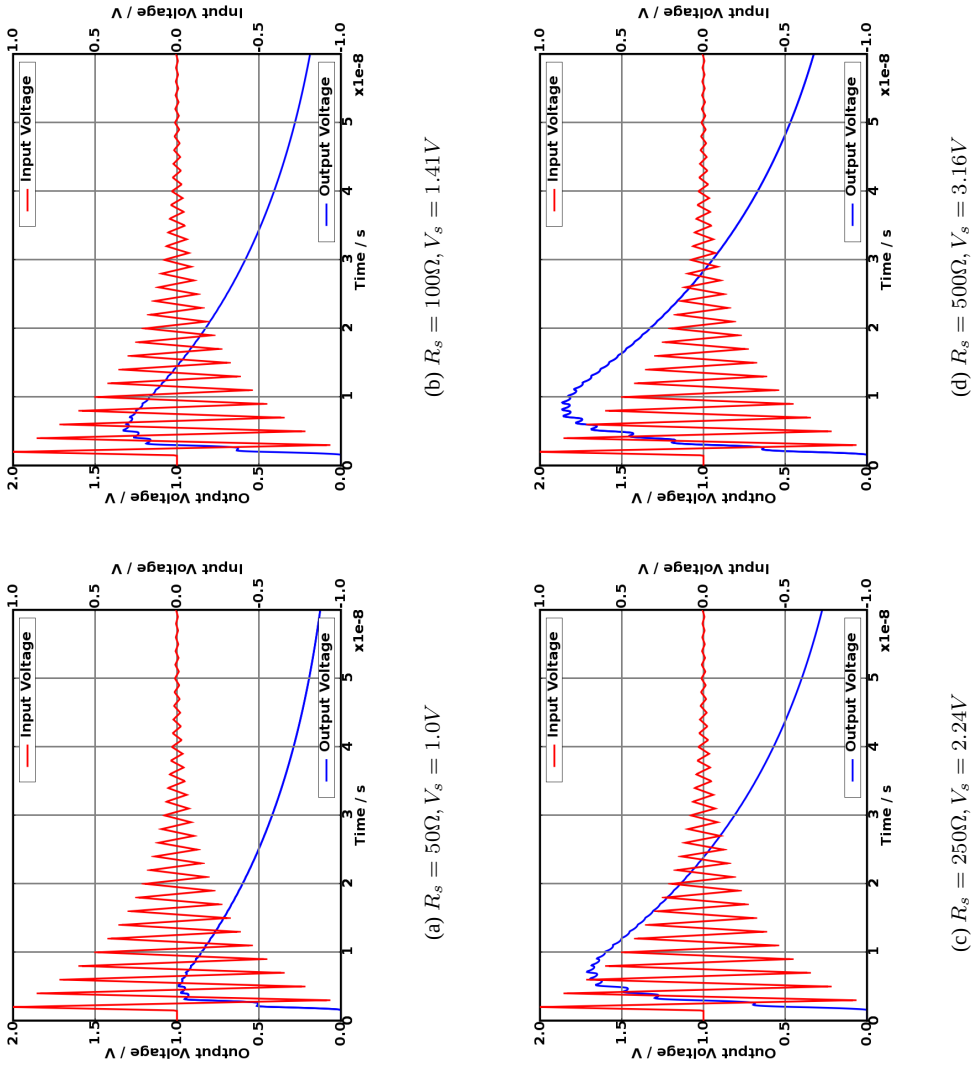

(a) $R_s = 50\Omega, V_s = 1.0V$

(b) $R_s = 100\Omega, V_s = 1.41V$

(c) $R_s = 250\Omega, V_s = 2.24V$

(d) $R_s = 500\Omega, V_s = 3.16V$

Figure 43: Output Voltages with Input Pulse Ringing

6 Noise and Distortion Analysis of Cascaded Systems

Cascade is a command line tool to calculate the noise and distortion perfomance of cascaded amplifiers. It works similar to agilent appcad and easier to use than ADS budget analyzer.

Gschem is the schematic entry of the GNU EDA Tools. It comes with a symbol library to create block diagrams for cascade. The schematic is then converted into the cascade format by **gnetlist**.

For the tests in FLASH the gain of the HERA electronics needed to be adapted.

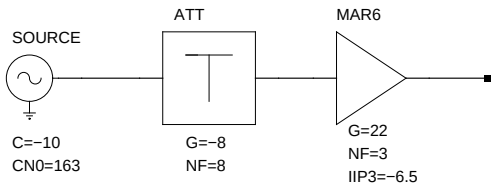

Figure 44: MAR6 Amplifier

Calculated Noise Figure = 11 dB

Substituting the MAR6 against MAR2 and reducing the input attenuator due to the lower amplifier gain im proves the noise figure by 7 db.

At the prototype we got a resolution improvement of about the same value.

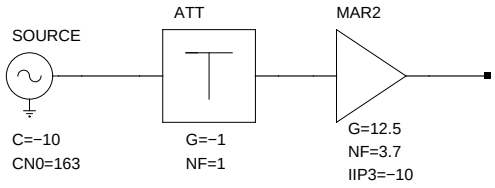

Figure 45: MAR2 Amplifier

Calculated Noise Figure = 4 dB

This example of cascade use was quite trivial. Cascade is capable of calculating noise and distortion performance of larger systems and is therefore an interesting evaluation tool for quick estimations of RF system performance.

7 Conclusions

7.1 Circuit Design

- Increasing the upper frequency limit will increase resolution.
- Changing from peak detector to double peak detector will improve resolution.
- Using high impedance detector driver will decrease nonlinearities and allows to take advantage of pulse ringing.
- It is possible to use the Time Multiplex BPM System not only at button BPMs but also at resonant striplines.[17]
- Todo: Temperature simulations.
- Is it possible/desirable to have an environment to simulate the complete BPM electronics and test it against the specifications?

7.2 Personal Opinions about Software Tools

- There is a large potential in Free Software Tools.
- One should do as much as possible with *Free Software*. [18]
- Concerning sophisticated features the free hardware design tools are somewhat behind the comercial products. Therefore at least one licence of ADS, Genesys, SMASH(?) or a similar program should be available.
- Due to high computing power consumption, especially in transient mode simulations, using a separate machine is appropriate.

[17] Can the Delay Multiplex Single Path Technique be used at other resonant BPMs, too?

[18] Buy better HW instead of expensive SW

A References

References

[1] Desler, Neumann et al. *Introduction to the A0 BPM System* http://beamdocs.fnal.gov/DocDB/0013/001361/001/bpm.pdf

[2] M.Krasilnikov *Note on BPM tests (August 2005) at PITZ (Draft)*

[3] M.Satoh et al. *Energy-Spread Feedback System for the KEKB Injector Linac* http://epaper.kek.jp/p05/PAPERS/RPAT088.PDF

[4] D.Cocq, G. Vismara *From Narrow to Wide Band Normalization for Orbit and Trajectory ...* http://www.slac.stanford.edu/pubs/confproc/biw98/vismara.pdf

B Software

References

[1] Python http://www.python.org

[2] IPython http://ipython.scipy.org/moin/About

[3] Numeric http://www.scipy.org

[4] Matplotlib http://matplotlib.sourceforge.net/

[5] Qucs http://qucs.sourceforge.net/index.html

[6] Gnucap http://gnucap.org/

[7] ROOT http://root.cern.ch

Circuit Simulation
some humbling thoughts…

Manfred Wendt

Fermi National Accelerator Laboratory, Batavia, IL 60510, U.S.A.[1]

Abstract. A short, very personal note on circuit simulation is presented. It does neither include theoretical background on circuit simulation, nor offers an overview of available software, but just gives some general remarks for a discussion on circuit simulator needs in context to the design and development of accelerator beam instrumentation circuits and systems.

BEAM INSTRUMENTATION DEVELOPMENT: FOR WHAT DO WE NEED CIRCUIT SIMULATORS?

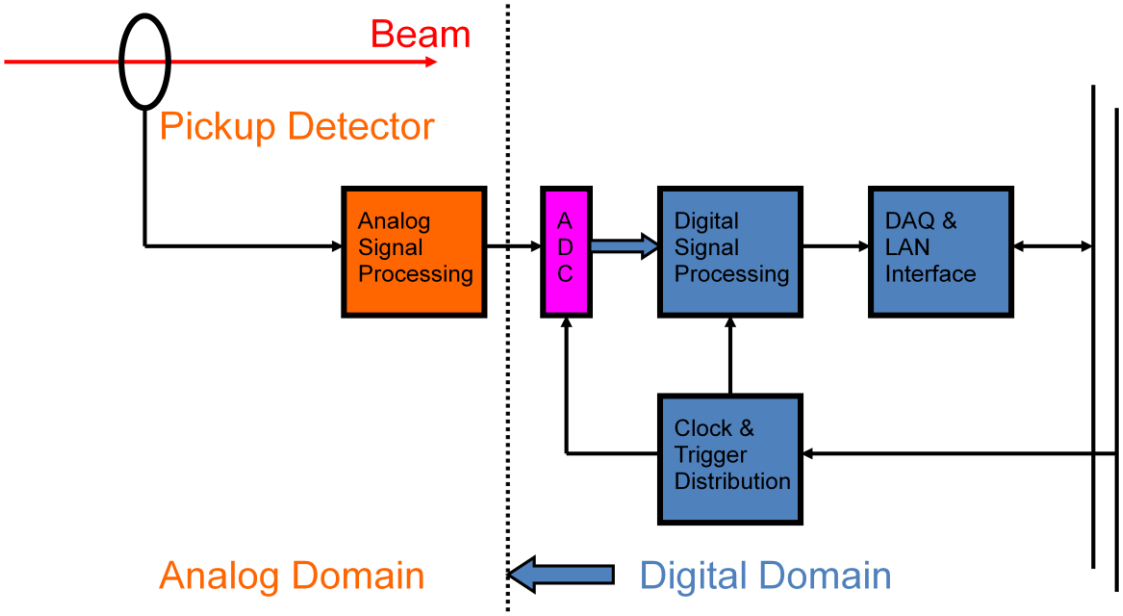

FIGURE 1. Schematic of a typical beam instrument, e.g. BPM, toroid, WCM, PMT, etc.

Fig. 1 illustrates a typical beam instrument used in a particle accelerator, consisting out of a pickup detector (often part of the beam pipe vacuum system), an analog front-end (Analog Signal Processing), and several "digital" blocks including the analog-digital converter (ADC). Before spending lots of funds in money and time for purchasing and working with a sophisticated circuit & system analysis software product, it is worth to discuss how and for what circuits it may be applied in the development of a beam instrument. Some personal observations are:

[1] This work was supported by Fermi National Accelerator Laboratory, operated by Universities Research Association Inc. under contract No. DE-AC02-76CH03000 with the United States Department of Energy

- As Fig. 1 indicates, the borderline between analog and digital domain in the signal processing chain is pushed further and further towards the detector, and this trend will remain.
- "Classical" circuit simulation tools, e.g. SPICE and its variants (time domain), Touchstone and similar products (frequency domain) are focusing on the circuit level simulation, usually in the analog domain.
- Model data is unavailable for many complex semiconductor components, e.g. ADCs, DACs, track&hold amplifiers, limiters, etc.
- Digital signal simulation is mostly based on vendor supplied simulators, and very product specific, e.g. Quartex II for Altera FPGAs, etc.
- Even today, there is no single simulation tool available to simulate a complete beam instrument, starting from the beam, through pickup, analog and digital signal processing, timing and triggering all the way up to the data management level at the LAN adapter.

A conclusion of these observations should not be to exclude circuit simulation from the development of a beam instrument. Even though a complete front to end simulation is neither available nor desirable, critical parts or subsystem (particular analog sections operating at RF or microwave frequencies) of the beam instrument may deserve an in deep circuit simulation and analysis, e.g.:

- Gain stages
- Passive sections (filters, diplexers, hybrids, sections with distributed components, i.e. transmission-lines).
- RF & microwave circuits
- Layout effects, cross-talk, reflections and grounding
- Noise and temperature analysis
- Pickup detectors (button, stripline, cavity and other monitors)
- High-speed digital I/O (CLK distribution, PECL & LVDL circuits, single-ended to differential transitions)

CIRCUIT SIMULATION SOFTWARE

We may categorize circuit simulation software as follows:

- **"Brainware":** Use pencil and paper and apply the Kirchhoff's and Ohm's laws for simple, often idealized sub-circuits. Big advantages are, in-deep understanding of the circuit and an analytical result. Unfortunately this method is limited to linear, sometimes oversimplified circuits.
- **Freeware:** The best known time domain circuit simulator – SPICE – actually is a freeware product, developed at the University of California at Berkeley. The latest version (3f5), as well as many variants are free available to download (google "free spice simulator").
- **$$$ware:** Professional circuit simulator products are often based on the original Berkeley SPICE, but add some handy features like schematic entry, a very flexible output display, data management, etc. SPICE or equivalent time domain circuit simulators are often combined with, or added to layout systems. High-end "design suites" consists out of a set of different simulators (often called "solvers"), sometimes including electro-magnetic (EM) modeling.

Circuit simulators:

- Fully **analyze** an electrical circuit based on implemented models for the circuit components.
- Often have limited **syntheses** capabilities.
- Usually solves the circuit topology by **numerical approximation**, thus no exact, analytical result is available.

The models for the circuit elements, i.e. the mathematical definition along with the parameters, used for the numerical computation in the circuit simulator, are of crucial importance:

- Lumped circuit elements are usually based on the ideal model formalism, e.g. capacitance, inductance, resistance. A real-world circuit component (capacitor, inductor, resistor) is more complex; typically has frequency, temperature, etc. dependent characteristics, "stray" elements and often non-linear effects.
- Distributed circuit elements are modeled based on known analytical solutions or approximation of the EM problem, usually solved in the frequency domain. This implies a limited parameter range, and a Fourier transformation (inverse FFT) has to be applied to use the model in the time domain.
- Nonlinear effects, temperature characteristics and noise behavior are available for some circuit models.
- Some circuit simulators offer the implementation of user specified circuit models and/or stimulation sources.

Circuit simulation software uses:

- **Linear solvers:** DC, AC, S-parameter, etc. simulation in the frequency domain at steady state.
- **Nonlinear solvers** (e.g. "harmonic balance"): Used for a small signal analysis around a specified DC working point. Offers spectral, distortion and other characterization of the system's frequency harmonics.
- **Transient solvers** (e.g. "SPICE"): Approximate solution of the circuit's system of differential equations. This time domain approach includes all transient effects with given initial values. The method may be limited when computing models of highly resonant circuit elements (resonators with very high Q-values).
- **Special solvers:** For arbitrary geometries of resonators, transmission-line components, antennas, etc. EM solvers are available to approximate the geometry applying Maxwell's equations. An S-parameter based solution is often available, thus the result can be used for further computations in a circuit simulator. Some analytical mathematical software products add circuit simulation routines as add-on to provide an analytical circuit simulation. Professional circuit simulation software usually includes statistical tools to optimize a set of circuit parameters to a given goal(s), which adds some limited circuit synthesis capability.

USING MATHCAD, MATLAB AND PSPICE FOR ELECTRONICS SIMULATIONS

José Luis Gonzalez, CERN, Geneva, Switzerland.

Abstract

During the conception and development phases of complex designs, electronics engineers usually need development tools that make the design faster and avoid breadboarding. Mathcad® and MATLAB® are among the most commonly used mathematical tools while PSpice® is certainly the most popular electronics simulator. This paper is not intended to be a tutorial; it only presents a few examples that illustrate how these programs have been used to ease designs.

INTRODUCTION

Constrained by increased project complexity and shorter design cycles, engineers rely ever more on analytical and simulation results before committing designs to hardware. A few examples will show the use of Mathcad® [1] and PSpice® [2] for electronics developments and MATLAB® [3] for beam data analysis.

USING MATHCAD

Mathcad lets engineers simultaneously design and document their projects, using a comprehensive set of mathematical functions. It is an efficient tool that integrates calculation results, graphs and text in a single worksheet, improving work verification and engineering collaboration. Mathcad is used in these examples to calculate the main parameters of some Beam Position Monitors (BPM) and plot their transfer functions.

Button type BPM

The button is an electrostatic monitor that uses the charge induced by the image current of a circulating beam. It generates a signal proportional to the beam intensity I_b and inversely proportional to the distance of the beam from the button. Its response can be evaluated using the "Spice" equivalent circuit of Fig. 1, where Z_∞ is the coupling impedance, C_e is the electrode capacity and R_l is the load impedance.

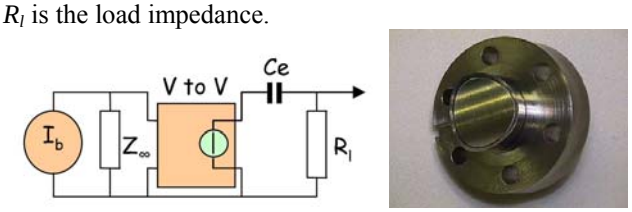

Figure 1: Simplified button equivalent circuit and actual view of the LHC button BPM.

On Fig. 2, the main parameters of the button are calculated using Mathcad and the worksheet can be modified easily to fit the same kind of BPM with different dimensions. Depending on its size, the electrode capacity usually ranges from less than 1pF to a few pF and the corresponding low frequency cut-off extends from some hundreds of MHz to several GHz.

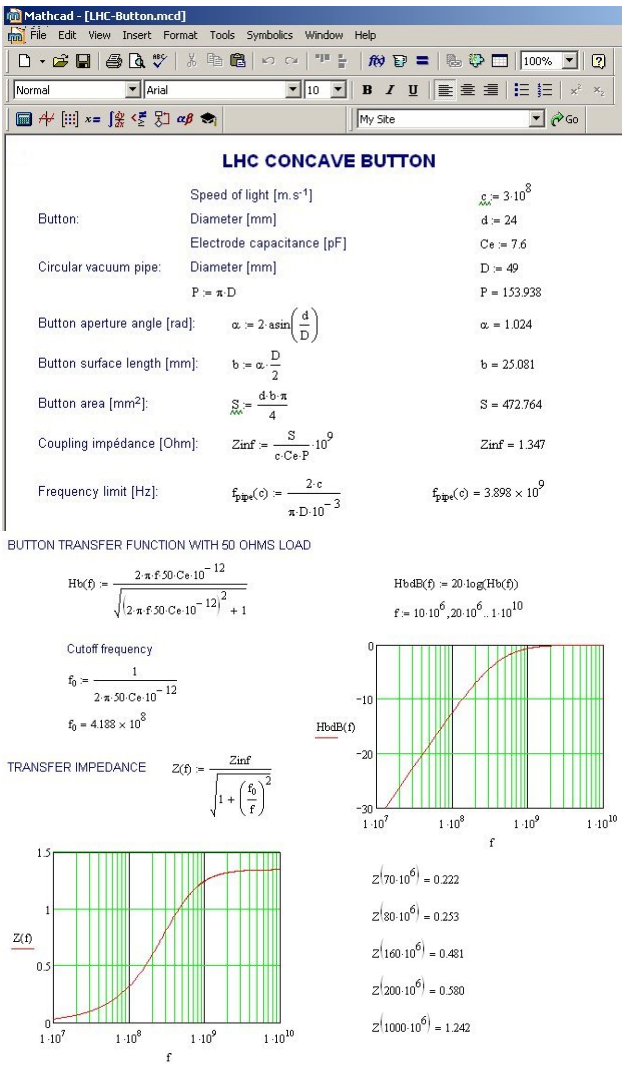

Figure 2: Mathcad worksheet for the LHC button showing the main parameters and the frequency responses.

The same approach can be applied to other button type electrodes, such as a High Frequency (HF) button where the electrode is simply the central conductor of a vacuum feedthrough. Its capacitance is about 0.6pF and the low frequency cut-off of this BPM is about 5GHz. Its transfer impedance is about 0.7Ω compared to the 1.4Ω obtained for the LHC button.

The LHC coupler

Couplers are devices that use the electromagnetic field of the beam to generate signals on strip-line structures. The

amplitude response, versus frequency, is periodic and it depends on the strip-line dimensions. The maximum is obtained for a frequency corresponding to $f_0 = c/4l$ and the minimum for $f_{min} = c/2l$, where l is the coupler length. Fig. 3 presents both the LHC coupler parameters and the frequency response.

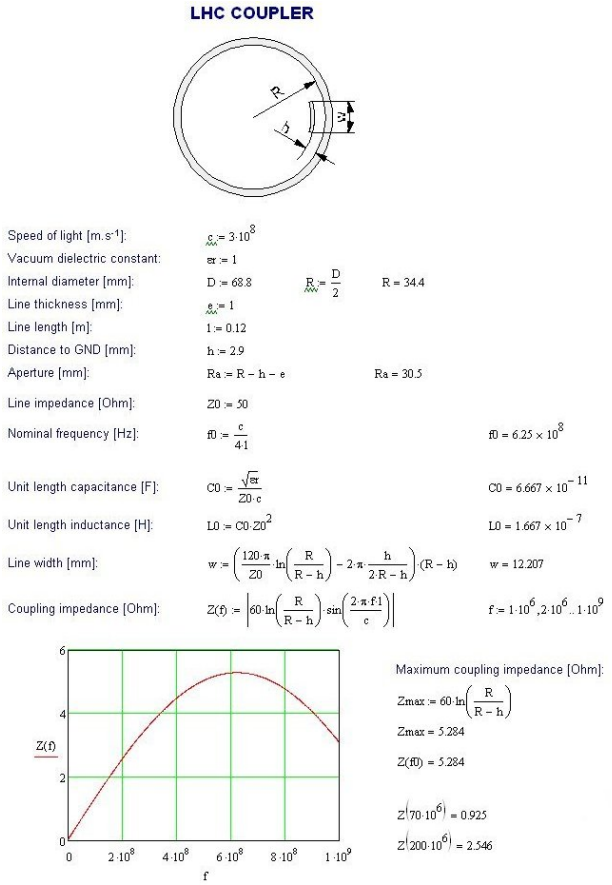

Figure 3: Mathcad worksheet showing the LHC coupler parameters and its frequency response.

SIMULATION WITH PSPICE

PSpice provides a complete simulation environment with schematic capture and plotting facilities. Analogue or digital models are available from many manufacturers. The "Optimizer" is an interesting feature that is presented here to improve the input matching of a filter.

LHC Button model

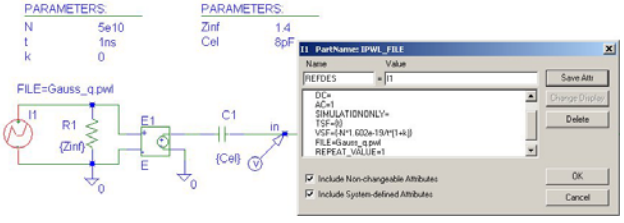

Figure 4: PSpice model of the LHC Button and beam definition using the current source settings.

PSpice parametric analysis can be used to easily change the design characteristics and immediately simulate the effects. In the example of Fig. 4, the BPM parameter values *Zinf* and *Cel* are directly derived from the previous Mathcad calculations. To generate a Gaussian pulse that models the beam, a piecewise linear current source is associated to the definition file *Gauss_q.pwl*, then the parameters *N*, *t* and *k* allow for signal scaling.

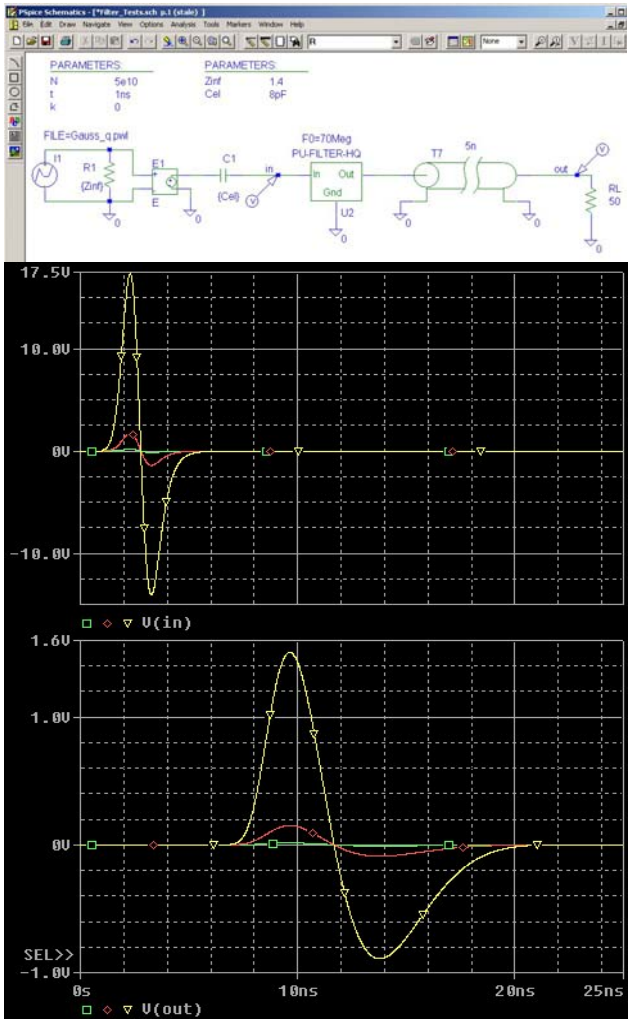

Figure 5: BPM and filter response to a Gaussian beam of 2.10^9, 2.10^{10} and 2.10^{11} charges.

In order to accommodate pulse shape variations during signal processing, the front end electronics of the LHC button BPM use constant impedance Bessel low-pass filters that *normalize* the pulse duration for each pair of electrodes. The schematic diagram of a loaded electrode and the transient analysis are shown on Fig. 5 with the parameter *N* varying from 2.10^9 to 2.10^{11} charges per bunch.

LHC Coupler model

The PSpice model *T2coupled*, which defines two coupled transmission lines, is used in Fig. 6 to simulate the LHC coupler response to the same Gaussian beam as for the LHC button BPM. Since the coupler transmission line is short (*len*=12cm) and made of copper material, the resistive *R* value of the model can be neglected. The

coupling resistance *Rcoupl* and the parameters required to describe T2coupled, L (unit length inductance) and C (unit length capacitance), have already been calculated in the Mathcad worksheet of Fig. 3.

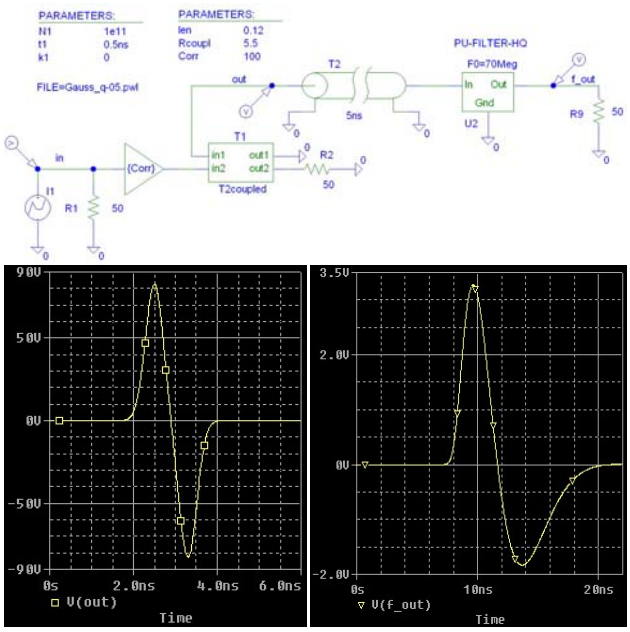

Figure 6: PSpice simulation of the LHC Coupler using the transmission line model and the filter.

Notice that the LHC coupler length is determined to get the same beam response as the LHC button BPM, which allows the use of the same processing electronics.

LHC Bessel Filter Optimization

As mentioned previously, the BPM signal must be low-pass filtered and, in order to avoid reflections, the LHC BPM front-end electronics must present an adapted load to the monitor electrode. This is done using the adapter network shown in Fig. 7, where *R1* and *C1* are high-pass elements and *Cr*, *Lr* and *Rr* can be optimized in order to reduce the input reflection coefficient S11.

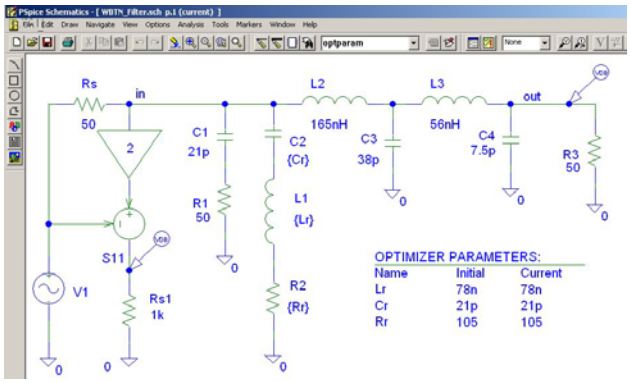

Figure 7: PSpice schematics of the LHC Bessel filter with the input matching network.

PSpice optimizer parameters are first filled with guess values and then the Optimizer helps finding the best component values that meet the performance goals and constraints that are defined in Fig. 8.

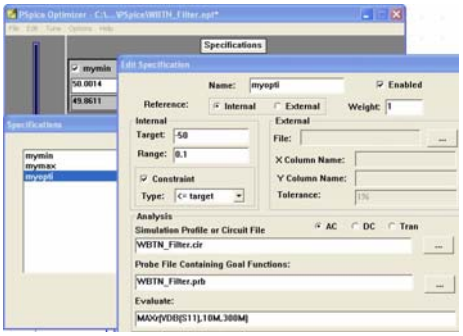

Figure 8: The PSpice Optimizer allows constraints and goal functions to be specified.

In this example, basic goals have been defined to meet a 50Ω input impedance and the constraint that S11 has to be less than -50dB. The response after using the optimizer results is shown in Fig. 9.

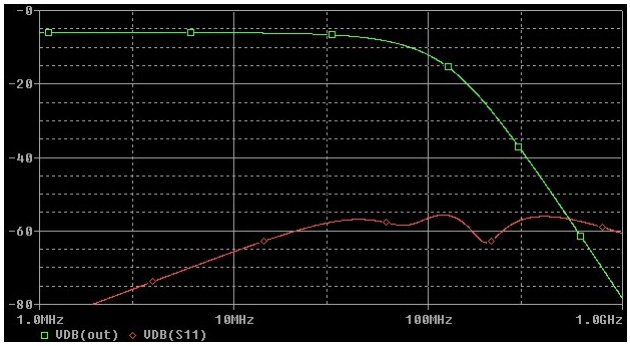

Figure 9: LHC Bessel filter response using the Optimizer results (78.5nH, 21.55pF and 105.5Ω).

However, to get these filters produced in large quantities, the specifications must be relaxed and a trimming capacitor can be used to fit the response within the specified limits of Fig. 10 (red curve). Notice that, in the high frequency range, the actual S11 measurement does not comply with the simulated results. This is due to the fact that, at these frequencies, the parasitic components of the inductors and capacitors cannot be neglected and then the models are not accurate enough.

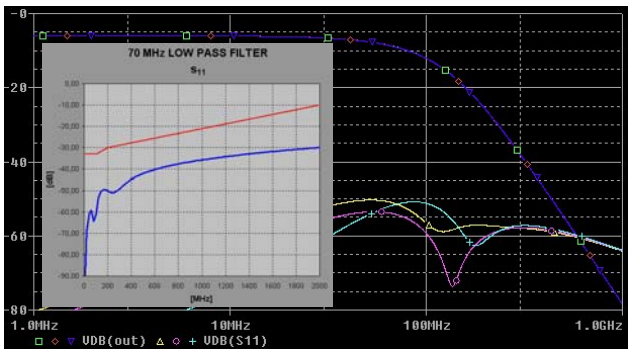

Figure 10: Parametric analysis using capacitor *Cr* and actual filter measurement. The red curve sets the upper limits of S11 during production.

DATA ANALYSIS USING MATLAB

MATLAB is a high level language, which provides an interactive environment for numeric computations, algorithm development, data analysis and visualization. Several MATLAB toolboxes allow specialized uses in a wide range of applications, including signal and image processing, control design, communications...

SPS Beam Data analysis

MATLAB easily handles both vectors and matrices. Fig. 11 shows the data from an actual measurement of an SPS beam, which has been stored in vector format (called *raw*) in a text file (*SPSdata.m*) for subsequent processing.

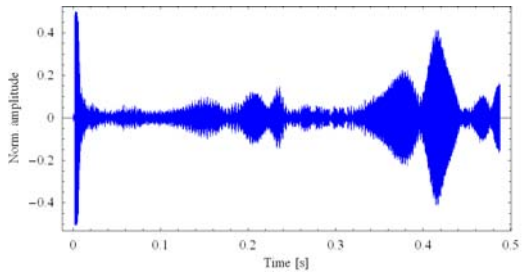

Figure 11: Actual SPS beam data acquisition.

The MATLAB development environment integrates the program editor (Fig. 12) and plot windows (Fig. 13) that can be generated when running the program.

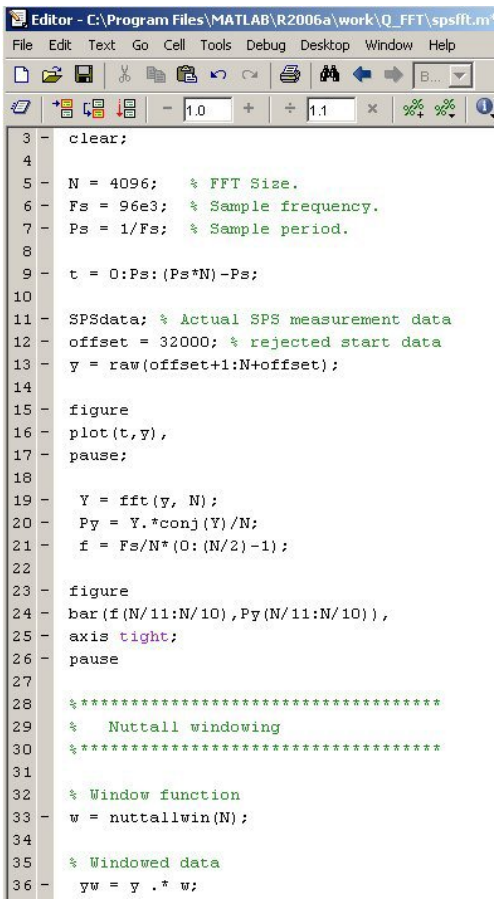

Figure 12: MATLAB code for beam data analysis.

When using the mathematical functions provided by the signal processing toolbox, it only takes a few lines of code to apply a standard *window* to the required beam data, calculate the corresponding FFT and display relevant results. Fig. 13 demonstrates the cleaning effect of windowing on the calculated spectrum for part of the data shown in Fig. 11.

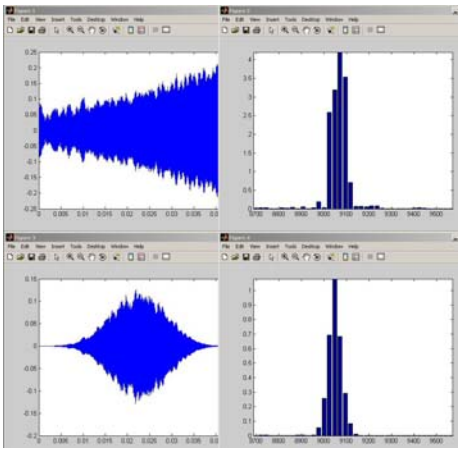

Figure 13: MATLAB display of the analyzed raw data or windowed data and the corresponding FFT results.

The same processing can be repeated to different sets of data that can overlap (sliding FFT principle), giving the result plotted in Fig. 14.

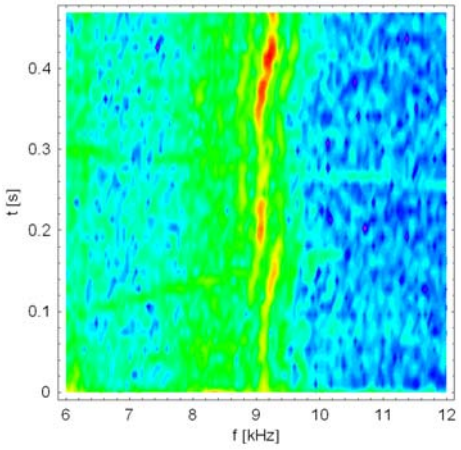

Figure 14: Continuous spectra of the SPS beam data.

CONCLUSION

Mathcad and MATLAB have proven to be efficient and powerful tools for the electronics engineer, both for data analysis and mathematical modeling.

PSpice has been an essential tool for simulating electronics designs and make developments faster.

REFERENCES

[1] Mathsoft Engineering & Education, Inc.

[2] Cadence PSpice.

[3] The MathWorks.

2nd half day: **BPM technology – simulation of electronics, measurements**

Chair: H.Schmickler (CERN)

Speaker/Institute; Title of talk

1.) **M. Wendt/FNAL** Development of a high resolution cavity BPM for the ILC cryostat
2.) **T.Traber/DESY** Simulations of frontend-BPM-electronics at DESY
3.) **M.Wendt/FNAL** Simulation of Frontend Analog-Electronics
4.) **J.Gonzalez/CERN** Using MathCAD, Matlab and PSpice to simulate electronics parts

In general: The main aim of the session was attained. The participants exchanged their point of view on particular features of the simulation tools and agreed on the level of detail one can get out of the model predictions.

In detail:

Add1) Very good agreement of design values compared to test measurements

Add2) A large variety of options has been explored before the realization of the first prototype PCB

Add4) Very comprehensive review of the functionality of modern tools. The talk has been suggested for a school/seminar with wider audience.

BPMS FOR THE XFEL CRYO MODULE

D. Nölle, N. Baboi, K. Knaack, D. Lipka, N. Mildner, R. Neumann, M. Siemens, T. Traber, S. Vilcins , DESY, 22603 Hamburg, Germany

Abstract

The European XFEL is based on superconducting accelerator technology developed in the context of the TESLA collaboration [1]. The accelerator itself consists of cryo modules equipped with 8 cavities, followed by a quadrupole/steerer package, a BPM and a HOM absorber. This contribution will present the layout of the BPM system for the cryo modules, describing the monitor itself, its integration into the cryo module. Additionally, the electronics concept will be discussed. Finally the results of beam measurements at FLASH using prototypes of the monitor and the electronics will be presented

INTRODUCTION

The accelerator complex of the European XFEL at DESY consist of a superconducting LINAC with a maximum energy of about 20 GeV. It is constructed out of 116 cryo-modules, with only a few warm sections intercepting the cold acceleration chain. The only monitor devices in the cold sections are BPMs, one per cryo module. They have to provide position and charge information along the LINAC.

Two BPM types are currently under investigation, a re-entrant cavity BPM developed by CEA in collaboration with DESY [2], and a button type BPM. The latter will be the topic of this paper.

Table 1: Requirements of the BPM

Parameter	Value
charge	0.1 – 1 nC
Bunch Spacing	200 ns (≥, arbitrary pattern)
Position Resolution	< 50 µm (Single Bunch)
Charge Resolution	1 %
#Datapoints	3250 within 650 µs @ 30 Hz
Length	170 mm
Beam Pipe	78 mm
Operation Temp.	4 – 20 °K

INTEGRATION INTO THE XFEL CRYO MODULE

The XFEL cryo module houses 8 TESLA cavities followed by a superconducting magnet block, consisting of a superferric quadrupole and a set of steerers. The BPM is connected to the vessel of the magnet. Components to follow are a gate valve and the HOM absorber. Fig. 1 shows the layout of the end of the cryo module in detail.

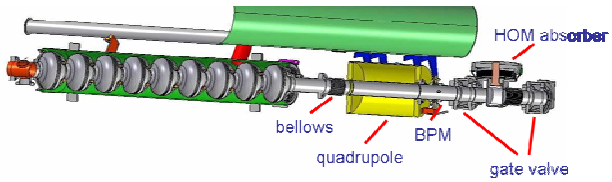

Figure. 1: Layout of the back part of the XFEL Cryo module.

In contrast to module BPMs at FLASH [3] (former TTF), the BPMs are flanged and not welded to the beam pipe. The BPM has a length of 170 mm, with two fixed, so called “cavity flanges” on both sides. The beam pipe diameter is 78 mm, the inner beam pipe has to be copper plated. Since the BPM is connected to the liquid He vessel of the quadrupole, the BPM will be at a temperature close to the 4 k level. The vicinity of the superconducting cavities requires a particle free inner volume of the BPM (Cleanroom Class 100). The alignment to the magnetic axis and orientation of the quad has to be better than 300 µm (transverse) and 3 mrad (roll angle) The cables of the BPM have to be a compromise between low cryogenic losses and RF properties.

BPM MECHANICS

Following the requirements on the mechanics inside the module a pickup monitor was designed. It is foreseen to mill the BPM out of a single piece, providing optimum tolerances and safety from the vacuum point of view. The alignment to the adjacent quadrupole will be based on field measurements of the quad and the use of dowel pins, included in the mechanical design of the BPM, in order to meet the tolerances mentioned before.

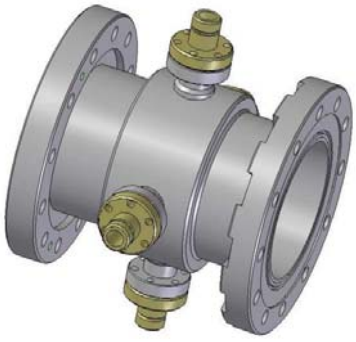

Figure 2: 3D Model of the BPM prototype

The design of a prototype is shown in Fig. 2. In order to meet the requirements at the lower charge limit, a feedthrough design with a larger button size of 15 mm is currently under investigation. Therefore, there will be some changes concerning the flanges for the feedthroughs and the feethroughs themselves.

ELECTRONICS CONCEPT

As mentioned in Table 1, the bunch to bunch distance in XFEL is as long as 200 ns. Furthermore, the requirement is a single bunch, single pass resolution better than 50 µm. These requirements are close to the performance of the electronics type used for the DESY electron rings, typically operating with a bunch spacing of 96 ns [4]. Here the signals of the 4 buttons are added onto a single cable after running through delay lines of certain length. Thus the electronics gets a sequence of 4 pulses for processing. The influence of the delaylines is taken out by means of calibration. Due to the use of a single electronics channel, one gets good stability properties. XFEL will use a modified and updated version of this scheme. Due to the geometry of the XFEL BPMs it easy to separate the vertical and the horizontal plane and to process them by separate electronics. Thus there will be one electronic per plane.

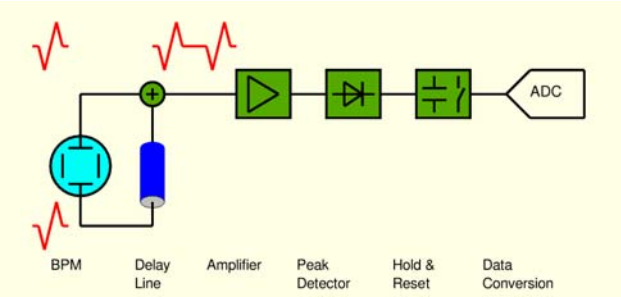

Figure 3: Block diagram of the BPM electronics for the pickup BPMs

In order to deal with drifts of the delay line network a test and calibration facility will be included in each electronic. It will allow to send and analyse test pulsed before or after each RF pulse of the linac, for testing and online calibration.

Since the will be various types of BPMs for XFEL this electronics has to be integrated into an overall framework of a BPM system. Currently this framework is under discussion with the colleges from PSI who plan to collaborate with XFEL on the warm BPM system. It is planned to integrate this electronics, including analog front end to ADC as a piggy pack board to be mounted on a common processing board. The cold BPM electronics would appear like an ADC unit to the processing board.

Based on the test setups the layout of the PCB for a prototype series is under development, and protype boards will be available for testing in summer 07. Beam test at FLASH are scheduled for fall 07.

BEAM RESULTS AT FLASH

A prototype of this XFEL BPM with adapted flange type (CF) and 8 mm buttons (as shown in Fig 2.) was installed in the FLASH LINAC. Several studies have been performed with this monitor and different test setups for the electronics. The result of a measurement with this BPM and a first electronics prototype is shown below.

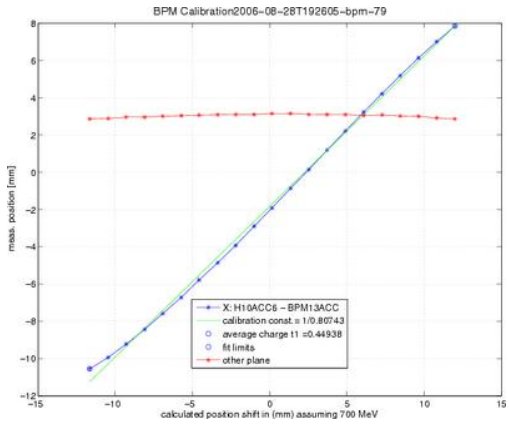

Figure 4: BPM response vs. steerer current at FLASH

The BPM was included in resolution measurements using correlation techniques [5]. For different charges in the range of 0.2 to 1 nC the resolution was measured to be better than 30 μm. Dynamic range of ±15 mm was also demonstrated, as well as a the required charge resolution of 1%.

CONCLUSION

In this paper the design and first measurements of a prototype for the BPMs in the XFEL cryo modules are presented. With the current design for a button type monitor and an electronics based on the scheme used at HERA, the requirements for XFEL can be met.

REFERENCES

[1] XFEL Technical Design Report, DESY 2006-97; XFEL.desy.de
[2] C. Simon et al, this proceeding.
[3] V. Ayvazyan, et al., “First operation of a Free-Electron Laser generating GW powerradiation at 32 nm wavelength”, Eur. Phys. J. D37 (2006) 297.
[5] R. Neumann, private Communication
[6] N. Baboi, “Resolution Studies a BPMs at the FLASH Facility at DESY”, Proc BIW 06, 227

KYOCERA Fineceramics GmbH
Fritz-Mueller-Str. 107
D-73730 Esslingen - GERMANY
Phone +49 (0) 711 93934-910
Fax +49 (0) 711939349-50
www.kyocera.de

Contents of presentations

1. Introduction of Kyocera
2. Our current activity of BPM feed-through
3. Introduction of Strip line type SR detector developed with Spring-8
4. Summary

Page 1 About Kyocera

Kyocera has been founded in 1959. Current total Kyocera group employees are about 61.000, Kyocera itself has 12.000 employees.
Our division for ceramic metallized products has about 300 employees.
Kyocera is producing metallized products from Semiconductor equipment to Medical , Avionics and Space Industry.

Page 2

1.583 mm length Ceramic chamber for LHC projects

Page 3

Kyocera has capability to produce Ceramic products. Our division can handle the process from metallization to firing , plating , assembly , brazing , welding and inspection process.

Page 4

Pls see a Kyocera BPM feed-through. It is a button electrode (or antenna) type BPM feed-through.

- Type A BPM has been using at Spring-8.
- Type B BPM has been using at KEK-B.

Both BPM can be used up to 7 GHz. Type A has big reflection at 8 GHz. And Reflection of Type B has controlled up to 18 GHz.

We can design ceramic feed-though to consider RF performance using RF simulation from the designing stage.

KYOCERA Fineceramics GmbH
Fritz-Mueller-Str. 107
D-73730 Esslingen - GERMANY
Phone +49 (0) 711 93934-910
Fax +49 (0) 711939349-50
www.kyocera.de

Page 5
Simulation Model result
We confirmed some ceramic model how to affect to RF performance of BPM. Kyocera did RF simulation to verify the ceramic diameter and thickness. We understand and have the experience that the frequency of resonance shifted to higher frequency to minimize Diameter of the ceramic disc , when we compare Model 1 ,2 and 3 ,

Page 6
Brazing strength in cold temperature
This is a result of metallized ceramic brazing strength in cold temperature. MoMn metallized ceramic was brazed between FeNiCo metal components by using AgCu brazing material. This test sample was immersed in Liq. N2 or Liq. He. Then brazed metal components were pulled top and bottom directions.

Page 7
Brazing strength test result
The X-axis is temperature and Y-axis is braking strength / brazing surface area.
We can see not so much degradation for pulling strength at low temperature.

However brazing strength is affected brazing flow condition. Our final conclusion was the influence of cold temperature was less than brazing flow condition. We could see same braking condition at three temperature conditions.

Final conclusion is that Ceramic brazing strength is enough for UHV applications at 4 K.

Page 8
Liquid N2 thermal shock test
This is the Liq. N2 thermal shock test result for stainless steel welded BPM.
This BPM was welded to 10 mm thick stainless steel to simulate actual installation on chamber.

No hermetic problem was observed after these sequences. Actual assembled BPM products survived in Cryogenic.

Page 9
List of BPM produced by Kyocera
This is a list of BPM produced by Kyocera before. Left side shows material of chamber or flange and described magnetic and non magnetic type.

KYOCERA Fineceramics GmbH
Fritz-Mueller-Str. 107
D-73730 Esslingen - GERMANY
Phone +49 (0) 711 93934-910
Fax +49 (0) 711939349-50
www.kyocera.de

Page 10 Page and Page 11

Example of BPM

Page 12

Prototype BPM
This is prototype BPM for J-Park. Cylindrical component are out of Alumina ceramic. Metallization was fabricated inside and outside of the ceramic tube. Each pattern metallization is connected to the center conductor of SMA Feed-through which was brazed outside of ceramic.

Page 13

Micro-strip line BPM
This product is used for the Synchrotron Radiation Monitor.

Page 14

The pulse length of Synchrotron Radiation is minimum 2 nsec at Spring -8.
Purpose of this product is SR positioning, Pulse strength and Timing monitor for trigger.

Page 15

This conventional W blade detector was not designed for high frequency signal. Half – width of out put signal is 2 nsec.

Thus, 2 nsec pulse length signal can not be separated.

Page 16

We considered high frequency design from Synchrotron Radiation detecting area. AlN ceramic substrate was brazed on slant surface of CuW. O.F.H.C made micro strip line was brazed at SR detecting area. Micro-strip line is matched 50 ohm impedance to optimize ceramic thickness and O.F.H.C line width.

KYOCERA Fineceramics GmbH
Fritz-Mueller-Str. 107
D-73730 Esslingen - GERMANY
Phone +49 (0) 711 93934-910
Fax +49 (0) 711939349-50
www.kyocera.de

Page 17

Gray color component is AlN ceramic. And slant shape metal is CuW. This detector was welded on Vacuum chamber at Synchrotron Radiation line in Spring 8. 2 nsec pulse signal was separated clearly using this developed detector.

Meggitt Safety Systems

CARE-N3 networking for HHH Conference
Held in Lueneberg, Germany
October 30th to December 1st, 2006

Meggitt Safety Systems Inc.
Report

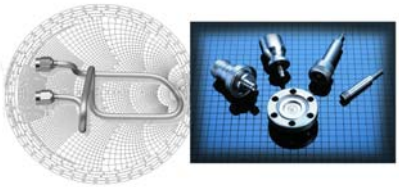

Presented by: Farzad Kialashaki

Meggitt Safety Systems Inc
1915 Voyager Avenue
Simi Valley
CA 93063
USA

Tel: +1 (805) 584 4100
Fax: +1 (805) 578 3400

www.meggittsafety.com
www.meggitt.com

MEGGiTT

Abstract

The presentation provided by Meggitt Safety Systems Inc. (MSSI) was aimed at providing the overall information about the company and to highlight MSSI's approach in designing and manufacturing the BPM and Feed-through for high energy physics communities worldwide. The goal was to inform the users about MSSI engineering and manufacturing capabilities in supplying hermetic BPM, feed-through and cable assemblies. It was of great value to interact directly with users and suppliers during the conference and be able to obtain the market needs and areas in need of improvement. MSSI has a long history of over 50 years manufacturing SiO2 insulated cable assemblies and hermetic connectors used by aerospace, nuclear and instrumentation market. The presentation also provided MSSI engineering and manufacturing capabilities and demonstrated BPM modeling using CST and HFSS. Although MSSI is capable of producing hermetic BPM and feed-through using ceramic to metal brazing, however, it was determined that the glass to metal sealing provides a more reliable seal and better electrical performance.

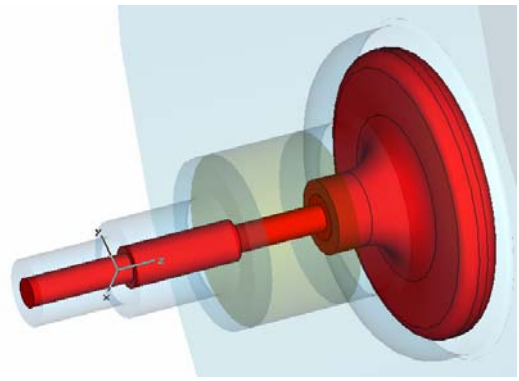

Outline

- Meggitt PLC organizational Chart
- Quality Management
- MSSI Business nature
- Cable product Line history
- Cable construction
- SiO2 Cable types
- Advantages of SiO2 cable
- Qualified SiO2 cables for Nuclear application
- Cable/Connector, BPM, engineering Capabilities
- Process Capabilities
- BPM modeling using CST and HFSS

Meggitt PLC organizational chart

The intent of presenting Meggitt PLC organizational chart was to demonstrate the market Meggitt serves and to provide additional information about the corporate products offered in case there would be an interest. The chart also showed the various locations in the areas worldwide that Meggitt is operating in.

Quality Management

MSSI operates within the guide lines of highly recognized quality systems such as ISO 9001 and NRC, which are the industry's standards and used worldwide. All products manufactured at MSSI go through vigorous inspections and all applicable requirements prior to shipment to the customer.

MSSI business nature

MSSI, based in Simi Valley, California, designs and manufactures various products such as silicon dioxide cable assemblies, BPM, feed-through, fire and smoke detectors and actuators.
MSSI's key markets are located in USA, Europe, Asia and North and South Africa. The market segments being served by MSSI and its products are High Energy Physics, Petrochemical, Aerospace, Nuclear, and Defense.

Cable product line history

The basic cable product, which was the SiO2 mineral insulated cable assembly with hermetic connectors, was developed back in 1946 to fulfill the industry's need for high performance/high temperature cabling. The product line was later acquired by Whittaker Corporation in 1979. Because of the nature of the SiO2 insulated cables and its characteristics and ability to withstand very high radiation exposure without any degradation, the cable was introduced to Nuclear market in 1980.

The cable product line remained a separate entity within Whittaker Corporation as Electronic Resources until its merger with a sister division Safety Systems Inc. in 1997. Whittaker Corporation was acquired by Meggitt PLC in 1999 and to date remains as MSSI.

Throughout all the name changes and acquisitions, the cable product line maintained most of the original staff and operators involved with the product. MSSI cable and connector products have been successfully used on various platforms since its inception and have proven to provide high reliability. MSSI always strives to improve the performance and reliability of its products and accommodate the industry's needs.

Cable construction

MSSI has been manufacturing stainless steel, all-welded hermetic cables with non-organic materials for applications in extreme environments for more than 40 years. MSSI has designed, developed and delivered radiation and temperature resistive Silicon Dioxide (SiO_2) insulated cable assemblies to the Military and Avionics Industry since 1960. The basic cable and connector technology is applied to a myriad of configurations in critical high temperature and vibration applications on various platforms. MSSI products are found wherever reliable performance in harsh environments is required.

The core technology in the MSSI cables is the use of silicon dioxide (SiO_2) as the dielectric insulator, resulting in extraordinary stability of the electrical and mechanical properties of this material under severe environmental extremes. The SiO_2 is extruded over the conductors, e.g., copper; or other alloys depending on the specific application. The extrusion process provides the design flexibility that facilitates the manufacture of an almost unlimited array of conductor configurations and sizes. The resulting extrusion is then loaded into a stainless steel (or other metal alloy) tube, and drawn down to size. In the final configuration, the SiO_2 maintains conductor position in the tube relative to the other conductors and the outer sheath maintaining precise spacing for stable electrical performance. The unique spherical shape of the SiO_2 particle holds the conductor spacing through cable bending operations, usually encountered during routine installation operations, hence electrical performance is not compromised in any way.

This characteristic permits forming and routing at installation with a very tight bend radius nominally three times the cable diameter without causing any damage to the cable. MSSI cable assemblies continue to operate in temperatures above 2000^{o}F.

SiO2 Cable types

MSSI offers a wide variety of cable/connector types with different material and construction to suit required applications. The configurations offered are coaxial, triaxial, shielded coaxial and twisted pair and multi-conductors.
All SiO2 cables are supplied with hermetic connectors, which are 100% helium leak tested.

The SiO2 cables offered by MSSI are used on a variety of applications in extreme environments and temperatures. Some of the most common applications are cryogenic, electrical power, RF/Microwave, control and instrumentation.

The type K thermocouple SiO2 cables are also available for application requiring such a device.

Advantages of SiO2 cable

The SiO2 cable is more superior than any other mineral insulated cable when it comes to performance and reliability. Some of the advantages are its amazing electrical performance stability at extreme temperature and pressure. Sio2 cables offer at least two decades better insulation resistance value at high temperature than any other mineral insulated cables.

Qualified SiO2 cables for Nuclear application

The SiO2 cable assemblies are widely used in nuclear power plants because of its resistance to high radiation dosage exposure in access of 100 Mega Rad. Different cable configurations utilizing various metals are used in different locations of nuclear power plants. The life expectancy of the SiO2 cables for nuclear application is 40 years.

Cable/Connector, BPM, engineering Capabilities

MSSI engineering department is staffed with wide range of disciplines such as electrical and electronic, mechanical, material, chemical, optical and software engineering group to provide solutions to customer needs.
MSSI engineering uses a number of state of the art software that is available to simulate and analyze the design. The software used are HFSS, FE structural, SFD, solid works, AutoCAD and various others.

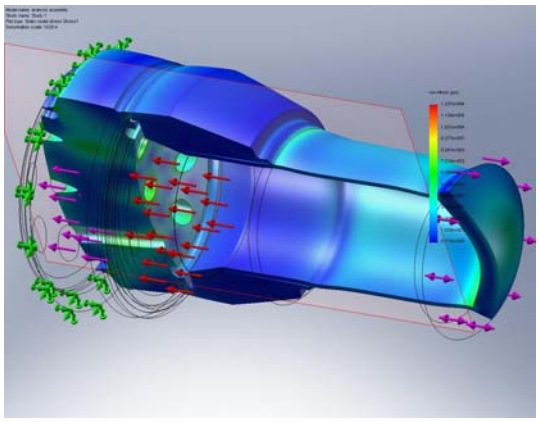

Process capabilities

MSSI possesses a range of manufacturing capacities in the areas of brazing, welding, glass to metal sealing, extrusion, heat treatment, metal forming and soldering. The brazing consists of different types; induction, filament, torch, and furnace. MSSI is equipped to use a GTAW, Laser, and resistance welding, as required and depending on application. For most applications the GTA or laser welding is used. The glass to metal sealing technique used by MSSI are either compression or matched/expansion. Heat treatments at MSSI are either vacuum, or annealing at H2 atmosphere.

BPM modeling using CST and HFSS

In order to demonstrate the engineering capabilities at MSSI and their utilization of available tools such as state of the art HFSS software a modeling of a known BPM and a new design BPM was presented. The modeling was conducted using the HFSS and CST to check the accuracy of the two systems. The first modeling was conducted on a known BPM with available actual capacitance test result. The modeling resulted in an acceptable capacitance value between the simulation and actual test result and proved a good correlation between the CST and HFSS.

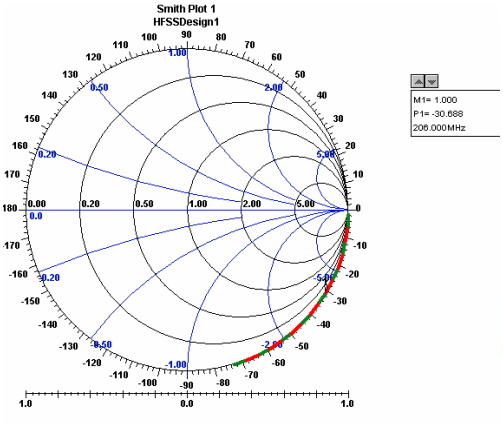

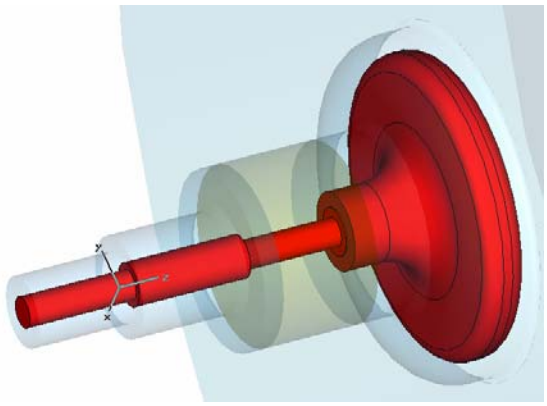

Experience with cold feedthroughs at DESY and short forecast of new cold feedthroughs at DESY

By Silke Vilcins, MDI, DESY

Introduction

This CARE workshop was dedicated to “Simulation of BPM Front-End Electronics and Special Mechanical Designs”. The third day of this workshop was specialized to cold BPM technologies.

This talk is given an express using feedthrough for beam position monitors in cold areas with the experiences of sixteen years lifetime in the HERA Proton accelerator. Further is in this presentation showing the cryogen test procedure of variety of feedthrough which are implemented in several beam position monitors at DESY. The goal for the future is to design a feedthrough, target-orienting to the application of the XFEL cold beam position monitor. To make a design concept, close to the technical design report, with all the mechanical and electricity specs to minimize all critical defects.

Contents

Past: Experience of cold feedthroughs in the storage ring HERA

A. Technical summary of the HERA proton BPM feedthrough

More than sixteen years, the in the TDR of HERA is showing a proton monitor which is installed in a cold module of HERA. At this time the experiences in cold tested feedthrough wasn’t presented. The experts in the diagnostic group of DESY decided for the Japanese company Kyocera for the cold feedthroughs. I don’t know the basic principles of this decision. DESY installed 220 proton monitors with four feedthroughs each (880 feedthroughs). The working temperature is 4K. The warm up (4 K to 330K) and the cool down (330 K to 4 K) processes need about ten days. The type of the feedthrough is a Kyocera type N. The body and the conductor material is Kovar, a Fe-Ni-Co alloy, with a CTE $5{,}0 * 10^{-6}$ K -1 20°C (CTE Coefficient of thermal expansion) The insulation material is Al_2O_3, exact A473, a material composition of Kyocera themselves. The CTE is 8,5 – 9,0, the exactly material composition can not be find out, because this is a topic of the manufacturing process of feedthrough companies. Kovar and Alumnia formed a good material combination for higher temperature applications.

B. Drawing and photos of this BPM and feedthrough

On this page a few drawings and photos will present the Kyocera feedthrough and the proton monitor of HERA.

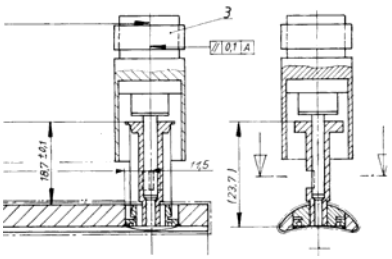

Fig. 1: Cross cut of the technical manufacturing drawing in a complete monitor with the antenna

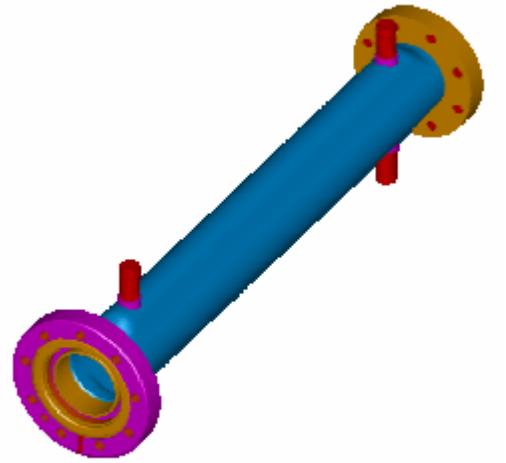

Fig. 2: The proton BPM (stripline) as a 3D view, courtesy to H.P. Gausepohl, DESY

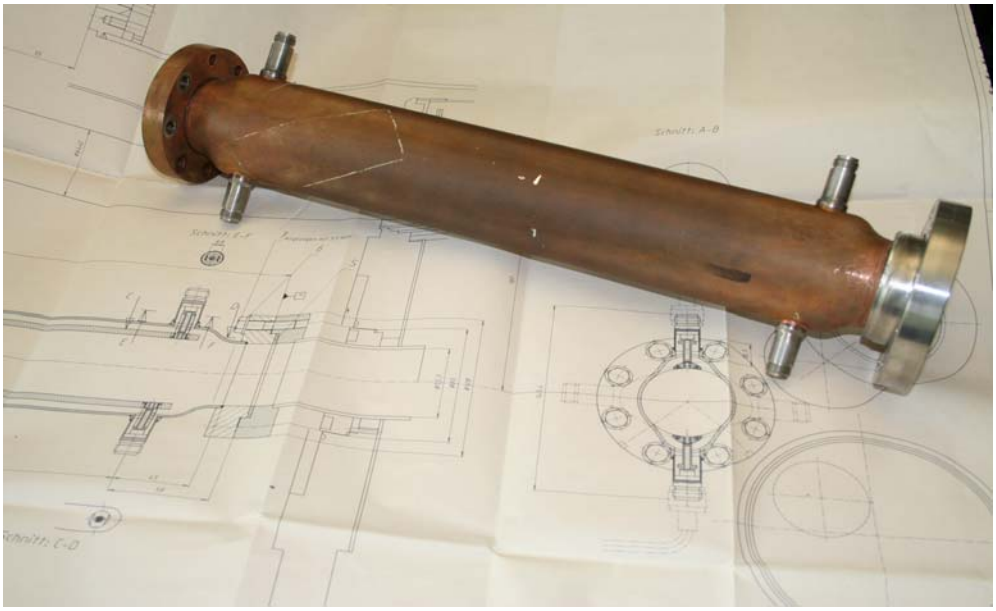

Fig. 3: Photo of a cold HERA proton BPM and its manufacturing drawing

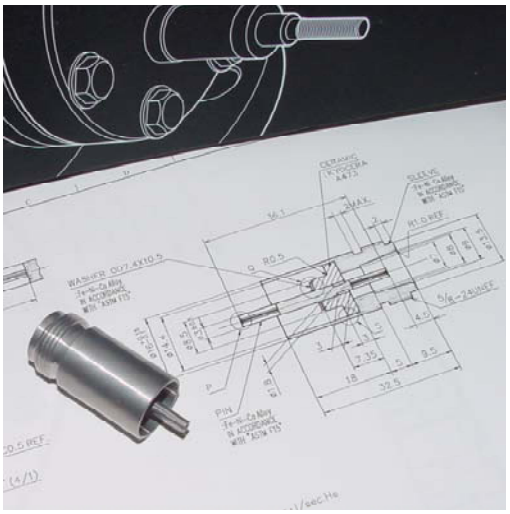

Fig. 4: Photo of an N type feedthrough, company Kyocera, and it technical drawing.

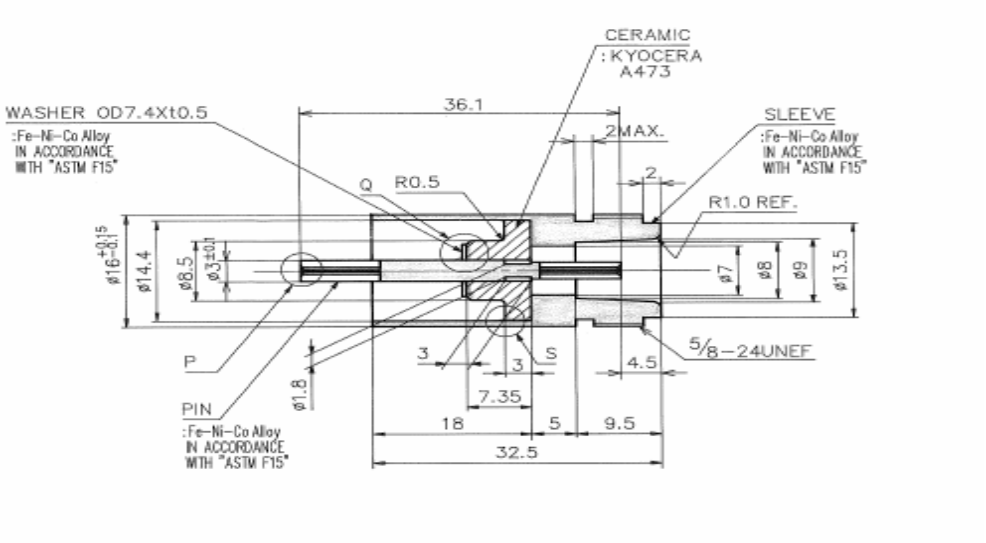

Fig. 5: The Kyocera feedthrough, technical drawing

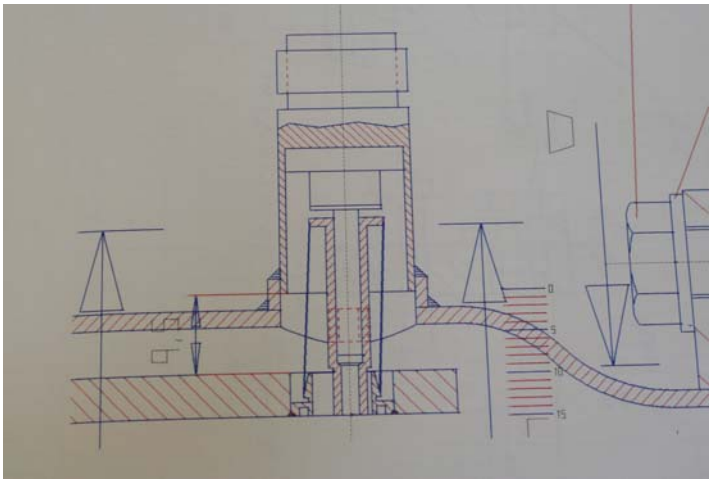

Fig. 6: A picture of an old longitudinal cut drawing showing connection point feedthrough to antenna

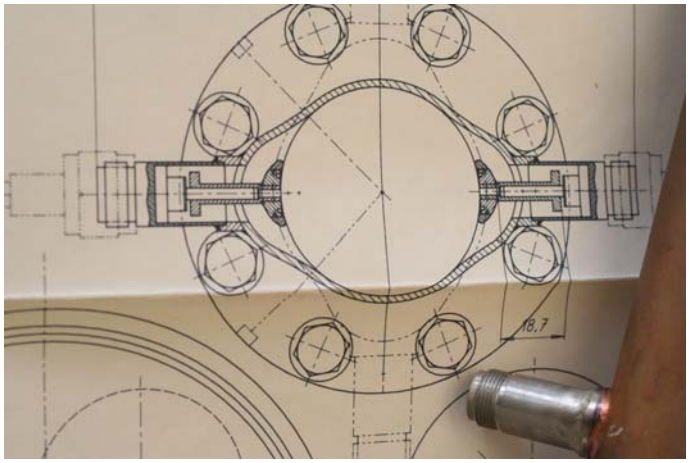

Fig. 7: Drawing of the cross section feedthrough - antenna

C. Lifetime results and conclusion

The experiences gained during these more than sixteen years of design, fabrication, testing, installations and operation with these feedthroughs are discussed in the following:

- Alumina and Kovar formed a good material combination respected to CTE.
- During the lifetime of HERA 10% of the feedthrough were broken. The leakages weren't exact detected, because it was very difficult to find the very tiny cracks. We did not invest any effort to analyse the problem. In case of a broken ceramic, we removed this antenna with two feedthroughs and replaced this antenna with two new feedthroughs. The feedthroughs were checked in advance only once of there high vacuum capability, but they were not tested by cold running cycles.
- The HERA experience shows that 10 % broken feedthroughs are too much for a design of a cold XFEL BPM feedthrough. And we learned it's very important to design a feedthrough matched to the application!

Now: Diploma work of two students at DESY, MDI entitled: "Ultrahochvakuum RF Durchführungen auf Tieftemperatureignungen testen, protokollieren und optimieren "

A. Short Technical summery of the test procedure

The European XFEL is designed on superconducting accelerator technology. The cryogenic accelerator modules consist of modules equipped with 8 cavities, followed by a quadrupole, a BPM and a Higher Order Mode coupler.

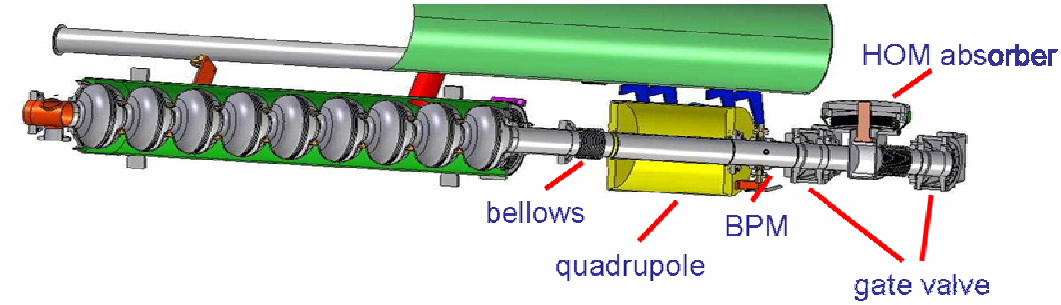

Figure 8 : Cross cut of a XFEL cryo module

The diploma work “Ultrahochvakuum RF Durchführungen auf Tieftemperatureignungen testen, protokollieren und optimieren “ was the first time at DESY, that a test procedure for feedthroughs under cryogenic atmosphere for more than a few feedthroughs was used.

Reasons for that procedure were to get more experience about design, manufacturing process and cryogenic test procedures of feedthroughs and to get a better understanding for the development of a new feedthrough for the cold button BPM of XFEL.

Feedthroughs from two different companies, four different types, were tested. Two flange versions and two feedthroughs especially design for welding directly into the BPM bodies were available and tested. We used want we had at this time in our group to gain the experience. On the base of that we might test other feedthroughs later. The boundary conditions of the test procedure were taken out of the XFEL Technical Design Report. Following points have to be attended:

- working temperatures of the feedthrough in the area of the cryo-modules is 4 K liquid helium
- the feedthrough has to be tested of ultra high vacuum suitability before going into the cold test cycles
- the feedthrough has to be mounted to the BPM body with a maximum reliability
- cool down to 4.5 K and warm up to 330 K as to cycle 10 times for each probe (using a test adapter with four feedthroughs)
- the leakage rate has to be checked after each cycle, (duration time was about 2 min.)

For applications in XFEL, the feedthrough has to be designed for its installation in particles free atmosphere, rinsing class 10 (this point wasn’t integrated in the cold test procedure).

B. Drawing and photos of the relevant testing feedthrough

A few picture of same mechanical parts for the testing procedure with mounted feedthroughs

Fig. 9: Meggitt flange feedthrough mounted to the test adapter flange

Fig. 10: Left side: Copper - silver plated flat gasket from VAT

Fig. 11: PMB feedthrough, for welding construction, also welded to the test adapter

Fig. 12: The Meggitt feedthrough, for welding construction, welded to a test adapter, knob diameter 15 mm.

Fig. 13: The flange version from PMB, France is shown.

Fig. 14: These two pictures show different tested feedthrough from PMB, France. The left shows a gold plated stainless steel button with molybdenum conductor brazed to AL_2O_3 ceramic insulator. Usable directly mounting with the BPM body. The design is based on a

DESY idea.The right picture presented a direct welding feedthrough, 11 mm stainless steel button, molybdenum conductor, brazed to $A_{l2}O_3$ ceramic insulator. (PMB standard design) Both feedthroughs are designed for an impedance of 50 ohms. And used under normal temperatures.

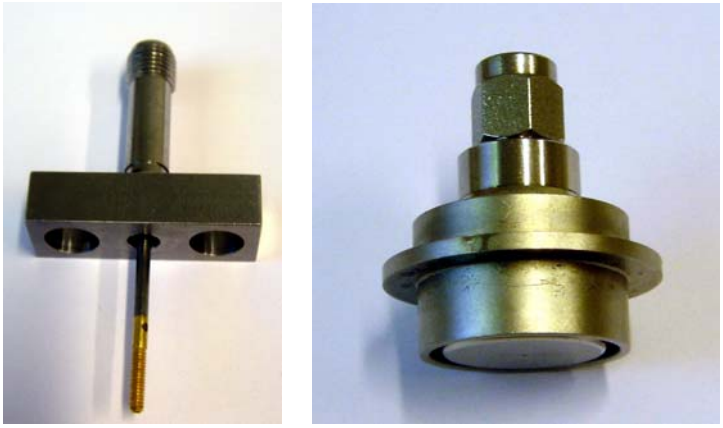

Fig. 15: These pictures show the two different tested feedthrough from Meggitt, USA. The left picture presented a direct welding feedthrough with a 15 mm stainless steel button, molybdenum conductor, fired to $A_{l2}O_3$ glass ceramic insulator. The right shows a gold plated CuBe pin with a metric thread ended to a molybdenum pin. The lead pin is fired to glass ceramic insulator. Usable directly to a flange, mounting with VAT flat seal to the BPM body. (A DESY designed feedthrough). Both feedthroughs are designed for an impedance of 50 ohms. Used under normal temperature and used under particle free atmosphere.

Pictures from BPM's with the tested feedthroughs in their accelerator.

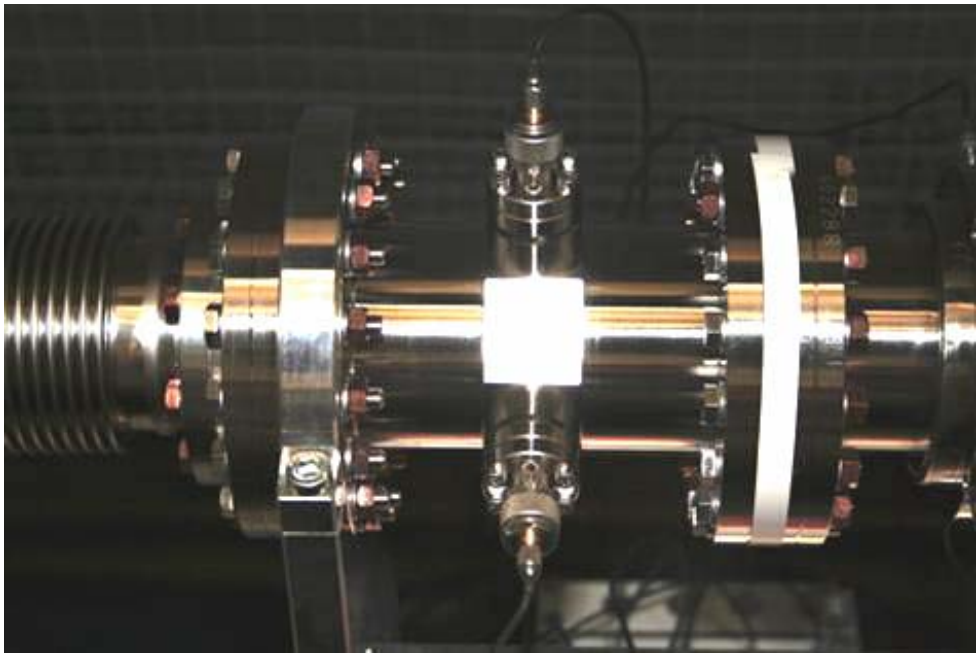

Figure 16: FLASH, first testing button BPM for a cold XFEL BPM (PMB feedthrough flange version with 8 mm gold plated knobs.

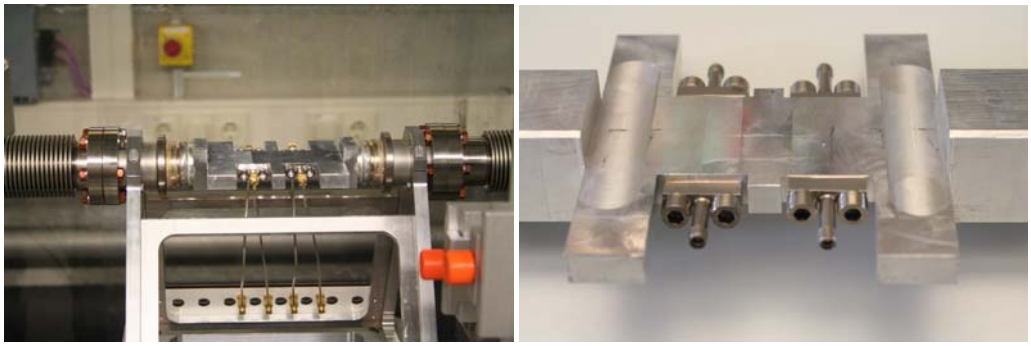

Figure 17: A flange version feedthrough from Meggitt, with a 1,6 mm diameter pin, installed in 2006 for testing BPM electronics at PITZ.

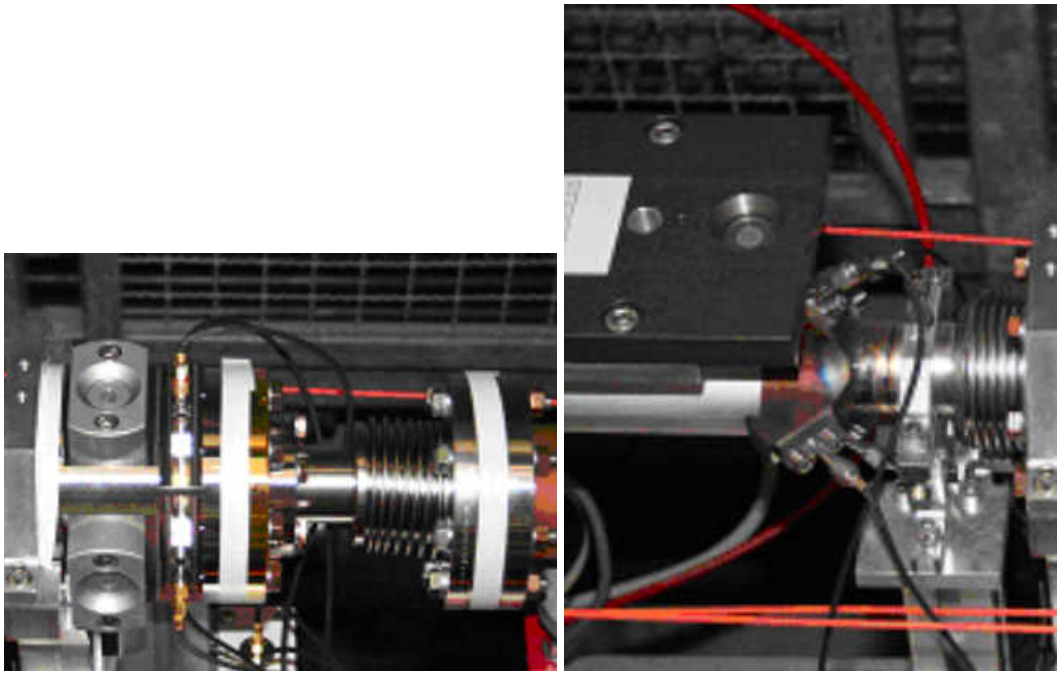

Fig. 18: Left: FLASH, the first PSI resonant Stripline with flanged feedthrough from Meggitt with a M 1,6 mm gold plated tread-end. Right: FLASH, Stripline BPM with flanged feedthrough from Meggitt, same feedthrough version is shown above.

C. Results of the cold test procedure

… NOT one of this feedthrough is broken….
This was an amazing conclusion for me. The testing procedure was very close to the real working environments. But this test was the first steps to get a better understanding of the interaction between every item of feedthroughs.

I mean exactly all of the elements that should be considered in a design of a cold feedthrough. To achieve the best results of the lowest failure rates we have to take care of the electric, RF and mechanical parameters and spec.

Goal is to design a cold feedthrough, with a minimum failing rate, nearly particular free and a suitable RF design for XFEL…

Earliest Future to Now: Design of a cryogenic feedthrough for XFEL

A. First design of a cold prototype BPM housing

The first design is made in the DESY group MVP, courtesy by Nils Mildner.

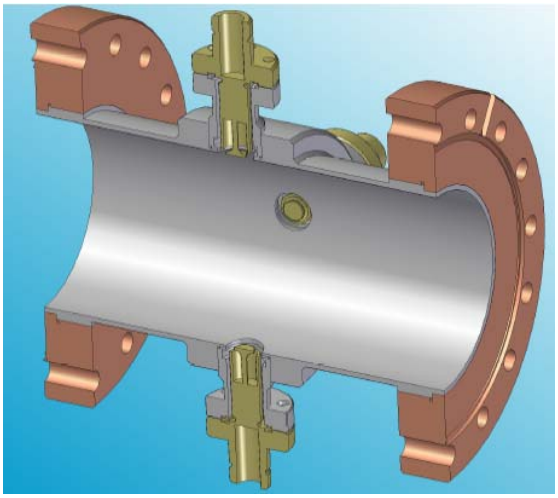

Fig. 21: Cross cut through the first prototype BPM housing. One of these prototypes is installing in FLASH, one is now mounted to a cryogenic module at FERMILAB and the last of this first prototype housing will be installed in a new module in Flash in spring 2008.

B. Design specs of a cold prototype feedthrough

Now I will give a short review of the components “Cold button BPM for XFEL” and give a forecast to the next steps, design aspects, technological issues and open points. Most issues have to be carefully viewed during the design phase and prototyping test phase to optimize the fabrication process to become a safe and efficient series product.

General

The electric requirements are designed for lower beam charge limit of 0.1 nC/bunch, a feedthrough design with a larger button size of 20 mm is currently under investigation.
The feedthrough will be optimized for RF properties up to about 2 GHz. Currently the design of a feedthrough is under investigation, starting from the first version.

BPM housing

The housing material has to be stainless steel AISI 316LN or 316L with a maximum magnetic permeability from 1,01 to 1,05 after all manufacturing process. The inner surface has to be copper plated. The flange design has to be compatible to the neighbour components in the XFEL modules. The alignment BPM to the quadrupole has to be specified to have an alignment item, guaranty the debit line between the quadrupole and the BPM after mounting in the cleaning room. The design has to integrate all requirements of particle free cleaning, mounting and operating.

The mechanical tolerances have to be relaxed as much as possible but the functionality of the BPM and the RF design parameters have still to be matched. Tight tolerances all along

the production chain let the cost grow up. A good design - does not over-specify the tolerances, - take care about mechanical deformations and - take a view on the quality check process. Tolerances should be designed as close as possible to your final product and to the required quality standards.

Feedthrough

The mechanical tolerances have to be as tight as necessary to guaranty the BPM resolution. A goal of the feedtrough design is to obtain the highest output voltage level as possible. Boundaries are the mechanical dimensions of the beam pipe.

The materials of the feedthrough are now for the prototype series:

a. Body and knob 316 LN, 316 L or 304 L stainless steel or titanium

b. lead conductor molybdenum per ASTM B365, copper beryllium or stainless steel (same as body material)

For using 316 L or 304 L the maximum value of magnetic permeability has to be between 1,01 to 1,05 after all manufacturing processes.

The actual design is a flange version, to minimize the failure rate during cleaning and mounting. Flanges versions are a little bit more expensive to welded versions, but for handling and mounting it reduces the process time. The flange versions are better for cleaning. The gap between knob and housing are optimized for rinsing processes. The vacuum seal between feedthrough and BPM housing is a normal Conflat copper gasket.

Another requirement is a reliable operation in the cryogenic environment of 4K. Therefore, extensive tests are foreseen. All feedthroughs of the series production will have to pass a cryogenic test. The test procedure is under investigation.

Also different assembly techniques like soldering or force fitting are evaluated. The diploma work has shown that the different tested feedthrough types, (soldered or force fitted designs) can be used at low temperature.

The feedthroughs have to be check of there hermetic leak tightness to $1*10^{-10}$ (mbar*l/s) before and after the cryogenic tests.

The last parameter is the heating resistance up to 150 °C for 4 hours.

Simulation

One of the simulations was to optimize the knob diameter to get a highest output voltage and find a good compromise to particular cleaning process. (Gap between knob and housing!)

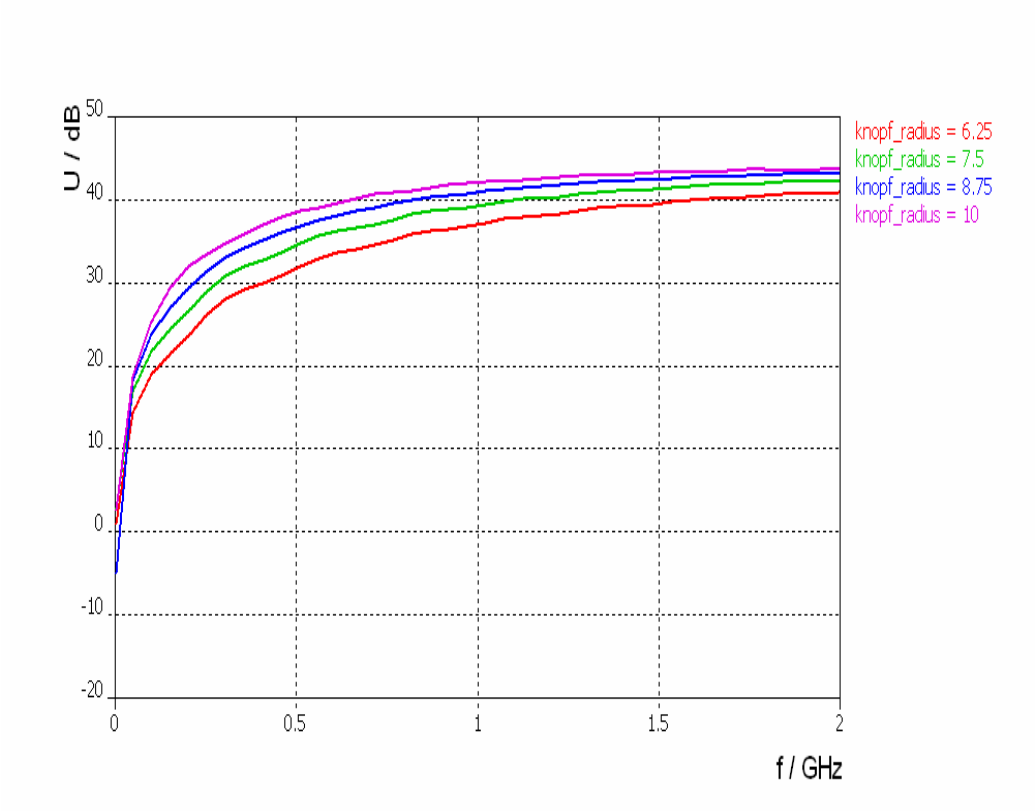

Fig. 22: The level of signal, as a function of frequency at feedthrough connection. Simulation done with 1 nC beam, 2 mm sigma length and 15 mm offset. The highest level provides the button with 20 mm diameter. All the simulation done by Dirk Lipka and Thomas Traber DESY

Drawings of the new prototype design…

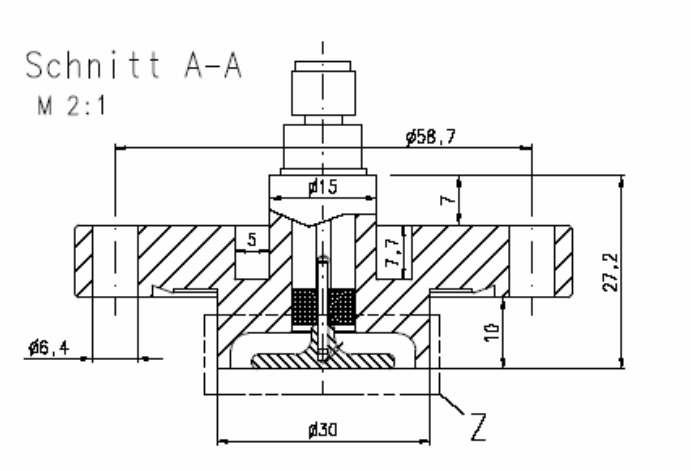

Figure 23: Cross section of the new design of the prototype, designed by Maike Siemens, DESY on 3D Cad System IDEAS.

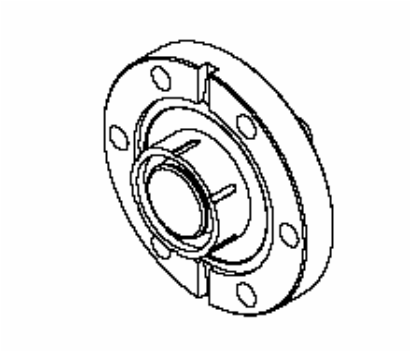

Figure 24: Isometric view of the new design of the prototype, designed by Maike Siemens, DESY on 3D Cad System IDEAS.

Summary

Schedule:

- Start design of the prototype feedthrough with FEM optimizing and RF calculations (Jan.07 – Feb.07) –in time-
- Redesign of feedthrough and fixing the BPM body design (Mar.07 – Jun.07) –in time-
- Fixing the specifications for the offer (Mar.07 – Jun.07) - delayed-
- Start writing the cold testing procedures (Mar.07 – Jun.07) –delayed-
- Start ordering prototyping series (Jul.07 – Dec. 07)
- Start of the series production (…Jun. 08)

Open points of mechanical design:

- Fixing the tolerances of feedthrough and BPM housing
- Alignment to the quadrupoles
- Vibrations uncritical for BPM resolution?
- MTBF for XFEL vacuum components has to be calculated and defined.
- Lifetime of the XFEL components.
- Writing of the cold test procedure
- Writing of ordering specifications for prototypes
- Design of the particle free mounting frames
- FEM simulation of the complete BPM, including all system components

Open points of electrical design:

- Fixing a few parameter, voltage, impedance, reflection..
- Radiation resistance

Open points of simulation:

- Simulation of the tolerances between feedthrough and housing
- Simulation the feedthrough position to axis
- Feedthrough position into housing
- Simulation the angle feedthrough to feedthrough

CARE-N3-HHH-ABI

Novel Methods for Accelerator Beam Instrumentation

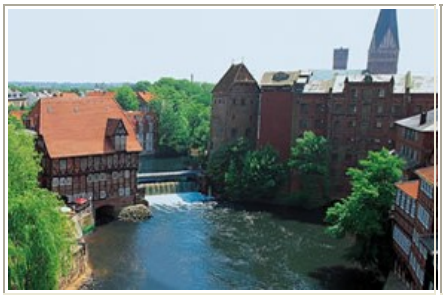

4th workshop

Simulation of BPM front-end electronics a
Special Mechanical Designs

30th of November and 1st of December 2006
Lueneburg, Germany

Design Choices for the cold LHC- BPMs

Christian Boccard, CERN AB/BI

Abstract

The 3rd half day of the CARE workshop was dedicated to special mechanical design and cold technology.
This presentation is not a complete and global review on the LHC BPMs design and fabrication. The goal is more to pinpoint particular aspects or technological issues to be carefully taken in account during each step of the design and fabrication process. It is also a chance to give other experts feedback on the experience gained during these years of development, design, fabrication, testing and final installation.

Outline

- Design parameters and choice
- BPM types in the LHC
- BPM Integration
- Components
- Bodies
- Buttons
- Striplines
- Cold Cables
- Cryostat feedthroughs
- BPM installation and Tests

Design parameters and choice

A lot of parameters have to be taken in account during the design phase leading to technology and material choices. Here are some examples:

- COST
- MEASUREMENT REQUIREMENTS
- BEAM STRUCTURE AND INTENSITY
- OPERATIONAL SCENARIOS
- ELECTRICAL CHARACTERISTICS
- FORESEEN LIFETIME OF THE ACCELERATOR
- INSTALLATION SCHEDULE
- ACCESS TO EQUIPMENT
- INTERVENTION WORK
- COOLDOWN TIME
- NUMBER OF THERMAL CYCLES
- NUMBER OF QUENCHES
- INTERFACE AND ENVIRONMENTAL CONDITIONS
- VACUUM
- PRESSURE
- RADIATION DOSE
- ACTIVATION

Some of these parameters will change during the development phase of the accelerator. I found it very useful that many of these parameters were summarized in a single working document. For the LHC, this document was stored under EDMS number 100513.

Early choice

One of the first choices to do was: Button or Striplines electrodes?
Arguments retained in favor of Buttons were:

- A welded Button electrode on a feedthrough is simple and robust.
- When fitted on a flange with a gasket, it is removable from outside the vacuum chamber and so can be replaced in case of leak or short-circuit.
- A diameter 24mm Button BPM is less cumbersome in longitudinal space compared to 120mm striplines.
- It is well adapted to short LHC bunches.
- Has little effect on longitudinal impedance.

On the other hand striplines were:

- More expensive to build.
- Less reliable due to the numerous small assembled parts.
- Requiring a precise machining or gap adjustment.
- More sensitive. However, this was not an advantage in the case of the cold LHC BPMs because of the power to be extracted from the cryostat and the heat load generated with the nominal beam current.

Given these pro and cons, the final choice (made in 1996) was for button electrodes for the arc BPMs with of course some directional striplines couplers around the experimental areas were directivity is needed. One can also state that this kind of choice is also greatly influenced by good or bad experience of people having already worked with each kind of technology.

BPM types in the LHC

How many types of BPM do you think we need in a machine like the LHC?

The first studies were concentrated on the standard cold BPM, 860 of them being needed for the arcs and dispersion suppressors. Then came the time to adapt to enlarged vacuum chambers; rotated aperture beam screens; experimental areas (with striplines). Some combined pick-ups were also designed to be shared with RF systems. The cold family was then completed with some other special cases requiring a particular integration.

With the warms areas, the number of BPM types was inflated drastically since the initial design due to the ever changing environment and parameters in these regions. The family was not completed until this year, with the special BPMs required for the beam dumping system and transverse diagnostics (long striplines, Tune and chromaticity measurements and wideband pick-ups)

At the end, it was necessary to construct, install and maintain a family of more than 30 Equipment codes and 1090 monitors. This diversity greatly increased the workload, as it was nearly as much work to launch and integrate a series of 5 BPMs as it was for the larger series of hundreds of monitors.

BPM Integration

The LHC BPMs are housed in the technical service module (QQS) on the connection side of the Short Straight Section (SSS), upstream of the beam 1 quadrupole. This is a crowded area shared with many other systems, leading to severe installation constraints. Given the number of components, people involved and interfering functions, every change done in the QQS during the development phase had to be well documented and made aware to all involved. This was done with the help of Engineering Change Request Procedures.

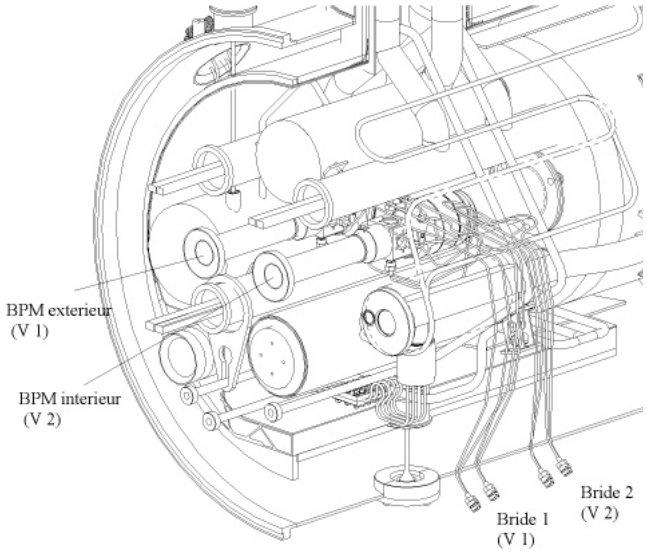

Given the restricted space, the BPM was since the beginning designed to be the input point for the cooling capillaries feeding helium to the Beam Screen. So once welded to the 5m long Beam Screen, the BPM is considered as a Vacuum component.

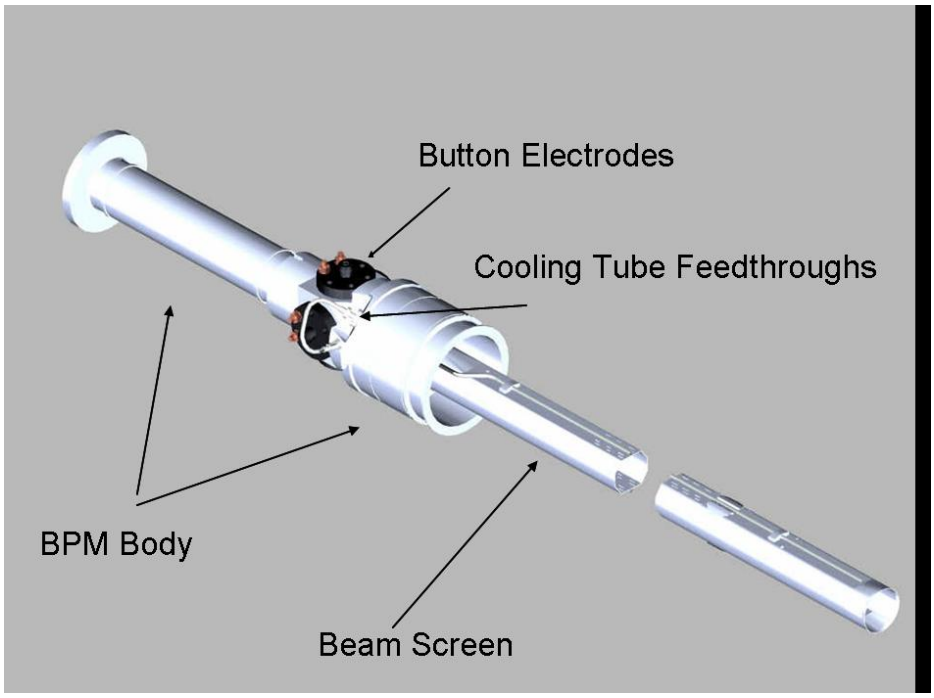

On the upstream side, the BPM flange is used to interconnect the SSS to the neighboring dipole magnet and at this end therefore has to satisfy the requirements of an interconnect component.

Exceptions to this standard integration scheme required even more work than the standard layout. The most difficult one to integrate was the directional coupler, named BPMS, situated in front of the Q2 magnet in the Q1-Q2 interconnect. Not only were these magnets designed by US collaborators, making integration of any CERN component more difficult, but given the proximity of surrounding bus bars, the BPM had to be rotated by 45 degrees in order to make it even possible to connect the coaxial signal cables.

Having learned with this first experience, (tooling development for the first arc BPMs was lengthy and costly) the integration concept was changed for the Enlarged BPM (BPMY). Here the monolithic arc BPM evolved to a modular concept with the aim of producing standardized components that could be adapted to other locations without the need for special tooling. It also took advantage of existing vacuum components such as the dipoles plug-in modules.

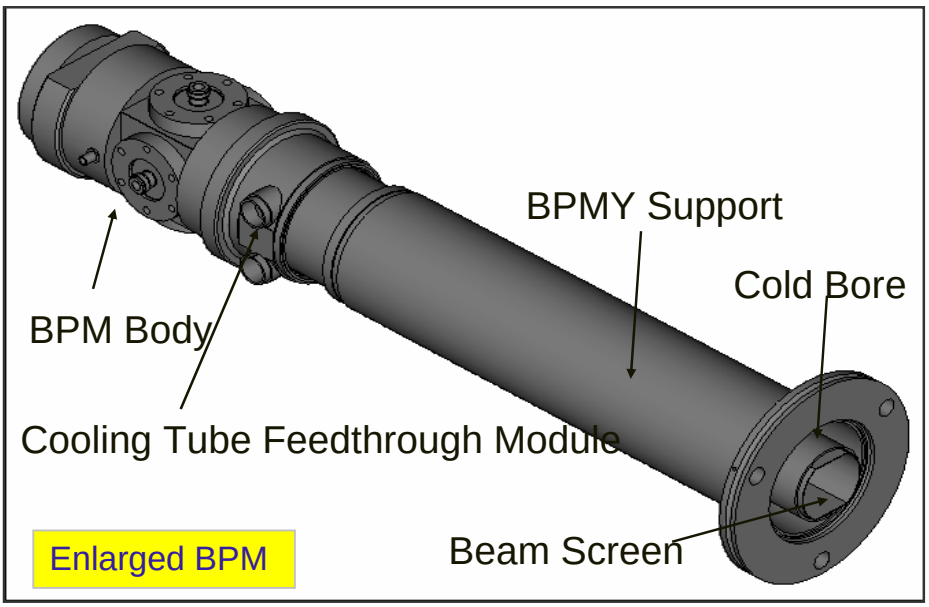

Modular concept of the Enlarged BPM.

Components

Let's now review the system components and see some particular aspects or technological issues that have to be carefully taken in account during the fabrication process.

Bodies

Mechanical tolerances

Given the functional specification, usually requesting measurements in the micron range, it is usual to specify tight mechanical tolerances during the mechanical design stage. This is promising but:

- Be sure to maintain these tight tolerances all along the production chain.
- Do not over-specify your design as tight tolerances immediately impact the cost of machining.

- Do not forget that the 3 axis metrological controls are long and expensive.
- Do not forget to take into account mechanical deformations (see below).

Simulations

In the same manner as Microwave Studio is useful in the design of electrical parameters, Ansys 3D proved to be very valuable in determining the expected mechanical deformations under pressure constraints or to show the thermal gradients along components.

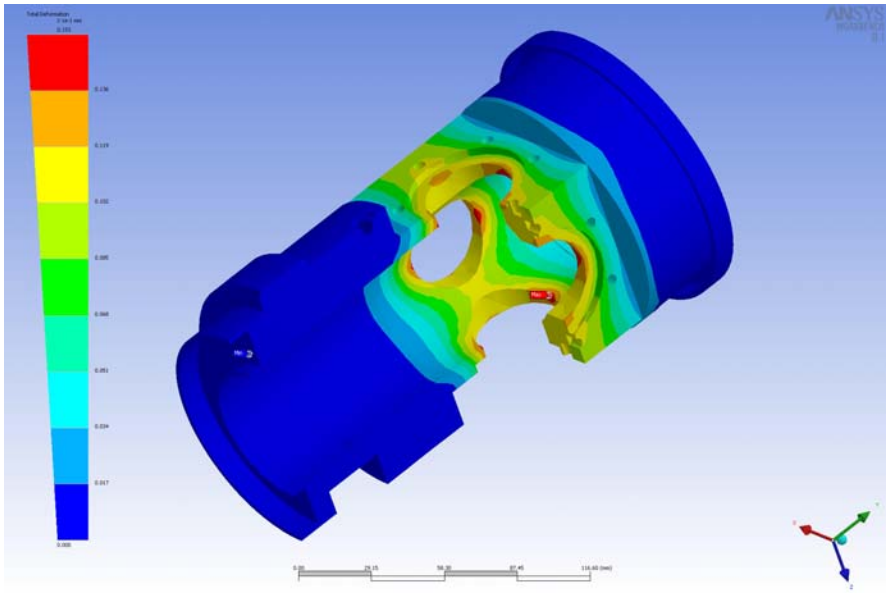

Material

Up to now, 50 leaks have been found in the LHC machine due to bad material (but not yet on BPM bodies). They were discovered after the welding of interconnect components. The reason behind these leaks was found to be due to macro-inclusions found in one batch of the forged austenitic stainless steel of type AISI 316LN used in the LHC.

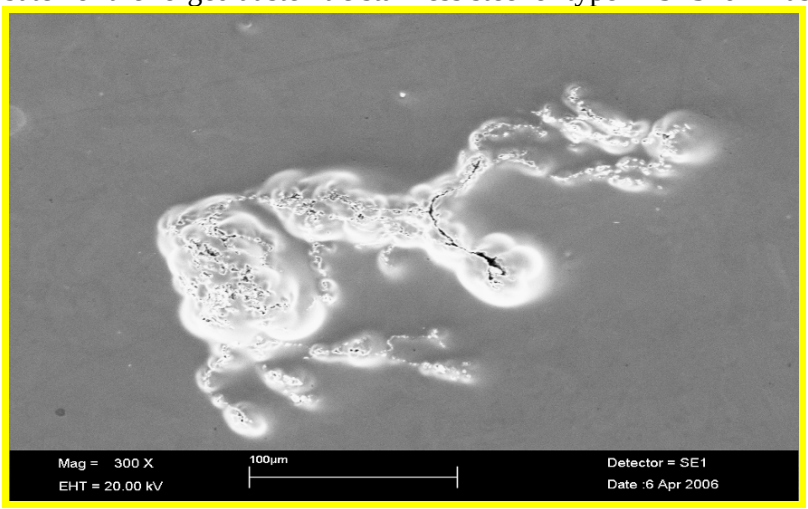

Picture from A. Gerardin

Leaks appeared around these inclusions due to the final stress applied on the material during welding. Such macro-inclusions can produce leaks on material thicknesses up to some millimeters.
To avoid this, a new material specification with an enhanced forging procedure is being issued to replace the current one issued in 1999 (CERN 1001-Ed. 3-02.08.1999).

Copper

The electroplated inner copper layer of 0.1mm thickness is mandatory to maintain the LHC longitudinal impedance. It also equalizes the temperature over the length of the BPM body.
Nickel being excluded due to its magnetic properties, gold is used as a strike between the steel and copper.
Perfect cleaning is the key for strong adherence. Witness samples were requested all along the fabrication to check process quality and copper RRR.
Poor adherence leads to blisters forming on the copper layer during the bakeout. It is important that such an eventuality is discovered well before the end of the fabrication process.

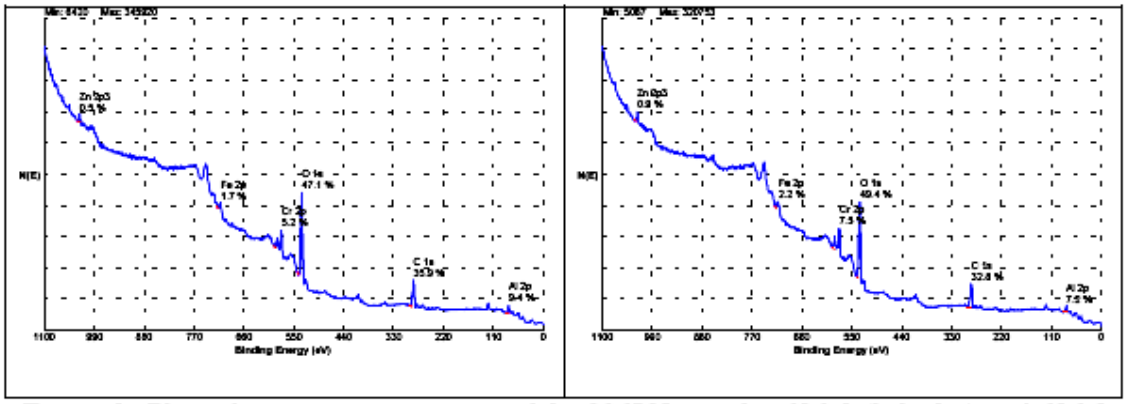

Figure 1: Photoelectron survey spectra of the 316LN samples 626-1 (left plot) and 626-2

Welding

Welds should be re-qualified regularly during production even with automated orbital welding machines. The internal welding surface should be such that the weld does not affect the copper plating.

Buttons

The curved BPM Buttons are the only non welded cold components of the LHC vacuum chamber. The component was designed to be exchangeable, fitted on a flange with a Helicoflex ® type gasket.

Feedthrough technology

Classical Ceramic Seal

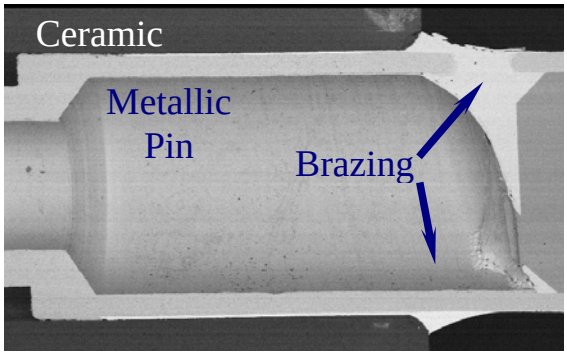

Glass-Ceramic Seal

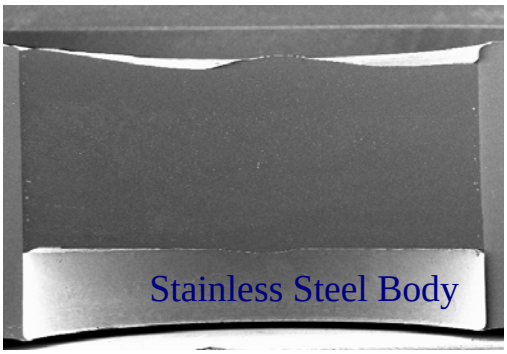

For the UHV coaxial feedthrough, glass metal technology was preferred to brazed ceramic after checks and analysis done on prototypes.

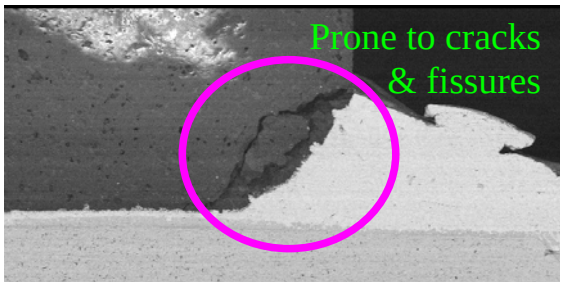

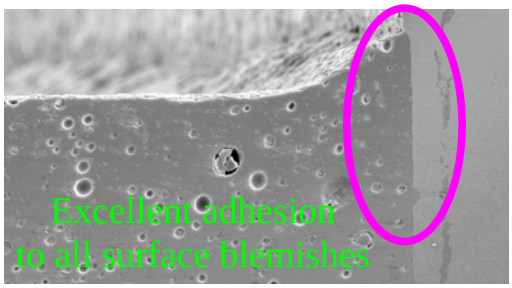

A close collaboration with the supplier allowed the design and fabrication steps to be optimized before the series production got underway.

The following systematic tests were carried out by the supplier:

- Mechanical measurements,
- 5 thermal shock cycles in liquid nitrogen
- Electrical checks,
- Leak test after bake out at 150 degrees for 15 hours.

Electrical tests and the pairing of buttons were carried out at CERN.
To measure the amplitude response and capacitance, a synthetic pulse from a Vector Network Analyzer is sent to the antenna of a test bench. A reference button is used to cross check the VNA calibration.

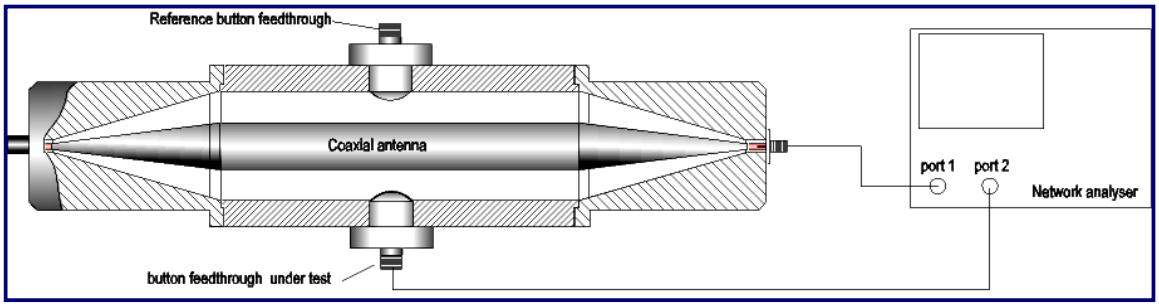

Button measurement test bench.

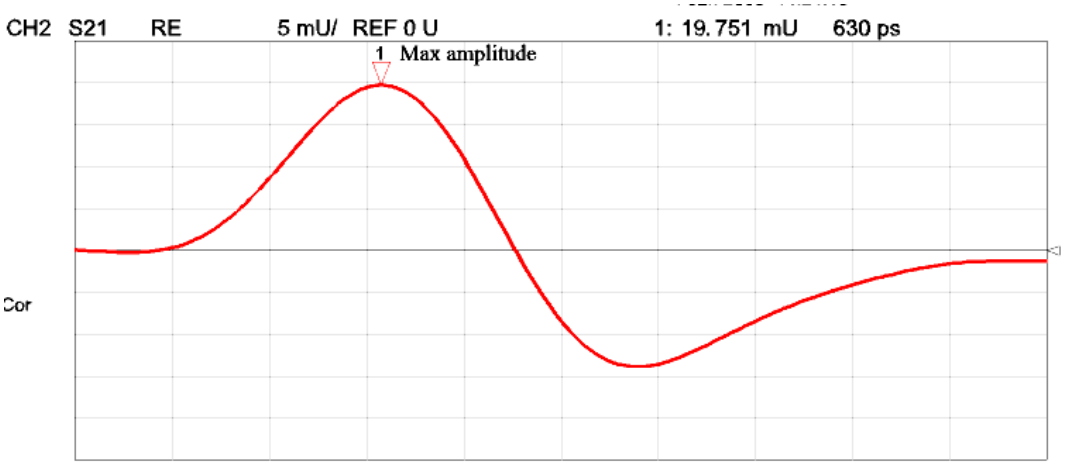

Pairing on amplitude response.

Striplines

The design consists of two parts:

1. Installed from inside the vacuum chamber, two coaxial assemblies are used to mechanically attach the electrode to the body.
2. Fitted from outside, glass ceramic to metal UHV feedthroughs (same technology as for the buttons) with a Helicoflex ® gasket gives the vacuum seal and electrically connects the electrodes to the N connectors on the outside of vacuum chamber.

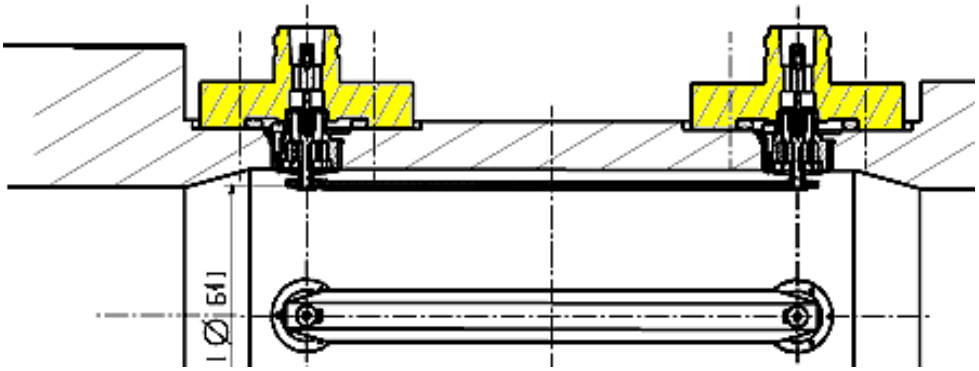

The insulator used for the coaxial assemblies inside the vacuum chamber must be UHV and cryo compatible, radiation resistant, mechanically stable and have low losses. Ultem was our material of choice.
On one side, a sliding contact allows for the thermal contraction of the electrode. A Rhodium – Gold contact was used for this as it has been shown not to stick at cryo temperatures.

The whole fixture is Electron Beam welded. The small weld on the 2mm diameter pin was finally done at CERN.

The electrode gap is not easy to trim with this design. After 3D metrological control of key points in the body, the spacer (2) is adapted in height and the electrode washer (5) welded.
The achieved directivity with this design is 28 dB with a high cut-off frequency of 70MHz.

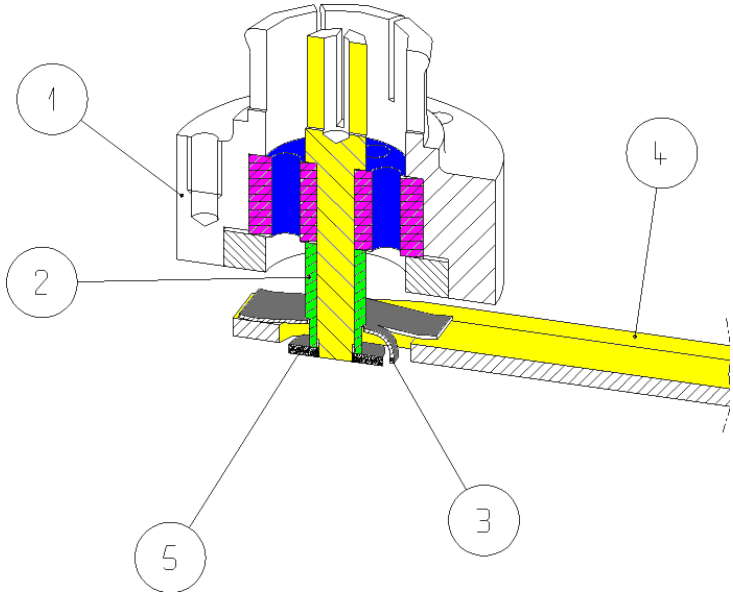

Electrical tests using a TDR were carried out in a cryogenic environment during the development to measure the contact resistance and impedance variation with temperature.
External inputs of the Vector Network Analyzer S Parameter set were used to switch the different instruments during temperature cycles.

Cryogenic Signal Cables

A strong specification

The cold semi-rigid coaxial cables have to meet some tough specifications:

- The cables must be compatible with a cryogenic environment, have high radiation resistance, be mechanically preformed, have a low heat transfer coefficient and VSWR, and most important, have good electrical stability under all these conditions.
- The electrical length difference was specified to be less than 10ps for the 4 cables associated with a single BPM

The dielectric materials under consideration included silicon dioxide, magnesium oxide and ultem (polyimide). The contract was finally awarded to KAMAN (US) for 4250 units in 2001 with the choice of a silicon dioxide foam (SIO2) dielectric. However, MEGGITT (US) took over KAMAN before the start of production.
A “Gold length cable reference” was used all along the fabrication to ease the pairing of cables, which helps the logistics on the CERN side as all cables of a particular type are now replaceable by any other of the same type.

Integration is a challenge

It was not possible to mount the first prototype in the QQS! A new integration design with a groove in the thermal shield was required to finally be able to mount the cables and eventually to allow their removal if one of them breaks.

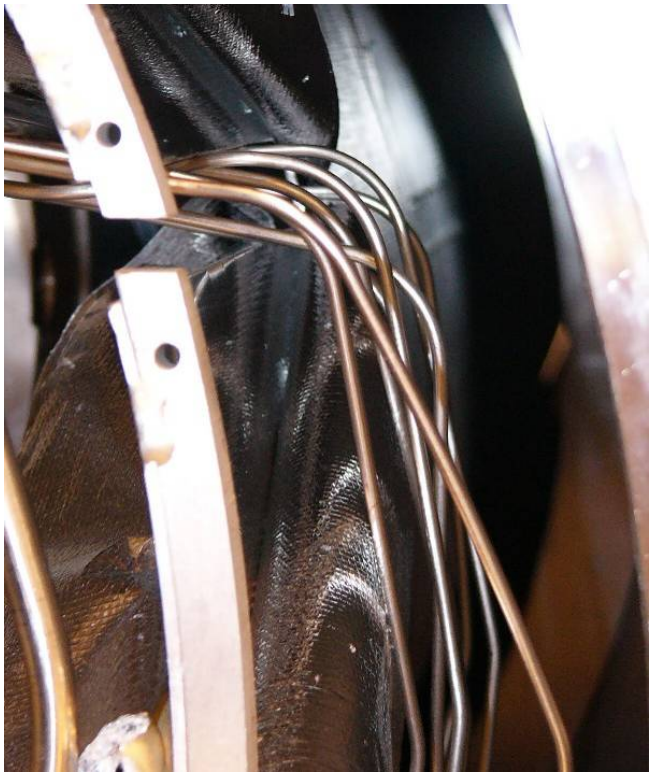

Forming was not found to be as accurate as was specified.

Other configurations

The design of 5 different forming configurations was required to fit to all the BPM types. The cabling of the directional coupler in front of the Q2 magnet is the worst, requiring in the tunnel during the interconnection process. This kind of configuration should be avoided for the safety of these fragile and expensive components

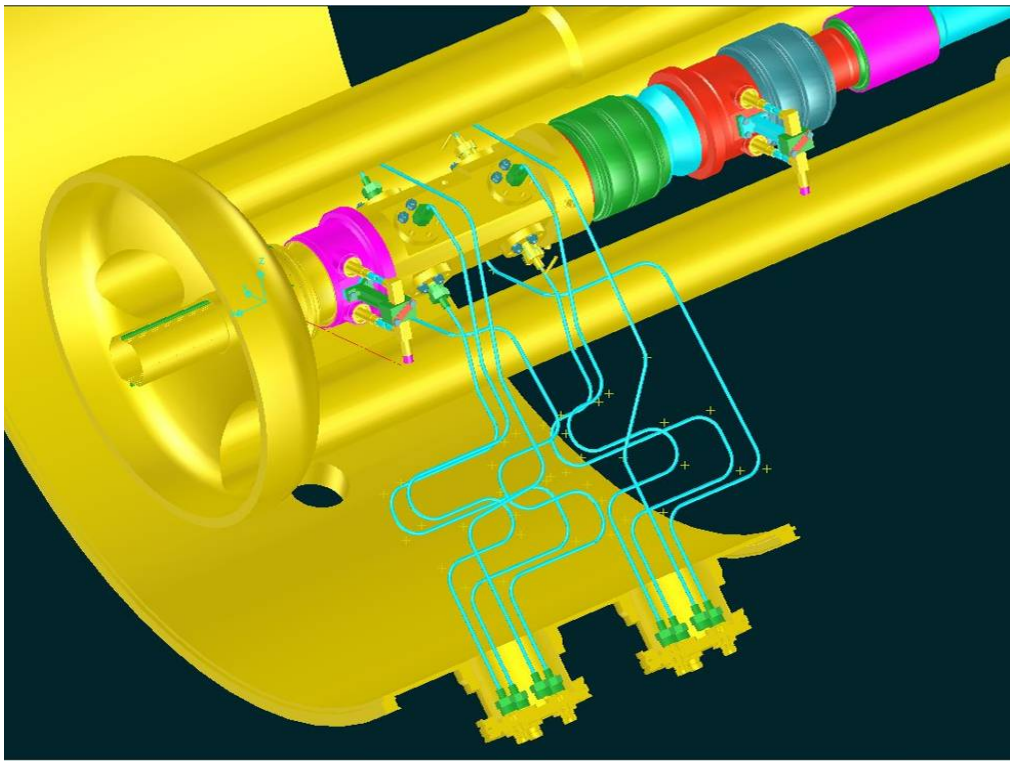

Cabling of the directional coupler in front of the Q2 magnet.

Finally, in order to avoid that the connector becomes unscrewed with thermal cycling, the connector nuts are locked in place by a twisted wire.

Cryostat feedthroughs

This warm component used to extract signal from the insulation vacuum has to withstand radiation and have a low VSWR.
Use of a DN100 flange with 4 N tight connectors with NBR (Nitride Rubber) gaskets in place of welded ceramic feedthroughs allowed us to gain a factor 10 in price.

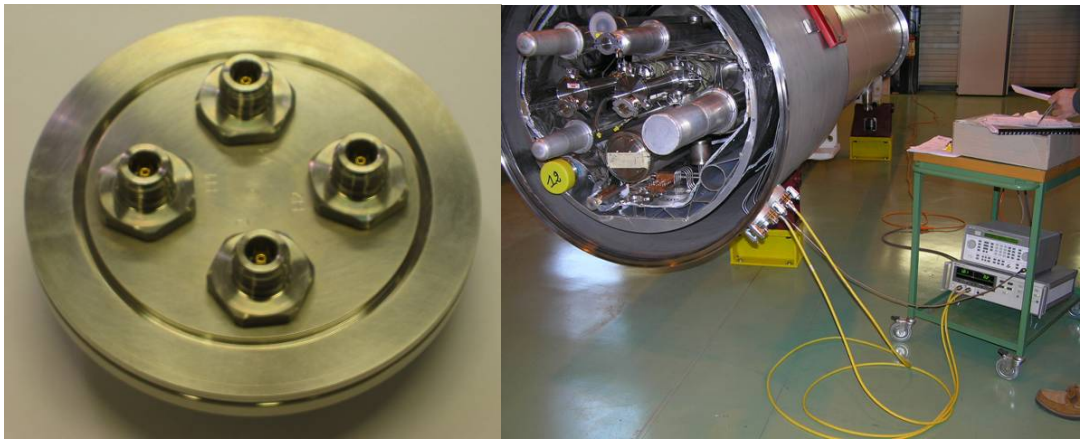

To detect any crossed cables during installation, a simple wiring test was included in the assembly work package.

BPM installation and Tests

BPM installation is part of a work package that is sub-contracted for the 480 SSS magnets.

Procedure:

- Weld the 5 m long beam screen to BPM body (contract)
- Select pairs of button feedthroughs for mounting (BI)
- Mount button feedthroughs (contract)
- Perform leak test (VAC)
- Insert BPM/beam screen assembly (contract)
- Spot weld BPM to support (contract)
- Measure and adjust position and tilt of BPM (Survey)
- Weld BPM to support (contract)
- Measure position and tilt of BPM (Survey)
- Install and connect BPM cables (contract)
- Mount warm feedthrough on cryostat (contract)
- Perform electrical test of BPM system (BI)

Worries:

The contract started slowly in December 2003 and technology transfer had to be repeated many times as the personnel changed regularly.
Magnet installation cannot wait! As this work package is one of the last before installation any non-conformities have to be treated rapidly.

Summary

- **Schedule**

All hardware has now been received after years of development (some of it just in time!)
Installation is now nearing completion (840 cold BPMs from a total of 956 are now assembled)

- **Budget**

We are currently within budget, but the original cryogenic cable budget was greatly underestimated.

- **Design**

Experience from previous machines at CERN and similar machines around the world proved to be extremely valuable in making some of the technical choices.

- **Specification**

Many of the issues related to materials could have been avoided if a timely global material purchase had been made at the project level. As it was, competition between different project engineers to order tons of material at the same could lead to delivery delays of up to 8 months.

- **Integration**

We learn all along the project ….
“What I would change if I would do it once again”

- **Construction and Installation**

Everything was slower than planned partly due to the large scale of the project and the limited manpower available.

LARGE HORIZONTAL APERTURE BPM FOR USE IN DISPERSIVE SECTIONS OF MAGNETIC CHICANES

K. Hacker, F. Loehl, H. Schlarb DESY, Hamburg, Germany

Abstract

A sub-5 μm resolution electron beam position monitor (BPM) with a 10 cm horizontal aperture is described. It was installed in the first bunch compressor chicane of FLASH in October 2006 and is required for a bunch-to-bunch energy measurement. It utilizes a stripline-pickup mounted perpendicularly to the beam direction to generate broadband electrical-pulses travelling to the left and right of the beam direction. The arrival-times of the broadband pulses will be measured through an electro-optical technique developed for a beam arrival-time monitor. In this paper, a comparison of simulations for the beam position monitor and measurements taken with an 8GHz bandwidth oscilloscope are presented.

INTRODUCTION

Energy jitter of the electron beam becomes transverse position jitter in dispersive regions of chicanes and after chicanes it becomes longitudinal and transverse position jitter. This longitudinal position jitter, or arrival-time jitter, presents a problem for the synchronization of external lasers to the electron beam. Since the low-level RF system alone cannot provide enough energy stability, a beam-based energy feedback is envisioned to stabilize the beam compression and arrival-time of the electron beam at the end of the accelerator. A monitor required for such a feedback system could be a high-resolution, large-horizontal-aperture BPM placed in the dispersive sections of magnetic chicanes.

A beam arrival-time stability of 30 fs (~10 μm at v=c) is desired for pump-probe experiments and mandatory for laser based electron beam manipulation at FLASH and the XFEL [1]. For an energy stability of 10^{-4} at FLASH, the transverse position jitter in the dispersive section of the first chicane becomes 34.5 μm and results in a longitudinal position jitter of 18 μm. A monitor for a feedback system should be able to measure the energy by a factor of three better than the desired energy stability and this means that the resolution for a beam position measurement in the chicane must be better than 6 μm and for a longitudinal time-of-flight path-length measurement it should resolve 3 μm.

A longitudinal time-of-flight energy measurement can be made with two beam arrival-time monitors: one before and one after the chicane, but a BPM energy measurement has an advantage given by the ratio of the R_{16} to the R_{56} terms. In the case of the first bunch compressor for the XFEL, this advantage in the required sensitivity of the monitor is a factor of six.

Standard BPMs can get better than 6 μm single-shot resolution, but they do not have the large horizontal aperture that the location in the dispersive section of the chicane requires, so a novel design must be chosen. A standard BPM could be placed on movers, but the large energy spread, space constraints, and the undesirability of bellows in a wakefield sensitive area rule out this possibility. Alternatively, an array of small, longitudinally-oriented striplines could be placed above the path of the beam to give a transverse beam profile, but experience with the multi-channel data acquisition, wire interference, calibration issues, and DC offset drifts of SEM grids suggests that this could be a difficult design to realize. Consequently, a rather simple perpendicularly mounted stripline concept was suggested, but it was noted that it could not achieve the required resolution with standard electrical processing techniques [2]. Thanks to the development of a broadband laser-based synchronization system, new optical-techniques for electrical-pulse phase measurement make the required resolution possible [3]. This system is being duplicated for commissioning with the chicane BPM in February 2007. Oscilloscope measurements of the beam transient from the BPM pickup demonstrate that it meets expectations.

VACUUM CHAMBER DESIGN

The design utilizes a cylindrical pickup within a cylindrically shaped vacuum chamber channel that lies over and perpendicular to the path of the electron beam (see Fig. 1). When the electron beam travels beneath this pickup, broadband electrical pulses travel to opposite ends of the pickup. The arrival times of the pulses are used to determine the position of the electron beam.

General Layout

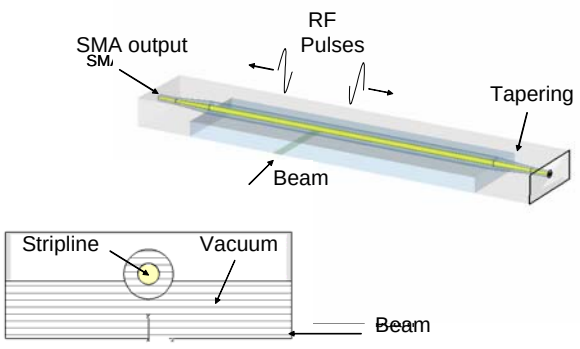

Figure 1: Perpendicularly-mounted stripline BPM pickup.

In Fig. 1, the perpendicularly mounted stripline is depicted in 3-D as well as in cross-section. Only the upper-half of the BPM is shown, since the lower-half is identical. The beam is represented by a thick line underneath the stripline. The central portion of the stripline is tapered on both ends from a 3 mm diameter to an SMA sized connector pin. The vacuum feedthroughs to SMA connectors are at the ends of the stripline.

Standard stripline designs do not have tapering from the pickup to the feedthrough, but instead have a larger radius pickup connected at a sharp angle to a smaller SMA connector sized feedthrough. The tapered design was chosen to improve the broadband transmission of the beam transient signal because it is undesirable to have an overlap between the signals of individual bunches within the macro-pulse and because the resolution of the optical phase measurement is improved by more broadband transient transmission.

Dimensions

Key dimensions of the BPM are listed below in Table 1.

Component	**Dimension**	**Specification**
Pickup	Radius	1.5 mm
Pickup Center	Height	5 mm
Channel	Radius	3.45 mm
Chamber	Half-height	4 mm

Table 1: BPM Dimensions

The ratio of the stripline pickup radius to the stripline channel radius was chosen based on a coaxial-cable impedance matching model. If the stripline channel were closed instead of open to the underlying beam pipe, the impedance would be 50 Ohms. Since the stripline channel is only a partial cylinder, the pickup assembly has closer to 60 Ohms impedance in both simulation and laboratory tests. This was the optimal configuration for coupling to the beam and throughput.

The height of the pickup assembly above the center of the beam pipe was also optimized through a simulation. The best coupling and throughput was achieved for a position where the bottom of the pickup was ~0.5 mm below the boundary of the beam pipe.

Construction

Considerations for the construction include:

- A ring shaped Alumina spacer is used to stabilize and align the pickup in the channel (for future designs, Vespel (polyimide) may be used).
- A mini-bellows design for the connection from the pickup to the feedthrough accommodates thermal expansion of the pickup.
- With flanges, the length is 130 mm and the width of the central chamber is 135 mm. (Parameters are adjustable for individual applications.)

OPTICAL PHASE MEASUREMENT

Beam Phase Monitor

To date, 30 femtosecond resolution has been achieved with the optical beam arrival-time monitor measurement [3]. It utilizes a broadband optical pulse (< 1 ps) from a master laser oscillator that is locked to the 1.3 GHz reference of the machine. The light pulse travels via fiber optics through an electro-optical modulator (EOM) which encodes the amplitude information of an RF pulse in the light pulse. Essentially, the light pulse samples the RF pulse. The modulated light pulse is then detected with a 50 MHz bandwidth photo diode and read out by a fast ADC that is clocked at twice the repetition rate of the laser and generated from the laser pulse itself. The method has only recently been tried and many possibilities for improving the resolution are still open.

Since changes in beam arrival-time produce a change in laser intensity, the measurement is limited by the steepness of the RF signal slope and the detection of the laser amplitude. Slope changes can distort the measurement, so it is best to measure at the zero crossing of the signal for an accurate phase measurement.

Beam Position Measurement

For the chicane BPM, the average of two outputs' phase measurements can also be used to measure the beam arrival-time, as long as the energy spread is constant. The difference of the two outputs' phase measurements gives the position. Alternatively, if the arrival-time is known from the phase monitor, the energy spread might be measured with the BPM.

It is anticipated that for each BPM output, the RF signal will be split for a low-resolution (large range) phase measurement, and the other output for a high-resolution (small range) phase measurement. A delay-line will use the low-resolution measurement to put a high-resolution measurement in range. The position of this delay-line plus the fine measurement given by the ADC gives the beam position. This delay line must have sub-micrometer resolution over 10 cm and be adjusted between macro-pulses (10 Hz) in order to keep the system measuring the beam transient at the zero crossing, thereby reducing the systematic errors of slope variation caused by beam charge fluctuations or transverse profile shape changes.

The slope variation from charge fluctuation scales linearly and should amount to no more than 3 percent, an amount for which one can correct with a toroid charge measurement. The shape dependence can be monitored with a synchrotron light monitor after the second bend of the chicane.

Interferometric schemes using either a CW laser or the master laser oscillator were also considered for this monitor, but the success of the arrival-time monitor's optical phase measurement has shifted the focus to a tried concept.

SIMULATIONS

In the Microwave Studio simulation, a Gaussian pulse was applied to the monopole mode of a waveguide port in order to simulate the electron beam. The output signals of the SMA connector ports were scaled according to a 1 nC electron bunch charge (Figs. 2 and 3).

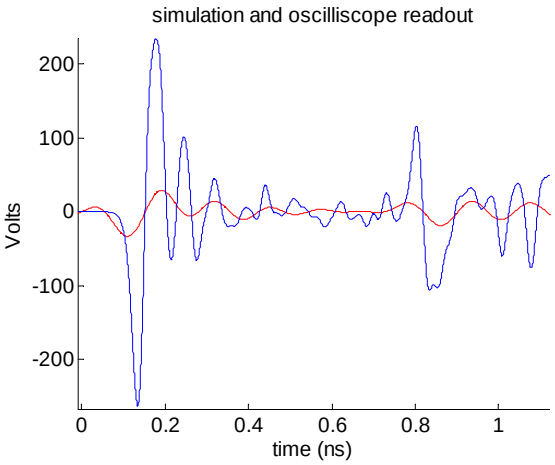

Figure 2: 50 GHz bandwidth simulation of BPM output (blue) and 8 GHz oscilloscope measurement. The reflected pulse (right) is undesired and is due to the impedance mismatch caused by the ceramic support.

The BPM response is linear over the entire horizontal aperture and is insensitive to small changes in the beam width and shape. Vertical position changes and charge fluctuations influence the amplitude of the signal but not the position measurement.

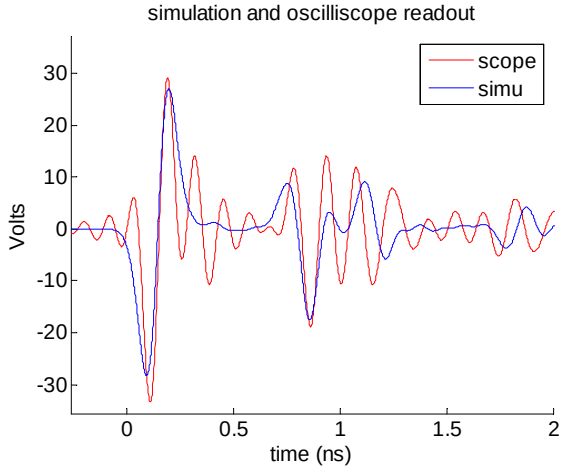

Figure 3: When the bandwidth of the simulation is the same as the bandwidth of the oscilloscope (8 GHz) good agreement is observed. The additional ringing on the oscilloscope signal is believed to be a scope artefact, but no conclusive test has been done.

The simulation did not include the 1 meter long cable between the pickup and the oscilloscope. The additional ringing observed on the oscilloscope signal is believed to be an oscilloscope artefact, but a conclusive test will be available in February 2007 when the optical front-end is commissioned.

MEASUREMENTS

The beam energy was changed through the adjustment of the accelerator section ACC1 RF amplitude and the beam position in the chicane changed as expected. The position was measured on an 8GHz oscilloscope by triggering the acquisition of the beam transient from one end of the stripline with the output from the opposite end (Fig. 4). This method should give ~150 um position resolution. The target resolution for the optical front-end is <5 um.

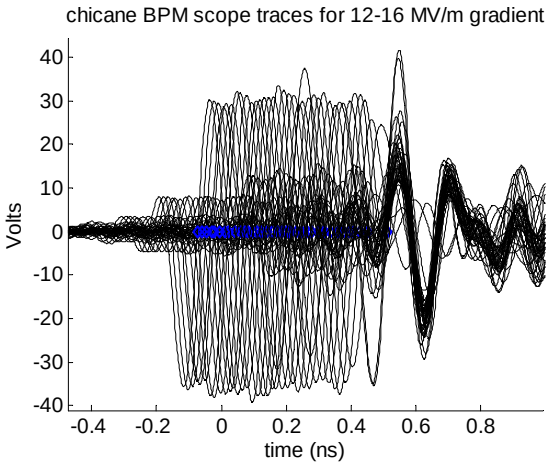

Figure 4: Beam transients for different beam energies.

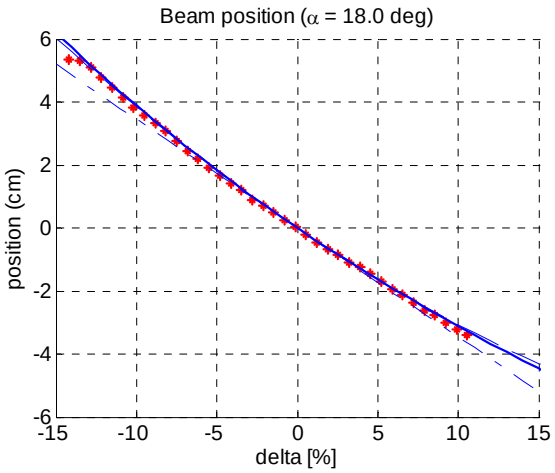

Figure 5: Beam positions for different beam energies for an angle of 18 degrees into and out of the chicane: measured (red*) and calculated R16, T166, R1666 (blue).

In Fig. 5, the measured values of the positions expected in the chicane for different beam energies (red) agree well with the calculated values (blue). The straight blue line is just the R16 term for the chicane and the curved lines include the higher order dispersion terms, T166 and R1666. The calculation was done for an angle into the chicane of 18 degrees. On the left end of the plot, the beam was clipped by the vacuum chamber and on the

right end of the plot, the gradient could not be increased any more.

In Fig. 6, the phase of the 1.3 GHz accelerating RF was changed and the beam position in the chicane changed in a sinusoidal form, as expected. When the bunch is further off crest, the energy spread, and therefore the transverse position spread, of the bunch is larger, but the length of the bunch is shorter. This situation seems like it could produce a position measurement error for very off crest beams, due to the difference in the arrival times of the head and tail of the bunch, but in reality the monitor always measures the centroid.

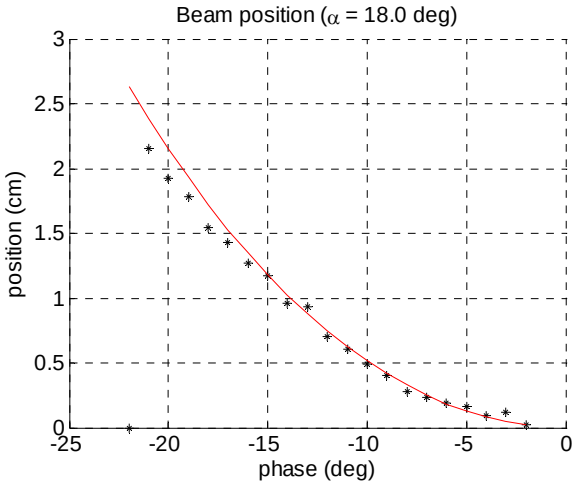

Figure 6: Beam positions for different beam energy chirps: measured (black*) and calculated (red). The phase of the accelerating RF was changed, creating a sinusoidal position change.

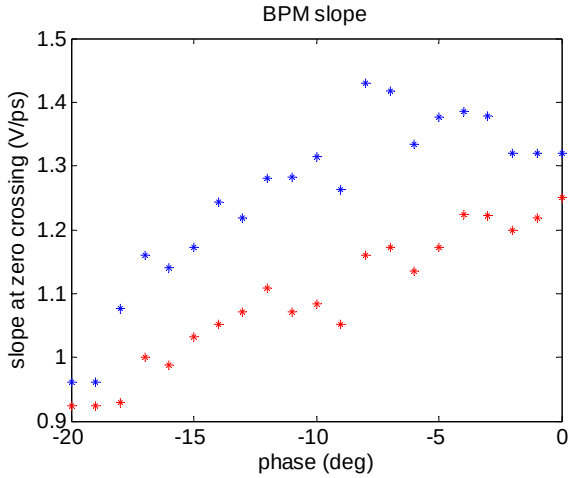

Figure 7: Slope at the zero crossing for different energy spreads. Negative phase corresponds to increased energy spread.

Fig. 7 shows the slope at the zero crossing for different accelerating RF phases. For the optical front- end, it is desirable to sample the transient as close as possible to the zero crossing because if one samples away from the zero crossing and then the bunch charge, the beam shape, or the vertical position changes significantly, then an error is introduced into the measurement from the resulting transient amplitude change. By sampling on the zero crossing the measurement is insensitive to amplitude changes. Nevertheless, it is good to see that bunch shape changes due to energy spread changes, do not drastically affect the slope of the transient.

FUTURE DEVELOPMENTS

A final version of the electro-optical front-end is expected to be completed by February 2007. The incorporation of the chicane BPM, upstream BPMs, the phase-monitor, and a bunch length monitor into an FPGA based bunch-to-bunch energy feedback will follow.

The phase monitor and the BPM can distinguish the energy jitter that results from injector timing jitter from the energy jitter caused by the acceleration RF phase and amplitude jitter. The bunch length monitor and the BPM can distinguish the RF amplitude jitter from the RF phase jitter. BPMs before the chicane can be used to remove incoming orbit jitter from the chicane BPM's energy measurement.

CONCLUSIONS

- The BPM is expected to have sub-5 μm resolution.
- It will have a 10 cm horizontal range for this first application in the first bunch compressor.
- It will be used in a bunch-to-bunch energy measurement.
- It will use an optical phase measurement developed for a beam arrival-time monitor.
- First results from the beam arrival-time monitor optical phase measurement give a sub-30 fs resolution with many options still open for improving the system's resolution.

ACKNOWLEDGEMENTS

Many thanks for design work and advice go to Jan Hauschildt, Dirk Noelle, Nicoleta Baboi, and Silke Vilcins-Czvitkovits.

REFERENCES

[1] X-FEL Technical Design Report Sect. 4.8 2006.
[2] Manfred Wendt, personal communication.
[3] F. Loehl et. al., "Beam Arrival-time Monitor", EPAC'06, Edinburgh, June 2006.
[4] K. Hacker et. al., "Large Horizontal Aperture BPM", EPAC'06, Edinburgh, June 2006.
[5] K. Hacker et. al., "Pickup Designs for an Optical Sampling Technique", FEL'06, Berlin, August 2006.

4th CARE-Meeting HHH-N3-ABI in Lüneburg, Germany

Simulation of BPM front-end electronics and Special Mechanical Designs

3rd half day: **Cold BPM Technology**
Chair: Kay Wittenburg, DESY

Invited talks:

1.	D. Noelle	DESY	Future cold BPMs at DESY (20 min)
2.	M. Nagata, K. Iwamoto	Kyocera	RF vacuum feed-through for cryogenic application
3.	F. Kialashaki	Meggitt	BPM and RF vacuum feed-through for cryogenic application
4.	S. Vilcins	DESY	Planned testprocedures for cold BPM-feedthroughs and experiences with cold BPM in HERA
5.	C.Boccard	CERN	Design Choices for the cold LHC-BPMs
6.	N. Baboi	DESY	A very special large aperture BPM at FLASH

Main remarks in the discussions:

- Talk 1: Overview of future cryogenic BPMs in XFEL/ILC, referring to talks to M. Wendt, C. Simon, T. Traber
- Talk 2 and 3: Overview of commercial products from two companies. Meggit prefers Glass to metal seal design while Kyocera works with ceramic to metal sealing. BPMs can be tested in factory with liquid N_2 temperatures. No significant difference to liquid He temperatures in the mechanical behaviour are expected. ("N_2 temperatures seems to be good enough"). Factories do not have liquid He test abilities.
- Talk 3: BPMs are modeled/simulated at Meggitt in CST and HFSS, with good agreement of the results.
- Talk 4: Experiences from HERA cold BPMs: No significant differences between horizontal and vertical BPM failure rate (expected that horizontal BPM is more affected, but at HERA it is 1/3 horizontal and 2/3 vertical failure rate). However, the auditorium expected that failures are mainly due to thermal stress of the whole BPM device (stripline). Therefore it is recommended to make cryogenic tests with the complete BPM included in the vacuum chamber.
  No experiences of cold BPM failures (leakage) available from RHIC or FERMILAB.
  It is not recommended to make more than 2 cryogenic cycles with feedthroughs which will be used later in an accelerator. Otherwise it might get too close to their lifetime-limit. 2 cycles are enough to find production faults.
- Talk 5: Also the cabling in the cryostat is an issue, not easy to get high quality FR cables with good thermal properties.
  Roughly estimated costs of a cold pick-up: Vacuum body ≈ 6000.- $ (note that the price of stainless steel increased very strongly (600% in last years), one button ≈ 200.- $, one cable ≈ 600,- $, warm feedthrough ≈ 600.- $ for 4 cables.